A critical review of proton exchange membrane fuel cells matter transports and voltage polarisation for modelling

Raphaël Gass^{a,b,*}, Zhongliang Li^{a,*}, Rachid Outbib^b, Samir Jemei^a, Daniel Hissel^{a,c}

^aUniversité de Franche-Comté, UTBM, CNRS, institut FEMTO-ST, FCLAB, Belfort, France

^bAix Marseille Univ, CNRS, LIS, Marseille, France

^cInstitut Universitaire de France

Abstract

Technologies based on the use of hydrogen are promising for future energy requirements in a more sustainable world. Consequently, the modelling of fuel cells, which are devices that convert hydrogen energy into electricity, is crucial to facilitate their optimal control to reach excellent performance while slowing down their degradation. To achieve this, a comprehensive study is needed that encompasses both well-established and the latest governing laws on matter transport and voltage polarisation for Proton Exchange Membrane Fuel Cells (PEMFC). Indeed, recent articles often use outdated or inadequate equations. Moreover, the lack of clear explanations regarding equation backgrounds and inconsistent incorporation of physical context, experiences, or model requirements hinder the comprehension of equations and contribute to their improper use. Further, specific research must also be conducted to construct more accurate models. This study aimed to provide a fair understanding of the current state-of-the-art PEMFC modelling to clarify the corresponding governing equations and their usage conditions and hypothesis . The given laws and equations can be used in most multi-dimensional, dynamic, and two-phase PEMFC models.

Keywords: Polymer electrolyte membrane fuel cell (PEMFC), Modelling, Water management, Hydrogen transport, Oxygen transport, Voltage polarisation

1. Introduction

As carbon-free, efficient, and broadly applicable disruptive innovations, decarbonised hydrogen technologies have garnered increased attention [1, 2]. The twenty-first century is engaged in a race against time to limit the global warming to 1.5°C above pre-industrial levels, as agreed in the Paris Agreement by 192 Parties in December 2015 [3]. Decarbonised hydrogen is a very promising candidate that can significantly impact several polluting sectors through relevant developments. For instance, it affects the decarbonisation of certain crucial industries, such as steel and fertiliser manufacturing, in the electricity storage for the development of renewable energies, and in transportation electrification [4]. Thus, hydrogen technology development has become a national priority for many different countries [1].

Currently, proton-exchange membrane fuel cell (PEMFC) is the most used fuel cell technology [5]. However, it suffers from limited lifetime which, among other current defaults, has hindered its spread in the global market [6]. Its life-span can be improved by considering, at a mesoscopic scale, the degradation processes that occur in the stack and then implementing it in an algorithm to control the fuel cell in real time. For this approach, fuel cell modelling is essential to study degradation. However, currently only a few algorithms can incorporate the physics involved in the stack while examining its ongoing degradation.

One of the many requirements to achieve this is the necessity of a good comprehension over the physics involved in water, hydrogen, and oxygen transport in the stack and on voltage polarisation. Although Jiao et al. [7], O'Hayre et al. [8] and Dicks et al. [5] presented comprehensive reviews on matter transport and voltage polarisation phenomena,

 $^{^*} Corresponding \ authors.$

in 2011, 2016, and 2018, respectively, a review covering the recent developments is required. Certain interesting and recent governing equations have not been mentioned in these reviews and must be considered. Consequently, often, recent articles do not employ the latest propositions, although they present greater precision in the results or more stability in the algorithms. Disruptive errors are also spreading in the literature and must be identified. In addition, a more comprehensive explanation of the background related to the governing laws and equations is necessary. Often, there are several equations that model the same phenomenon. Thus, these must be synthesised within one paper and be differentiated in terms of the physics involved, the experiences, or the model needs related to them. Furthermore, a synthetic gathering of key constant values present in the whole literature must be considered to have an overview of the commonly accepted constant values, the ones that result in disagreements, and the ones that are poorly considered.

This study also exploited the opportunity to construct new equations. First, we combined several expressions to create new equations that are either more stable, more precise, or which consider more phenomena. Subsequently, to reduce the complexity of generating an algorithm and inspired by the work of Pukrushpan et al. [9], we proposed simplified boundary conditions at the inlet and outlet of the gas channel, to provide draft results before modelling the auxiliary systems. All the given governing laws and equations can be adapted in any multi-dimensional two-phases model. Figure 1 illustrates the matter flows considered in this study, wherein, the flows are directed according to the thickness of the stack. This facilitated the graphical representation; however, flows in other spatial dimensions are possible, although minor.

In this study, first, matter transports are discussed while considering the flow of each molecule at stake at each place of the stack. Water transport dissolved inside the Nafion[®] membrane is examined first. Then, liquid water transport in the catalyst layer (CL), gas diffusion layer (GDL), and gas channel (GC) is considered. Thereafter, vapour transport and then hydrogen, oxygen, and nitrogen transports in all these three regions are discussed. Subsequently, voltage polarisation is addressed. Finally, in the appendixes, other useful equations are mentioned, synthesis of the constant values found in the literature and of the hypothesis considered in this study are given, and certain demonstrations are presented.

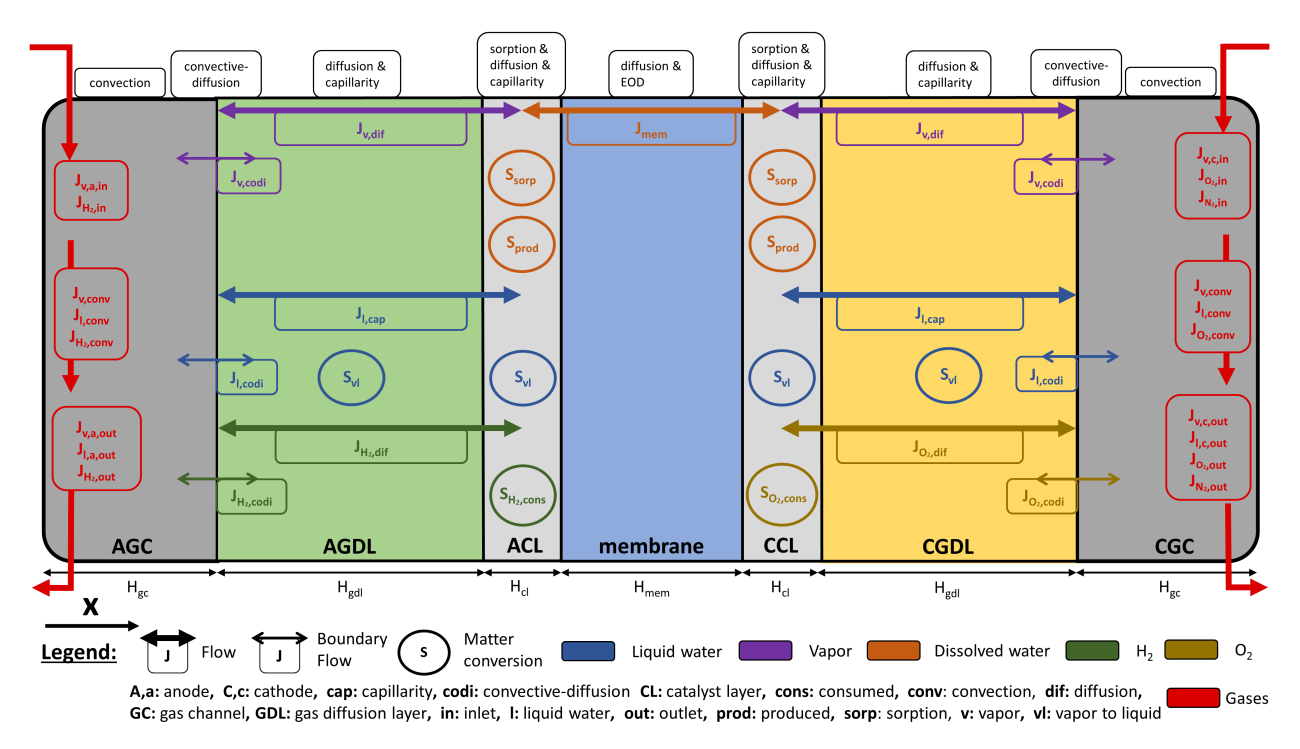


Figure 1: Schematic of a single PEMFC with the matter flows illustrated

2. Water transport in the membrane

State-of-the art polymer electrolytes, such as Nafion[®], have noticeable ionic conductivity only in a wet state. As discussed in Section 2.3, protons are transported in the membrane owing to dissolved water in it. Thus, this hydration must be considered to facilitate good working conditions.

Notably, in studies on PEMFC, the active area has been commonly used as the surface reference for the different flows. Species evolve in different materials with different volume accessibility. However, the active area, which is the surface of the MEA without the gasket, is a common surface for all the materials and is thus a good reference. Moreover, it is also the surface for which the current density is defined. This reference is useful to consider the molar transfer from one element to another without errors, and hence, the governing equations in this study use constants such as porosity ε , which facilitate a return to the active area.

2.1. Water content: λ

In the Nafion®membrane, water is present in an unusual form. It is absorbed by the sulfonated side-chains $(-SO_3H)$ in liquid phase [5]. Thus, it is interesting to quantify the water in the membrane using the water content variable λ . By definition, the water content corresponds to the number of water molecules per charged site $SO_3^-H^+$ in the membrane.

$$\lambda \triangleq \frac{n}{n_{SO_3^-H^+}} \tag{1}$$

where n (mol) is the number of moles of water, $n_{SO_3^-H^+}$ (mol) is the number of moles of the sulfonic acid group, and $\stackrel{\triangle}{=}$ refers to an equality by definition.

Further, λ must be considered in the CL. Indeed, a thin layer of ionomer adheres to the catalyst metal particles [5], and so a fraction of the CL volume is the electrolyte. This necessitates the use of ε_{mc} , which is the ionomer volume fraction in the CL defined in (2). It is then interesting to note with an index the location of the water content λ_{mem} in the membrane or λ_{cl} in the catalyst layer. Although both of are continuously linked, the governing equations are different, and this notation would simplify the writing of the differential equation for λ dynamic behaviour. However, the omission of this index allows for the designation of both locations.

$$\varepsilon_{mc} \stackrel{\triangle}{=} \frac{V_{\text{ionomer in CL}}}{V_{\text{CL}}} \tag{2}$$

2.2. Schroeder's paradox

In a membrane electrode assembly (MEA), the membrane and catalyst layers are in close contact. Water can travel from one element to the other. However, the amount of water absorbed by the membrane is not the same as water may in saturated vapour or pure liquid phase in the catalyst layer. In liquid phase the quantity absorbed is considerably higher. This is, at first glance, a paradox as dissolved water in the membrane theoretically reaches an equilibrium with water activity, which is equal to 1 for both saturated vapour and pure liquid water. Both equilibriums should then be the same. This phenomenon is referred to as Schroeder's paradox in recognition of the searcher who discovered it in 1903. This is prevalent in many polymers such as perfluorosulfonic acid (PFSA) polymer (e.g., Nafion®). Although this subject is not fully understood, many studies have focused upon it. Liquid water changes the morphology of the polymer, transforming it from a strongly hydrophobic matter to a hydrophilic one. With liquid water, the Nafion®hydrophilic sulfonated side-chains ($-SO_3H$) initially inside the matter, can reach the surface of the membrane, as shown in figure 2, to attract and absorb water. However, vapour absorption first requires vapour condensation at the ionomer interface. This additional step explains why less water is absorbed in the vapour regime and why the time scales are significantly larger [7].

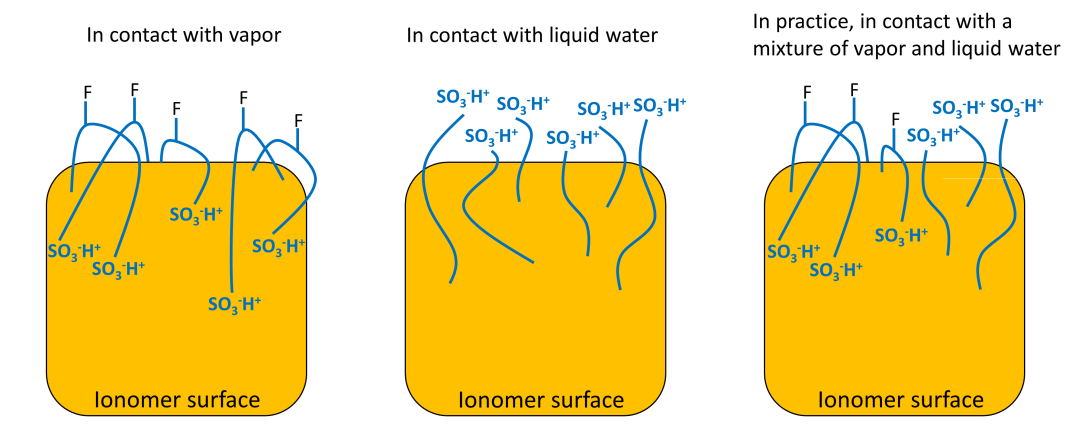


Figure 2: Illustration of PFSA membrane surface morphology when it is in contact with vapor and liquid water [7].

2.3. Water flow in the membrane: J_{mem}

There are two dominant water transport mechanisms in the membrane: a diffusive flow and an electro-osmotic drag (EOD). The expression of these flows is initially based on the model of Weber and Newman [10, 11] from the concentrated solution theory [12]. However, their expressions are mathematically complicated and use theoretical variables that are not practical for global modelling; such as, the chemical potential of water μ . Consequently, their expressions have been evolved to more functional forms without losing any information. The following expressions are demonstrable using the concentrated solution theory, although their final form is different from their initial one.

Diffusive flow is expressed as a Fick-like expression [13], using the gradient of λ and an associated diffusion coefficient D, which is not constant but a function of λ . This is done to express this gradient as the derivative of λ with x, which is the space variable in the direction of the thickness of the cell, as shown in Figure 1.

EOD corresponds to the water molecule drag with protons transport in the membrane. Protons travel in the membrane by hopping between adjacent water molecules (Grottus mechanism) or in the form of hydronium complexes H_3O^+ that cause them to drift (vehicle mechanism). Through this second phenomenon, protons carry water with them from the anode to the cathode [7, 14]. Springer et al. assumed in 1991 [13] that EOD is proportional to the current density and to the water content. They then found a constant EOD coefficient based on measurements in Nafion®117. Their work, shown in the expression of J_{mem} as (3), has been extensively used in the literature [7, 13, 15–18].

$$\boldsymbol{J_{mem}} = \frac{2.5}{22} \frac{i_{fc}}{F} \lambda \, \boldsymbol{\imath} - \frac{\rho_{mem}}{M_{eq}} D(\lambda) \, \boldsymbol{\nabla} \lambda \tag{3}$$

where J_{mem} ($mol.m^{-2}.s^{-1}$) is the water flow in the membrane, i_{fc} ($A.m^{-2}$) is the current density of the fuel cell per unit of cell active area, F ($C.mol^{-1}$) is the Faraday constant, ρ_{mem} ($kg.m^{-3}$) is the density of dry membrane (ionomer), M_{eq} ($kg.mol^{-1}$) is the equivalent molar mass of ionomer represented by the dry mass of the membrane over the number of moles of SO_3^- , D ($m^2.s^{-1}$) is the diffusion coefficient of water in the membrane, and ι is a unit vector along the x-axis. However, since 1991, significant enhancements in Nafion® membrane have been made [19] and the EOD on these new membranes may differ. It would thus be interesting to reproduce the EOD calculation in order to obtain more accurate models.

A different expression for the EOD exists in the literature [7], although it is less employed and equally outdated. It is expressed as (4).

$$J_{EOD} = \begin{cases} \frac{i_{fc}}{F} \mathbf{i}, & \lambda \le 14\\ [0.1875\lambda - 1.625] \frac{i_{fc}}{F} \mathbf{i}, & \lambda > 14 \end{cases}$$
(4)

where J_{EOD} ($mol.m^{-2}.s^{-1}$) is the EOD flow of water in the membrane.

Models other than that of Springer have been sparingly used for the flow of water through the membrane. They are mentioned in Dickinson et al. work [20].

2.4. Diffusion coefficient: $D(\lambda)$

110

Notably, the amount of water dissolved in the membrane impacts its diffusion coefficient. Under sufficient hydration, the molecules of a polymer backbone form water-filled micro-channels with SO_3^- groups attached to their walls. Depending on the water content, the membrane structure has different number of conducting channels, mean radius, and forms [14], as shown in Figure 3. This directly affects water diffusion, which benefits from high hydration, through bigger channels, less tortuosity, and less friction. Thus, this dependency must be considered in the diffusion coefficient, which cannot be constant. It must be a function of λ .

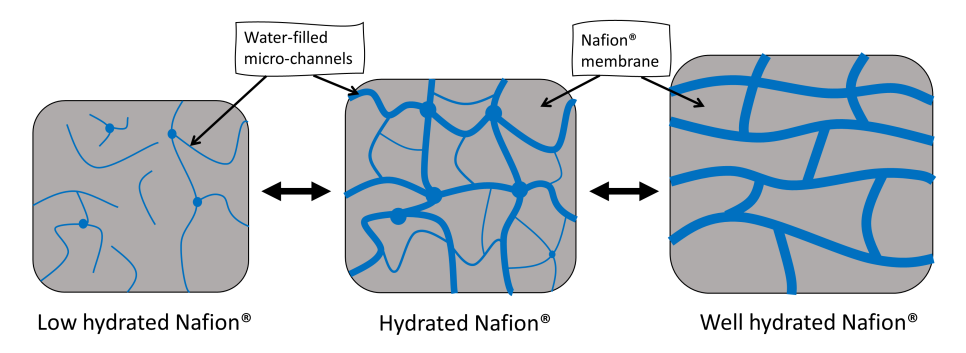


Figure 3: Illustration of PFSA membrane morphology at different levels of hydration.

The diffusivity of dissolved water in the electrolyte was usually determined based on the curve fit of experimental data. There are two expressions that are commonly used, and both are based on Zawodzinski's data provided in 1991 [21]. The first one expressed as (5) was presented by Springer et al. in 1991 [7, 13]. The second one as expressed as (6) was presented by Motupally et al. in 2000 [7, 15, 18, 22–24].

$$D(\lambda) = \begin{cases} 2.692661843 \times 10^{-10}, & \lambda \le 2\\ 10^{-10} e^{2416 \left[\frac{1}{303} - \frac{1}{T_{fc}}\right]} [0.87 [3 - \lambda] + 2.95 [\lambda - 2]], & 2 < \lambda \le 3\\ 10^{-10} e^{2416 \left[\frac{1}{303} - \frac{1}{T_{fc}}\right]} [2.95 [4 - \lambda] + 1.642454 [\lambda - 3]], & 3 < \lambda \le 4\\ 10^{-10} e^{2416 \left[\frac{1}{303} - \frac{1}{T_{fc}}\right]} [2.563 - 0.33\lambda + 0.0264\lambda^2 - 0.000671\lambda^3], & 4 < \lambda < 17 \end{cases}$$
(5)

$$D(\lambda) = \begin{cases} 3.1 \times 10^{-7} \lambda \left[e^{0.28\lambda} - 1 \right] e^{-\frac{2436}{T_{fc}}}, & \lambda < 3\\ 4.17 \times 10^{-8} \lambda \left[161e^{-\lambda} + 1 \right] e^{-\frac{2436}{T_{fc}}}, & 3 \le \lambda < 17 \end{cases}$$
(6)

where T_{fc} (K) is the fuel cell temperature. In practice, it is considered as equal to the cooling fluid temperature measured at the outlet of the stack.

Notably, an inversion of the coefficient 2436 in the exponential has been applied in certain recent papers [7, 15, 24]. Moreover, both of these expressions do not consider water content values greater than 17. The suitability of these relationships for higher λ is not guaranteed.

Upon examining figure 4, it is evident that the difference between the two correlations is not negligible, and there is no conclusion indicating the more accurate one. In fact, the two correlations have both been widely used for PEMFC modelling [7, 13, 22].

However, the sharp change in the diffusion coefficient raises the difficulty for performing numerical simulations. This peak is induced by the procedure of correction, which involves differentiation of experimental data and may not be consistent with reality. The kinetics of channel formation in Nafion®membranes upon water uptake and even geometry of channels are not well understood. Moreover, the situation is complicated by the fact that the structure of the membrane depends on the method of material pre-treatment. Exposing the membrane under different hydration and thermal conditions leads to the formation of different pore structures and thus to different macroscopic properties

of the membrane. However, as discussed previously, it is reasonable to consider that low water content leads to lower mean pore radius in the membrane, which presumably hinders water diffusion [14]. Therefore, there should not be any peak and diffusivity must be a growing function of λ .

Measurements conducted later in 1998 by Van Bussel et al. [25] have validated these physical considerations. These measurements yielded almost constant diffusivity coefficients in the range $\lambda \in [10, 22]$ and reduced to zero for $\lambda < 5$. Kulikovsky et al. fitted these values in 2003 and proposed the function expressed as (7) [14, 23, 24]. This equation, which has been emphasised, appears to be more representative of the physical phenomena at stake. However, its drawbacks are that the measurements were performed using outdated membranes, as is the case with the two previous equations [19]. Moreover, the temperature dependency was here lost. This expression was fitted with data at 80°C.

$$D(\lambda) = 4.1 \times 10^{-10} \left[\frac{\lambda}{25.0} \right]^{0.15} \left[1.0 + \tanh\left(\frac{\lambda - 2.5}{1.4}\right) \right]$$
 (7)

Figure 4 presents a comparison of the three proposed equations for the diffusion coefficient at 80°C. We suggest using Kulikovsky model [14], although it should be further improved by incorporating temperature considerations and using modern membranes in the measurements.

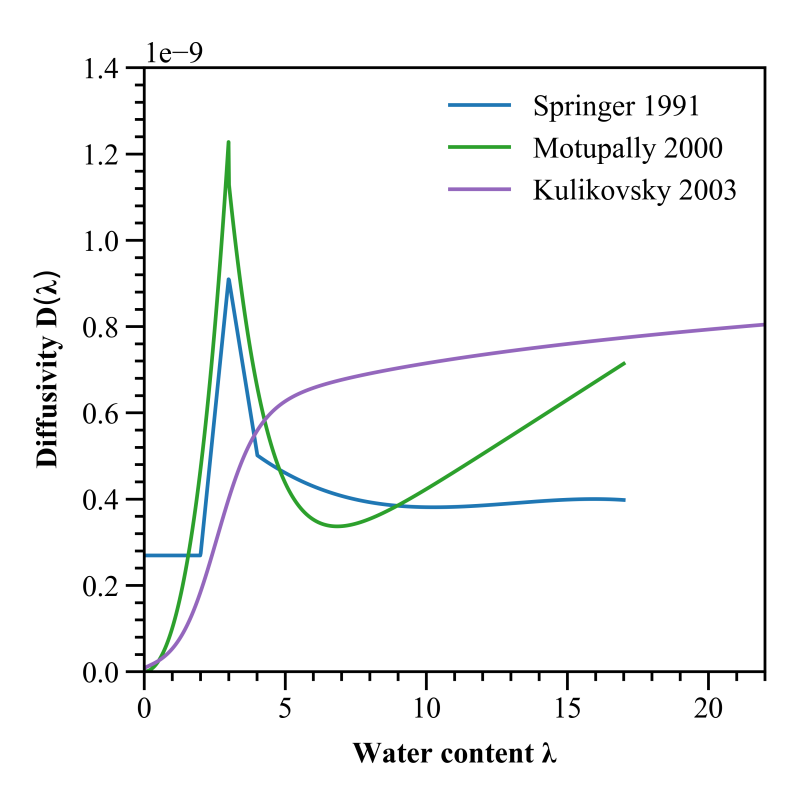


Figure 4: Comparison of the three expressions of the diffusivity coefficient of the membrane at 80°C

2.5. Equilibrium water content of the membrane: λ_{eq} - an overview

To calculate the sorption flow between the membrane and the catalyst layer, as presented in 2.8, first, the equilibrium water content of the membrane λ_{eq} (discussed here), and the water activity a_w , as in 2.6, must be understood. However, this sorption flow is complex and the literature appears incomplete. An overview is presented in Sections 2.5 and 2.6 based on an evaluation of the evolution of the models. Further, in-depth explanations with new proposals are presented in Section 2.7.

One effective method of quantifying the exchange flow between the membrane and the catalyst layer involves comparing the current water content in the catalyst layer, λ , with its equilibrium value, λ_{eq} , as presented in Section

2.8. The equilibrium water content of the membrane λ_{eq} is a variable that is experimentally accessible, and is a function of the water activity a_w . Subsequently, $\lambda_{v,eq}$ must be differentiated from $\lambda_{l,eq}$. Here, $\lambda_{v,eq}$ refers to an equilibrium of the dissolved water with vapour at the surface of the membrane, with a certain activity a_w , whereas $\lambda_{l,eq}$ refers to an equilibrium with pure liquid water. The difference between $\lambda_{l,eq}$ and $\lambda_{v,eq}$ with saturated vapour is noticeable and is referred to as the Schroeder's paradox, as discussed in Section 2.2.

Two well-known experiments, that are widely accepted in the scientific community, have been conducted to present an equation for λ_{eq} . The first experiment was proposed by Springer et al. in 1991 [13], using the data provided by Zawodzinski et al. in 1991 [21]. It was performed exclusively on a Nafion®117 membrane at 30°C for $\lambda_{v,eq}$ and at 80°C for $\lambda_{l,eq}$. It is expressed as (8) [7, 9, 13, 17, 18, 21, 23, 24, 26]. The second experiment was proposed by Hinatsu et al. in 1994 [27] and is expressed as (9)[20, 22, 27, 28]. They provided an equation for $\lambda_{v,eq}$ that could fit on experiments conducted on several types of membranes: Nafion®115, Nafion®117, AC-12, and FL-12. It was conducted at 80°C, which is the usual temperature for PEMFC working conditions. For $\lambda_{l,eq}$, the results depended on the type of membrane and it is the expression for Nafion®117 which is there considered. Moreover, a temperature dependency was incorporated in the expression. As the experimental conditions proposed by Hinatsu et al. are more realistic than those of Springer et al., their results are more preferable. Zawodzinski et al. also conducted experiments at 80°C in 1993 [29], which were expressed as an equation by Ye in 2007 [30]. However, the study by 'Hinatsu et al., became widespread. As discussed previously, all of these measurements are outdated for modern models as membrane structures and experimental protocols have improved during the last decade [19]. However, they are still widely used. A graphic comparison of these expressions for $\lambda_{v,eq}$ is shown in Figure 5.

$$\lambda_{eq}^{S \, pringer} = \begin{cases} \lambda_{v,eq} \, (a_w) = 0.043 + 17.81 a_w - 39.85 a_w^2 + 36.0 a_w^3, & a_w \in [0, 1] \\ \lambda_{l,eq} = 16.8 \end{cases}$$
 (8)

$$\lambda_{eq}^{Hinatsu} = \begin{cases} \lambda_{v,eq} (a_w) = 0.300 + 10.8a_w - 16.0a_w^2 + 14.1a_w^3, & a_w \in [0,1] \\ \lambda_{l,eq} = 10.0 + 1.84 \cdot 10^{-2} T_{fc} + 9.90 \cdot 10^{-4} T_{fc}^2, & T_{fc} \text{ in } ^{\circ}\text{C here} \end{cases}$$
(9)

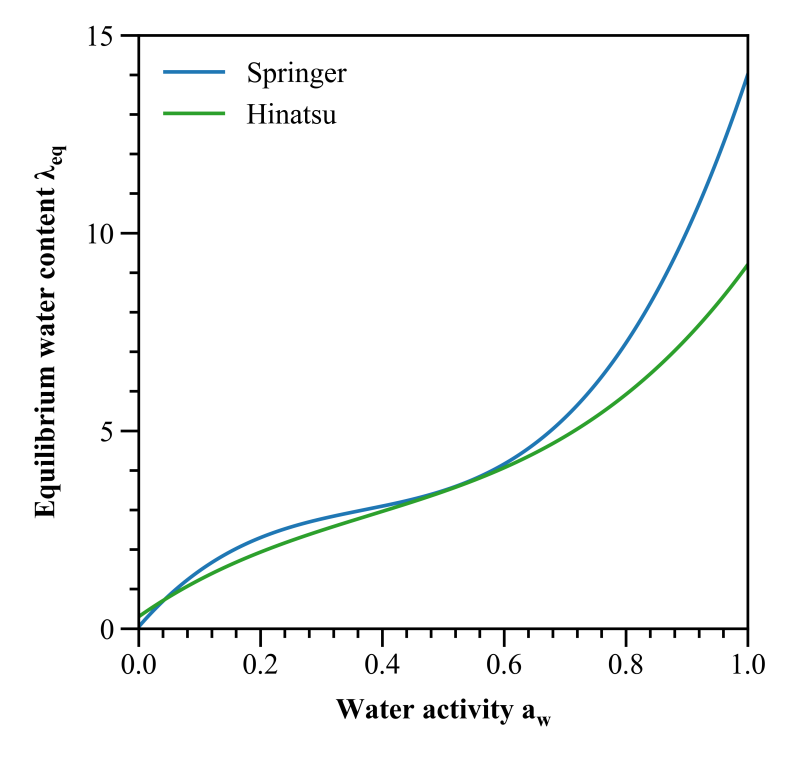


Figure 5: Comparison between Springer's and Hinatsu's expressions for $\lambda_{v,eq}$.

Both these expressions were fitted on experimental data. Till date, the methodology is fully acceptable and only the use of more advanced experimental protocols and membranes yield different results. However, the link between $\lambda_{v,eq}$ and $\lambda_{l,eq}$ is subject to discussions and requires further extensive theoretical research. Next, the ideas proposed in the literature are addressed and a new approach is presented in Section 2.7.

To determine this link, Springer et al. first considered that their expression for $\lambda_{v,eq}$ is suitable at 80°C, although the measurements were performed at 30°C [13]. This is not necessary in case of the study by Hinatsu et al. Then, Springer et al. linked the water activity a_w to both the vapour and liquid water, although this is uncommon. For $a_w \in [0, 1]$, only vapour existed, and for $a_w > 1$, liquid water coexisted with saturated vapour. Then, they considered a a_w value considerably greater than 1 and concluded that $a_w = 3$ is a good value for having only pure liquid water, which occupies all the cavity volume of the triple points zone. The arbitrary choice of $a_w = 3$ and the new expression of a_w connected to both vapour and liquid water were not explained in their study, which are obstacles for the comprehension of their model. However, these obstacles did not curb its ubiquity in the literature and an adapted expression for a_w has been consequently presented. This is discussed Section 2.6. Finally, a linear expression was arbitrarily used for connecting $\lambda_{v,eq}$ at $a_w = 1$ to $\lambda_{l,eq}$ at $a_w = 3$, as expressed in (10) [7, 9, 13, 17, 18, 21, 23, 24, 26]. Considering this model, having $a_w \ge 3$ is either unlikely or impossible; thus, the value of 16.8 is either maintained for higher a_w or higher values should not exist [26]. However, it is difficult to provide precise rules as this construction is incomplete and subjective. Still, this model has been perpetuated in all the subsequent studies. The expression by Hinatsu et al., has been adjusted in the same manner at 80°C, which yields (11).

Moreover, the fact that the expression of $\lambda_{l,eq}$ by Hinatsu et al., in (9), incorporates a temperature dependency is very useful. It allows the adjustment of the equations to the real working temperature at $a_w \ge 1$. At $a_w \le 1$, an interpolation between the equations of 'Springer et al., and Hinatsu et al.,' could eventually be undertaken to obtain λ_{eq} at a more precise temperature.

$$\lambda_{eq}^{Springer}(a_w) = \begin{cases} 0.043 + 17.81a_w - 39.85a_w^2 + 36.0a_w^3, & a_w \in [0, 1] \\ 14 + 1.4[a_w - 1], & a_w \in [1, 3] \end{cases}$$
(10)

$$\lambda_{eq}^{Hinatsu}(a_w) = \begin{cases} 0.300 + 10.8a_w - 16.0a_w^2 + 14.1a_w^3, & a_w \in [0, 1] \\ 9.2 + 4.3[a_w - 1], & a_w \in [1, 3] \end{cases}$$

$$(11)$$

As evident, these equations are built in two parts, which result in stiffness at $a_w = 1$. Consequently, oscillations occur during the implementation of the models. To improve the numerical results, the liner expression 'for $a_w \in]1, 3]$ by Springer et al., has been changed by Bao et al. who presented a unique and general equation for all a_w values [31]. As the connection between $\lambda_{eq}(a_w = 1)$ and $\lambda_{eq}(a_w = 3)$ was arbitrarily made linear, at first sight, no impediments were observed to this change. This is discussed in Section 2.7. However, Bao et al., interpreted Springer's work differently. They considered that there is a discontinuity at $a_w = 3$, where λ_{eq} increases from 16.8 to 22 [31]. In our analysis, the value of 22 is provided for experiments conducted at 100°C whereas 16.8 is evaluated at 80°C. Only one of them must be chosen depending on the working temperature, which is 80°C in our case. Thus, we slightly modified the expression proposed in [31] to obtain a more adapted equation, which is expressed as (12) [15, 31].

$$\lambda_{eq} = \frac{1}{2} \left[0.043 + 17.81 a_w - 39.85 a_w^2 + 36.0 a_w^3 \right] \cdot \left[1 - \tanh \left(100 \left[a_w - 1 \right] \right) \right]$$

$$+ \frac{1}{2} \left[14 + 2.8 \left[1 - \exp \left(-K_{\text{shape}} \left[a_w - 1 \right] \right) \right] \right] \cdot \left[1 + \tanh \left(100 \left[a_w - 1 \right] \right) \right]$$
(12)

Different values of the mathematical factor K_{shape} allow the experimenter to model a smooth transition ($K_{shape} = 2$) or a sharp jump ($K_{shape} = 20$) between the "two ends of Schroeder's paradox" [31], as shown in Figure 6. It is important to remember that this is purely a mathematical model formulated for modelling purposes and that the physics considerations are lost at this point. In this study, the use of a small K_{shape} , such as $K_{shape} = 2$, is suggested to ensure that we do not stray excessively far from the physics involved, as discussed in Section 2.7. At this point, it is apparent that a better theory on equilibrium water content must be formulated to connect the physical considerations of $\lambda_{v,eq}$ to $\lambda_{l,eq}$.

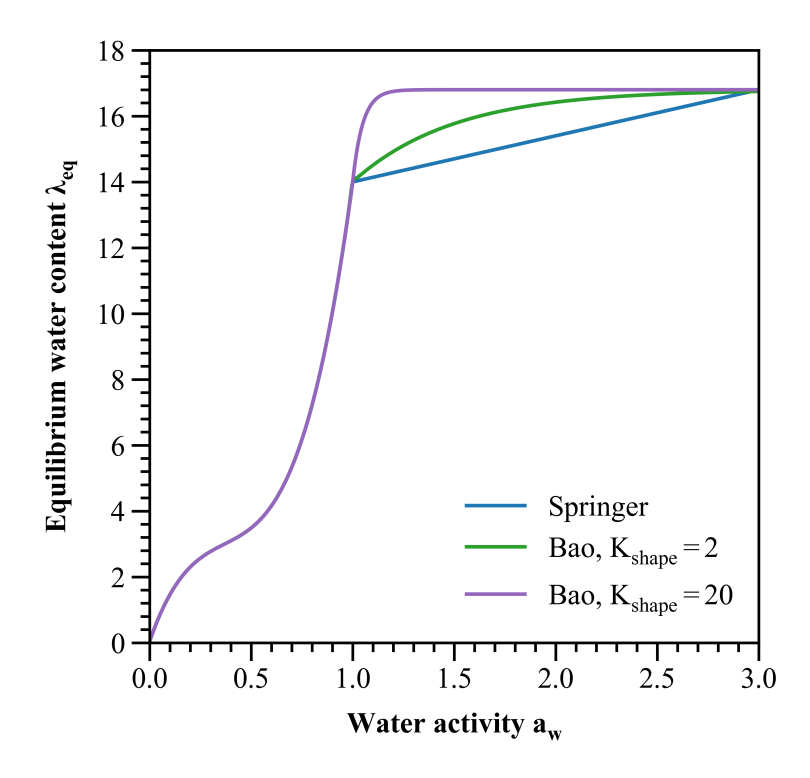


Figure 6: Comparison between Springer's piece wise expression and Bao's function for water content equilibrium with different values of K_{shape}

Finally, the expression for λ_{eq} proposed in this study is expressed as (13) and has been emphasised. It is built using Hinatsu's expressions at 80°C while adhering to the form proposed by Bao et al'. This expression is compared with that of Springer et al., in Figure 7.

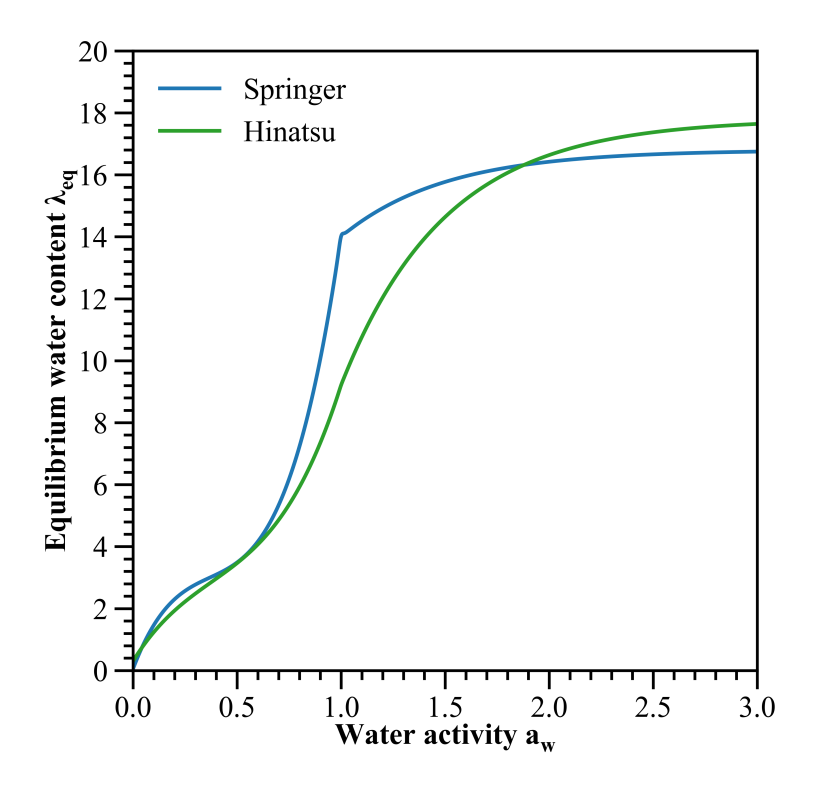


Figure 7: Comparison between Springer's and Hinatsu's expressions for λ_{eq} at 80°C, using Bao's form.

$$\lambda_{eq} = \frac{1}{2} \left[0.300 + 10.8a_w - 16.0a_w^2 + 14.1a_w^3 \right] \cdot \left[1 - \tanh\left(100\left[a_w - 1\right]\right) \right] + \frac{1}{2} \left[9.2 + 8.6 \left[1 - \exp\left(-K_{\text{shape}}\left[a_w - 1\right]\right) \right] \right] \cdot \left[1 + \tanh\left(100\left[a_w - 1\right]\right) \right]$$
(13)

2.6. Water activity: a_w - an overview

The water activity a_w , in this study, quantifies the ability of water to humidify the membrane from the catalyst layer. According to the Schroeder's paradox, the more condensed the membrane the better the results. Two different definitions, (14) and (15), are widely accepted in the literature; however, the use of one against the other has, to the best of our knowledge, never been explained. We considered this as an important lack of information that often creates confusion. Thus, this Section attempts to explain both these definitions. Furthermore, a new approach is proposed in Section 2.7.

The original definition, which is expressed as (14), has been proposed by Springer et al., [13] and pursued by Ge et al. [28]. If only vapour is considered, a_w is equal to the water humidity as is commonly considered in all areas of physics. However, a_w is allowed to be greater than 1 and to increase until 3, which corresponds to a mixture of vapour and liquid water. The value of $a_w = 3$ refers to only pure liquid water.

$$a_{w} \stackrel{\triangle}{=} \begin{cases} \frac{P}{P_{sat}} = \frac{C}{C_{sat}}, & \text{for pure vapor} \\ \text{ideal gas law} \end{cases}$$

$$3, & \text{for pure liquid water}$$
(14)

where P(Pa) is the vapour pressure, $P_{sat}(Pa)$ is the vapour saturated pressure, $C(mol.m^{-3})$ is the vapour concentration, and $C_{sat}(mol.m^{-3})$ is the vapour saturated concentration.

The drawback of this model is that no explanation has been provided regarding the characterisation of a_w when its values are higher than 1. It is implicitly mentioned that the expression of $\frac{P}{P_{sat}}$ is sufficient, which is questionable. When vapour is fully saturated at $a_w = 1$, condensation starts and vapour pressure diminishes to create liquid water. However, condensation is not instantaneous and more vapour can be introduced in the control volume through desorption or diffusion, which counterbalance the condensation and leads to a pressure increase; eventually $a_w > 1$. However, the greater the $P > P_{sat}$, the greater the amount of condensation (as discussed in Section 3.8). Thus, a_w is not likely to increase significantly. Springer et al., considered an arbitrarily a limit of 3 for a_w , which, for them, corresponded to the water activity of pure liquid water. However, this value could not be attained considering only vapour in water activity a_w . Thus, although it is acceptable to have $\frac{P}{P_{sat}} > 1$, it is unlikely to increase until 3. Two extrapolations are then possible to present acceptable results with a mixture of vapour and liquid water. One such method has been extensively employed in the literature and explained below. The second method is a new approach proposed in this study and discussed in Section 2.7.

Within the scientific community, liquid water is often considered in the expression of a_w in addition to vapour [7, 17, 18, 24]. Regarding Springer's work, a_w is reconstructed following certain rules. First, $a_w \in [0, 3]$. Then, $a_w \in [0, 1]$ corresponds to a vapour phase in the catalyst layer whereas $a_w \in [1, 3]$ fits a mix of vapour and liquid water. Finally, a_w grows with the condensation of water. One method of fulfilling all these requirements is expressed as (15). However, it is not the only solution as any power can be added to s for fulfilling these criteria. There are no clues that (15) is the more accurate one for modelling the fuel cell.

$$a_w \stackrel{\triangle}{=} \frac{P}{P_{sat}} + 2s \underbrace{=}_{\text{ideal gas law}} \frac{C}{C_{sat}} + 2s$$
 (15)

where s is the liquid water saturation (explained in 3.1)

This idea offers the advantage of being suitable for use in one-directional (1D) models as vapour and liquid water are considered as one unique and homogeneous fluid. It is a global perspective. However, it must be noted that this is a model that incorporates only a few physical aspects. Using a coefficient of 2 in $\frac{P}{P_{sat}}$ + 2s counterbalances the fact that a_w is extended from 1 to 3 as the results would be the same when using $\frac{P}{P_{sat}}$ + s with a_w only extended from 1 to 2. This is further explained in Section 2.7.

Finally, there is another equation in the literature [15, 26], which is less employed. This expression, expressed as (16), is an extrapolation of the activity definition for vapour of (14). Here, liquid water is considered as a gas and its concentration in the pore volume is considered. However, we strongly discourage the use of this equation as it is not compatible with Springer's model. Indeed, the equation which governs λ_{eq} is only suitable for an activity between 0–3 and the value of 3 is established for only liquid at the interface with the membrane and the catalyst layer. However, with this last equation, for $s \in [0, 1]$ we obtain $a_w \in [0, 5072]$! It is thus clear that this equation yields false results.

$$a_{w} \stackrel{\triangle}{=} \frac{P_{\text{vapor+liquid}}}{P_{\text{sat}}} \underbrace{=}_{\text{ideal gas law}} \frac{C[1-s] + \frac{\rho_{H_{2}o}}{M_{H_{2}o}}s}{C_{\text{sat}}}$$
(16)

2.7. New method of interpreting λ_{eq} and a_w

Previously, Sections 2.5 and 2.6 presented an overview of the current use of λ_{eq} and a_w in the literature. Further, there limitations were highlighted. Thus, to improve the theoretical expression of the sorption flow between the catalyst layer and the membrane in the fuel cell, a new approach is proposed here.

As evident, different experiences yield different expressions for λ_{eq} . When vapour is in contact with the membrane, it is $\lambda_{v,eq}$. Whereas, when liquid water is in contact with the membrane, it is $\lambda_{l,eq}$. Previous studies attempted to link them as one entity, as if vapour and liquid water were the same. Thus, the notions of $\lambda_{v,eq}$ and $\lambda_{l,eq}$ disappeared under λ_{eq} . Another idea involved considering them as two distinct entities to render $\lambda_{v,eq}$ and $\lambda_{l,eq}$ separate. A net separation between the two phases in the CL was considered. With this, vapour and liquid water have different behaviours in the CL and must be modelled differently with spatial distinction. Then, in a same area, dissolved water interacting with vapour yields a λ_{eq} value different from that in case of dissolved water interacting with liquid water. The former used the polynomial equation of $\lambda_{v,eq}$ and the latter reached the value of $\lambda_{l,eq}$. This consideration offers the huge

advantage of suppressing the idea of an activity of 3 for a_w and the linear link between $\lambda_{v,eq}$ and $\lambda_{v,eq}$. The water activity maintains its common form $\frac{P}{P_{sat}}$ and only corresponds to vapour.

However, this idea requires either of following two conditions. First, a very precise three-dimensional (3D) model is required, and subsequently, several sorption flows in the catalyst layer must be considered, one for each vapour or liquid water zone. Second, the proportion of liquid water at the membrane surface compared to the vapour one must be known, and subsequently, a global λ_{eq} built on these proportions must be considered. We believe that the latter idea is more relevant as it does not require the use of a precise 3D model and thus leads to a good compromise between physics and computing time. However, it needs a function φ_{sp} (SP for surface proportion). This function accepts the liquid water saturation s, which is the known volume proportion of liquid water in the pore volume, as presented in 3.1, and outputs the corresponding surface proportion that a volume of liquid water requires for the total CL surface. However, φ_{sp} appears complex and not that prevalent in the literature. The resulting λ_{eq} is highlighted in 17.

$$\lambda_{eq}\left(a_{w}, \mathbf{s}, T_{fc}\right) = \lambda_{v,eq}\left(a_{w}\right)\left[1 - \varphi_{sp}\left(\mathbf{s}\right)\right] + \lambda_{l,eq}\left(T_{fc}\right)\varphi_{sp}\left(\mathbf{s}\right)$$
(17)

It is noticeable that the linear link between $\lambda_{v,eq}$ and $\lambda_{l,eq}$ proposed by Springer in (10) is reachable using (17). Indeed, using the hypothesis of fully saturated vapour ($a_w \in]1,3]$ for Springer), Springer's values for $\lambda_{v,eq}$ and $\lambda_{l,eq}$ and a very simple φ_{sp} function for which the surface proportion is equal to the volume proportion: $\varphi_{sp}(s) = s$, it is possible to obtain the following development.

$$\lambda_{eq} \left(a_w, \mathbf{s}, T_{fc} \right) = 14 [1 - \mathbf{s}] + 16.8 \mathbf{s}$$

$$= 14 + 1.4 [1 + 2 \mathbf{s} - 1]$$

$$= 14 + 1.4 \left[\frac{P_{sat}}{P_{sat}} + 2 \mathbf{s} - 1 \right]$$

$$\approx 14 + 1.4 [a_w - 1]$$
(18)

Springer's proposition implies that the volume proportion of liquid water in the CL pores is identical to its surface proportion, which is an important simplification. A more accurate relation for φ_{sp} is needed to propose a better model. This also leads to another consideration. The link between $\lambda_{v,eq}$ and $\lambda_{l,eq}$ proposed either by Springer et al., or Bao et al., and shown in Figure 6, incorporates a certain physical meaning. For Springer, the linearity of the link induces that $\varphi_{sp}(s) = s$. Thus, for Bao, it is not possible to accept any value for K_{shape} as all of them induce implicitly one expression for φ_{sp} . Thus, it appears reasonable to use the value of $K_{shape} = 2$ for having an expression close to but bigger than the linear equation; meanwhile, an accurate expression of φ_{sp} is obtained.

Furthermore, it is then tangible based on the previous development that the number 3, in Springer's extension of a_w from 1 to 3, does not have any absolute importance, provided the number 2 is used in $a_w = \frac{P}{P_{sat}} + 2s$. They counterbalance each other, and any value can be considered for the maximum of a_w , provided it is counterbalanced in the expression of a_w .

Springer's proposition also requires that vapour is always fully saturated when liquid water is in the stack. However, although it is frequently true, it is not always the case. One scenario could be indeed that liquid water appears next to vapour over-saturation. Then, for certain reasons, vapour is quickly removed out of the stack in sufficient proportion such that vapour becomes under-saturated while liquid water does not have the time to fully evaporate. Then, the mentioned hypothesis supporting (10) is invalid in this case. The proposed relation in (17) does not suffer from all these drawbacks.

Finally, the procurement of φ_{sp} has another useful consequence in this model in terms of the calculation of the overpotential η_c as presented in Section 9.3. It facilitates the determination of the value of s_{lim} , which is the limit value of s for which the entire surface in the triple point region is occupied by liquid water.

2.8. Water sorption at the ionomer/CL interface: J_{sorp}

In the catalyst layer, at the triple points, there is a water conversion between the pore regions, where vapour and liquid water exist, and the membrane where water is in a dissolved form. This water conversion, referred to as S_{sorp} in study (Figure 1), corresponds to a water absorption or a desorption and occurs in the entire volume of the catalyst layer. It is different from a flow, which is matter transport from one volume to another through a surface. This conversion

happens in one volume and is then volumetric. Because of the discontinuity of matter at the interface, Fick's law does not characterise this flow. More complex phenomena are indeed at stake, which complicate the existing laws. Thus, these laws have been improved during the past decades [7, 16, 28]. In this part, the authors have attempted to provide a clear and accurate expression of the sorption term S_{sorp} , based on the most recent and original studies [17, 18, 28, 32].

First and foremost, the following general expression (19) is commonly accepted in the community [7, 17, 18, 24, 32, 33]. It corresponds to the sorption of vapour and liquid water to dissolved water in the membrane.

$$S_{sorp} = \gamma_{sorp} \frac{\rho_{\text{mem}}}{M_{\text{eq}}} \left[\lambda_{\text{eq}} - \lambda \right]$$
 (19)

where γ_{sorp} (s^{-1}) is the sorption rate.

This expression is meaningful. Indeed, λ_{eq} represents the value of λ at equilibrium. It is a virtual variable. Thus, as long as λ is different from λ_{eq} , a water flow exists between the membrane and the catalyst layer seeking equilibrium.

The coefficient $\frac{\rho_{\text{mem}}}{M_{\text{eq}}}$ facilitates a conversion of the water content to the water concentration in the membrane to finally express a water flow. However, to eliminate the need to track the membrane swelling in the model, Springer et al. converted his widely used results for a dry membrane model [13]. This idea was pursued in most of the subsequent studies, and this is why the constants ρ_{mem} and M_{eq} are used in these equations.

Finally, the sorption rate coefficient expresses the velocity of this sorption. For a given gap between $\lambda_{\rm eq}$ and λ , the value of γ changes S_{sorp} and renders the flow as more or less important. This important coefficient has been evaluated in different ways and sometimes misemployed. It was challenging to determine sorption/desorption rates γ in an actual PEMFC, and somewhat arbitrary values, ranging as $0.1-100~s^{-1}$, were generally used in the literature [32]. The value of $\gamma = 1.3 s^{-1}$ is the most encountered [7, 24].

However, it was determined through experiments that the sorption rate of water is not constant. It depends on the volume fraction of water in the membrane and the absorption and desorption rate of water are also different. Ge et al. [28] presented a more accurate expression for S_{sorp} in 2005. It was then slightly modified by adding H_{cl} term to it [34], and is expressed as (20) [17, 18, 28, 32].

$$S_{sorp} = \gamma_{sorp} \frac{\rho_{\text{mem}}}{M_{\text{eq}}} \left[\lambda_{\text{eq}} - \lambda \right]$$
 (20a)

$$\gamma_{sorp} = \begin{cases} \gamma_a = \frac{1.14 \cdot 10^{-5} f_v}{H_{cl}} e^{2416 \left[\frac{1}{303} - \frac{1}{T_{fc}}\right]}, & \text{for an absorption flow} \\ \gamma_d = \frac{4.59 \cdot 10^{-5} f_v}{H_{cl}} e^{2416 \left[\frac{1}{303} - \frac{1}{T_{fc}}\right]}, & \text{for a desorption flow} \end{cases}$$
(20b)

$$f_{v} = \frac{\lambda V_{w}}{V_{\text{mem}} + \lambda V_{w}} \tag{20c}$$

where f_v is the water volume fraction of the membrane, V_w $(m^3.mol^{-1})$ is the molar volume of water, and V_{mem} $(m^3.mol^{-1})$ is the molar volume of dry membrane.

The coefficient ε_{mc} , as discussed in Section 2.1, should have been added in this equation to consider the volume fraction of the ionomer in the catalyst layer. Indeed, the sorption flow appends in the catalyst layer where the ionomer is only a fraction of the overall volume. This fraction is not universal and depends on the stack conception. This variable should then be considered for more precise modelling. Adding tortuosity considerations with ε_{mc}^{τ} would have been even better (as seen below in Section 4.2). However, in both sets of values for the sorption rate, the separation of ε_{mc} from these constants has not been made. It is probably implicitly contained in these coefficients and as their experimental values were not mentioned in the original papers, it is not possible to extract it. Thus, ε_{mc} cannot be used with these experimental results, although it would have been suitable for more precise modelling.

One important question remains. In a biphasic state for water in the catalyst layer, is S_{sorp} a vapour, a liquid matter conversion or both? Ge et al. provided an answer to this. If liquid water is fed, it would be in direct contact with the membrane. The water content of the membrane at the membrane/GDL interface is assumed to be instantly in equilibrium with liquid water [28]. Thus, S_{sorp} is originally a vapour matter conversion.

Finally, Hu et al. [16] proposed to separate S_{sorp} into two matter conversion when water is in two-phase, one for vapour $S_{sorp,v}$ and the other for liquid water $S_{sorp,l}$. The use of liquid water saturation variable s was proposed to weight this cutting. This idea is presented in (21). However, we discourage the implementation of this idea. This

is because after implementing this in our own models, we obtained undesirable results. Immediately after crossing the saturated value and the apparition of liquid water, vapour concentration decreased until it became undersaturared, whereas liquid water still existed. Both of them reached an equilibrium. Indeed, with this law, once liquid water appears, it has the ability to interact with condensed water in the membrane and not only with vapour. Thus, the above equilibrium is made possible as liquid water evaporation in the cathode and its transport to the GC is balanced by liquid water sorption from the membrane. We believe that this type of equilibrium must not happen and thus S_{sorp} must only be a vapour conversion matter.

$$\begin{cases}
S_{sorp,v} = k_{sorp} \frac{\rho_{mem}}{M_{eq}} [1 - s] \left[\lambda_{eq} - \lambda \right] \\
S_{sorp,l} = k_{sorp} \frac{\rho_{mem}}{M_{eq}} s \left[\lambda_{eq} - \lambda \right]
\end{cases}$$
(21)

2.9. Water production at the interface of the triple points: S_{prod}

Water is mainly produced by the classic and expected fuel cell reaction at the triple point interface in the cathode catalyst layer. This water production is mainly related to i_{fc} , which corresponds to the current generated in the external circuit. However, it is also related to i_{sc} , which corresponds to the short circuit current density (discussed in Section 9.4), when the reaction occurs normally but the electrons have passed through the membrane instead of the external circuit. This equation is expressed as 22.

It is unclear whether it is initially produced in vapour, liquid, or dissolved form in the membrane. Similar to Jiao et al. [7], we propose the implementation of this matter conversion term of the membrane in the triple points zone to consider a water production in dissolved form. However, it is very easy to change this assumption by placing the following matter conversion term in another differential equation.

$$S_{\text{prod}} = \begin{cases} \frac{i_{fc} + i_{sc}}{2FH_{cl}}, & \text{in the CCL} \\ 0, & \text{elsewhere} \end{cases}$$
 (22)

where S_{prod} ($mol.m^{-3}.s^{-1}$) is the water production in the membrane at the triple points zone, H_{cl} (m) is the catalyst layer thickness.

Additional water is also produced in the stack as a result of the crossover of hydrogen and oxygen, as discussed in Section 7.2. This is referred to as S_{co} . However, this time water can be produced in both anode and cathode catalyst layer. This water production must be directly linked to the crossover flows, again assuming that these flows pass instantaneously through the membrane, as if it were of zero thickness. Moreover, it is assumed that all the matter that has passed through reacts instantaneously to yield water [35]. The associated equation is expressed as (23).

$$S_{co} = \begin{cases} 2 \cdot S_{O_2,co}, & \text{in the ACL} \\ S_{H_2,co}, & \text{in the CCL} \\ 0, & \text{elsewhere} \end{cases}$$
 (23)

where $S_{i,co}$ ($mol.m^{-2}.s^{-1}$) is the crossover flow of molecule i (hydrogen or oxygen) discussed in 7.2. Finally, the corrected expression of S_{prod} is expressed as (24).

$$S_{\text{prod}} = \begin{cases} 2k_{O_2} \frac{RT_{fc}}{H_{cl}} \nabla_m C_{O_2}, & \text{in the ACL} \\ \frac{i_{fc} + i_{sc}}{2FH_{cl}} + k_{H_2} \frac{RT_{fc}}{H_{cl}} \nabla_m C_{H_2}, & \text{in the CCL} \\ 0, & \text{elsewhere} \end{cases}$$
(24)

2.10. Water content dynamic behavior

In the membrane, water content is governed by the following molar balances (equation 25a) [15] and boundary condition (equation 25b). Two differential equations are employed. Indeed, contrary to the bulk membrane, in the catalyst layer the membrane corresponds to only a fraction of the overall volume. This influences the governing

equation with the addition of the ionomer volume fraction ε_{mc} (Section 2.1). Finally, it is noticeable that, ε_{mc} is not linked with the tortuosity. This link must only be considered for the expression of the transport flows.

$$\begin{cases} \frac{\rho_{\text{mem}}}{M_{\text{eq}}} \frac{\partial \lambda_{\text{mem}}}{\partial t} = -\nabla \cdot \boldsymbol{J}_{\text{mem}}, & \text{in the bulk membrane} \\ \frac{\rho_{\text{mem}} \varepsilon_{\text{mc}}}{M_{\text{eq}}} \frac{\partial \lambda_{\text{cl}}}{\partial t} = -\nabla \cdot \boldsymbol{J}_{\text{mem}} + S_{\text{sorp}} + S_{\text{prod}}, & \text{in the CL} \end{cases}$$
(25a)

$$J_{mem}^{cl,mem} = \mathbf{0}$$
, at the ionomer border (25b)

3. Liquid water transport in the CL and GDL

3.1. Liquid water saturation: s

400

During the working of PEMFC, the amount of water generated by the chemical reaction along with the vapour present in the inlet moist gas can be sufficient to reach vapour saturation and subsequently form liquid water in the stack. This quantity must be controlled as it reduces the ability of the reactive gases to interact and thus reduces the voltage. Owing to being a compressed phase, liquid water is densely located on the matter surface of the catalyst layer and impedes the interaction of gases with it.

To have a comprehensive quantity, liquid water is measured using the liquid water saturation variable s.

$$s \stackrel{\triangle}{=} \frac{V_{\text{liquid water}}}{V_{\text{pore}}} \tag{26}$$

The values of s are between 0 and 1, 0 for the absence of liquid water and 1 for only liquid water in the pore"s stack. Three phenomena govern liquid water evolution: capillarity, convection, and condensation/evaporation. Each of them are discussed in the subsequent subsections.

3.2. Liquid water flows inside the electrodes and at their border

Inside the CL and the GDL, liquid water is mainly transported by a diffusive force: capillarity. It is named in this work $J_{l,cap}$ and studied section 3.3. In addition, a second flow exists: $J_{l,conv}$. It is a consequence of gases motions, which haul liquid water and thus referred to as a convective flow. However, as studied in Section 3.6, it is a minor flow compared to the capillary action case and is often neglected. Darcy's law is used to characterise both of them. Finally, the sorption flow at the GDL/GC border is reasonably considered equal to the convective-diffusive flow at the GC interface side: $J_{l,cc}$. It is discussed in Section 3.7.

3.3. Liquid water capillary flow in the CL and GDL: $J_{l,cap}$

The capillary flow $J_{l,cap}$, expressed as (27), indicates the ability of liquid water created inside the electrode matter with vapour condensation to naturally diffuse through it [7, 17, 23, 26, 30]. Capillarity is a specific case of diffusivity for liquid phase. This equation is similar to Fick's law, with a matter gradient ∇s , and a variable diffusive coefficient D_{cap} . Darcy's law enables this construction, as discussed in Section Appendix D.1.

It is noteworthy that (27) is derived from experiments involving water permeation through beds of sand, which represents a significant simplification when compared to water permeation through the GDL. However, it appears to be the best model currently available in the literature [7]. Thus, new and relevant models are crucial. In this case, the porous environment is considered homogeneous, its deformation negligible, and water flow must be sufficiently slow to have a small Reynold's number under stationary conditions [36]. The effect of gravity is also usually neglected in the stack. However, this flow (27) is historically expressed as $kg.m^{-2}.s^{-1}$, whereas, all the other flows in the literature are expressed as $mol.m^{-2}.s^{-1}$. This formulation is retained in this review and adjustments are made to the differential equations to incorporate this.

$$\begin{cases} J_{l,cap} = -D_{cap}(\mathbf{s}, \varepsilon) \, \nabla \mathbf{s} \\ D_{cap}(\mathbf{s}, \varepsilon) = \sigma \frac{K_0}{\nu_l} \left| \cos \left(\theta_c \right) \right| \, \sqrt{\frac{\varepsilon}{K_0}} \, \mathbf{s}^{\mathbf{e}} \left[1.417 - 4.24 \mathbf{s} + 3.789 \mathbf{s}^2 \right] \end{cases}$$
(27)

where J_{cap} ($kg.m^{-2}.s^{-1}$) is the capillary flow, σ ($N.m^{-1}$) is the surface tension of liquid water, K_0 (m^2) is the intrinsic permeability, v_l ($m^2.s^{-1}$) is the liquid water kinematic viscosity, θ_c (°) is the contact angle of GDL for liquid water, e

is the capillary exponent, and ∇ is the gradient notation. To provide a better comprehension of this expression, certain additional information are presented in (Appendix D.1).

It is noticeable that we decided to place an absolute value on $\cos(\theta_c)$ although this is not frequently done. This is helpful for always having a positive diffusion coefficient D_{cap} to retain the negative sign commonly present in any mass balance. In the literature, with $\cos(\theta_c)$ being negative, the negative sign sometimes disappears in the global equation. This renders the appropriate comprehension of the equation and the comparison between different sources difficult.

Moreover, the capillary exponent e is an empirical one. This name and this letter are proposed in this study to consider several values of e that exist in the literature. Indeed, the value of 3, named cubic correlation, is widely used. It originates from sand/rock-type porous media with typical porosity of 0.1–0.4. As a PEMFC catalyst layer is quite similar to sand/rock in terms of porosity and morphology, liquid and gas permeabilities in the catalyst layer are calculated using the following cubic correlations. However, in recent studies, e is suggested to be between 4.0–5.0 for GDL porous matters with high porosities between 0.6–0.8. The cubic correlation may overestimate liquid permeability, particularly at low liquid saturation [7, 17, 23, 30, 33]. These considerations are synthesised in (28).

$$\begin{cases} e = 3, & \text{if } \varepsilon \in [0.1, 0.4] \\ e \in [4, 5], & \text{if } \varepsilon \in [0.6, 0.8] \end{cases}$$

$$(28)$$

Finally, for information only, it is worth knowing that $J_{l,cap}$ (as well as $J_{l,conv}$ in Section 3.6) is based on Darcy's law, which is applicable only for creeping flow. This is a reasonable assumption inside the GDL and the CL. However, for modern stacks that exploit the complex flow-field in the GC, such as the use of baffles, and which are operated under high current densities (> $1A.cm^{-2}$), convective flows in the GC can penetrate the GDL. In these critical conditions, Darcy's law is not suitable. Here, Darcy-Forchheimer's law is used to consider the additional inertial effects. Further information can be found in the study by Kim et al. [37].

3.4. Intrinsic permeability: K_0

The intrinsic permeability K_0 is a measure of the ability of a porous matter to allow fluids to pass through it. The permeability of a medium is related to the porosity, but also to the shapes of the pores in the medium and their level of connectedness. It is a physical property of the matter. The Tomadakis and Sotirchos (T&S) model (equation 29) for an effective diffusivity can be used to calculate single phase permeability in random fibrous and porous media [24, 38, 39]. Notably, copying errors persist in the literature related to the use of this equation 29. The one considered in this study corresponds well to the original expression [38].

$$K_{0} = \frac{\varepsilon}{8 \ln(\varepsilon)^{2}} \frac{\left[\varepsilon - \varepsilon_{p}\right]^{\alpha+2} r_{f}^{2}}{\left[1 - \varepsilon_{p}\right]^{\alpha} \left[\left[\alpha + 1\right] \varepsilon - \varepsilon_{p}\right]^{2}}$$
(29)

where r_f (m) is the carbon fibre radius, obtained at $4.6 \cdot 10^{-6}$ m [39] or $3.16 \cdot 10^{-6}$ m [24], ε_p is the percolation threshold porosity, obtained at 0.11 [24, 39], and α is a fitted value, obtained at 0.521 for in plane direction and at 0.785 for through plan direction [24, 39].

Another element that is often neglected in the literature must be considered in the calculation of the intrinsic permeability. This is the compression of the GDL, described by Bao et al. [40]. Indeed, when the cells are assembled together, a pressure is applied to them to ensure that the gases between each compartment are sealed. This compression causes deformations in the structure of the GDL and therefore causes changes in the transport properties within it [41]. It is therefore necessary to modify the previously proposed model. The advantage of the proposal by Bao et al. is that it fits any model for calculating the effective diffusivity before compression with the simple addition of an exponential coefficient to account for it. However, this study has a limitation. It can only be used for structures with a porosity of approximately 73% or 60%. Fortunately, this concerns a large part of the current GDL. Thus, the model of Tomadakis and Sotichos augmented by the work of Bao et al, which can be renamed by the TSB model, yields the following intrinsic permeability given equation 30.

$$K_{0} = \frac{\varepsilon}{8 \ln(\varepsilon)^{2}} \frac{\left[\varepsilon - \varepsilon_{p}\right]^{\alpha+2} r_{f}^{2}}{\left[1 - \varepsilon_{p}\right]^{\alpha} \left[\left[\alpha + 1\right] \varepsilon - \varepsilon_{p}\right]^{2}} e^{\beta_{1} \varepsilon_{c}}$$
(30)

where β_1 is a fitted value which varies with the porosity and the matter diffusion direction according to the following table 1 and ε_c is the compression ratio of the GDL, which is defined as the ratio of the thickness reduction to the thickness of uncompressed GDL. According to Yim et al. [42], a value of 30% for ε_c , which corresponds to high GDL compression, is feasible and exhibits good performances. A minimum value of 15% should be given to ε_c for low GDL compression.

$oldsymbol{eta}_1$	in-plane	through-plane		
$\varepsilon \approx 0.6$	-5.07	-3.60		
$\varepsilon \approx 0.73$	-3.51	-2.60		

Table 1: Different values of the fitted parameter β_1 according to the porosity and the diffusion direction of gases.

Table 2 presents a comparison between the value given by these equations and values found in other works.

	TSB	T&S	Hu [16, 26]	Yang [18]	Wang [23]	Ye [30]	Meng [33]	Wang [43]
$K_0^{gdl}(m^2)$	$3.4 \cdot 10^{-13}$	10^{-12}	$7 \cdot 10^{-13}$	$3 \cdot 10^{-12}$	$2 \cdot 10^{-15}$	$23 \cdot 10^{-12}$	10^{-12}	10^{-12}
	$(\varepsilon = 0.6)$	$(\varepsilon = 0.6)$	$(\varepsilon = 0.5 - 0.6)$	$(\varepsilon = 0.7)$	$(\varepsilon = 0.5)$	$(\varepsilon = 0.7)$	$(\varepsilon = 0.6)$	$(\varepsilon = 0.7)$
$K_0^{cl}\left(m^2\right)$	Ø	$1.4 \cdot 10^{-14}$	0	$3 \cdot 10^{-14}$	$5 \cdot 10^{-17}$	$2 \cdot 10^{-15}$	10-13	10^{-13}
		$(\varepsilon = 0.25)$		$(\varepsilon = 0.2)$	$(\varepsilon = 0.12)$	$(\varepsilon = 0.2)$	$(\varepsilon = 0.12)$	$(\varepsilon = 0.3)$

Table 2: Comparison between the value given by Tamadakis and Sotirchos model and values found in other works

3.5. Water surface tension: σ

460

Surface tension refers to the force that maintains a fluid at a specific geometry, which corresponds to its minimal surface interface with another fluid; here, its liquid water with air. This allows the two fluids to minimise the energy at their interface. In case of water, it is only a function of the temperature. It can be calculated using equation 31 [44].

$$\sigma = 235.8 \times 10^{-3} \left[\frac{647.15 - T_{fc}}{647.15} \right]^{1.256} \left[1 - 0.625 \frac{647.15 - T_{fc}}{647.15} \right]$$
(31)

This equation yields at 80°C : $\sigma = 0.0627 \text{ N.m}^{-1}$, which is close to the mainstream value in PEMFC literature of 0.0625 N.m^{-1} [16–18, 24, 26, 43].

3.6. Liquid water convective flow in the CL and GDL: $J_{l,conv}$

Before proceeding, it is important to note that this liquid water convection flow $J_{l,conv}$ is not that prevalent in previous studies. It is sometimes neglected by certain models, as in the unsaturated flow theory (UFT) [45, 46], and sometimes cleverly but rigorously disappears in others, as in the multi-phase mixture model (M^2) [46]. It will finally be neglected in this study; however, we still discuss it here. The different theories that allow to proceed without its use and the resolution methods to consider when it is present are discussed in this part.

Then, a description of $J_{l,conv}$ is provided. As soon as liquid water is generated with vapour condensation, these molecules are affected by gases motion. The diffusive flow of gases hauls liquid water molecules with their movement. This flow, which is also a consequence of the use of Darcy's law for calculating $J_{l,cap}$, is expressed as 32 [7, 34] and is demonstrated in Appendix D.1.

$$\boldsymbol{J}_{l,conv} = \frac{\rho_{H_2O}\mu_g}{\mu_l} \frac{\mathbf{s}^{\mathbf{e}}}{[1-\mathbf{s}]^{\mathbf{e}}} \boldsymbol{u}_g \tag{32}$$

where $J_{l,conv}$ $(kg.m^{-2}.s^{-1})$ is the convective flow of liquid water, μ_g (Pa.s) is the gas mixture dynamic viscosity, μ_l (Pa.s) is the liquid water dynamic viscosity, and u_g $(m.s^{-1})$ is the gas mixture velocity.

There are several theories that allow this flow to be neglected. First, the unsaturated flow theory (UFT) [45] states that the pressure of the gas phase in the two-phase mixture is constant along the porous media. This important reductionist assumption implies that the pressure variation of the liquid phase is equal to the capillary pressure variation, that is, the gases are immobile in the porous medium using Darcy's law and thus $u_g = 0$ (see demonstration Appendix D.1 for details). The convective flow of liquid water is thus cancelled out. This theory has been widely deployed in the fuel cell literature of two-phase flow through porous media.

The UFT theory was not used in this study because the assumption of a constant gas pressure in the stack is very limiting. It is only this convective flow $J_{l,conv}$ that has been assumed to be negligible and is therefore not considered further in this study. This assumption, although reductive, is justifiable. First, in terms of magnitude, this flow is not that major compared to the capillary flow. Moreover, for the cathode, liquid water is affected by both vapour and O_2 motions in the electrodes. However, vapour and O_2 have comparable flows in opposite directions. Thus, their impact on liquid water is balanced. As a consequence, u_g is small. This leads to a minor convective flow.

For further information, it is possible to do a more complex modelling. However, it would result in much more complex equations and higher computing times because of the necessity of using Cauchy momentum equation to obtain the velocity field. Whereas, in the model presented here, this is not necessary. Indeed, the velocity is not involved in the system of partial differential equations (except in the GC, which can be circumvented with 1D modelling) and thus, only the continuity equation can be used to solve this system, which is much easier to do. The classical method for considering this convective flow phenomenon, which can be renamed as the multi-phase approach [46], involves keep $J_{l,conv}$ as it is in 32 and to complete the system of equations with the Cauchy momentum equations. $J_{l,conv}$ is then considered in the liquid water saturation dynamic behavior (36a) by using $\nabla \cdot \left(J_{cap} + J_{l,conv}\right)$ instead of $\nabla \cdot J_{cap}$, as done by Wu et al. [34].

However, another method has been developed to significantly reduce the number of equations involved, which are very large in the classical method, although Cauchy momentum equations are still required. This is the multi-phase mixture model (M^2) and involves considering the differential equations of each matter present in different phases (here water vapour and liquid water) as being a single multi-phase mixture. Consequently, the interactions between phases disappear because the vision is more global. This method therefore allows to cancel both the liquid water convective flow $J_{l,conv}$ and the terms of evaporation and condensation of water S_{vl} , as dicussed in Section 3.8. Furthermore, the M^2 method offers the advantage of being as accurate as the classical approach and does not require any additional reducing assumptions. However, it requires a slight revision of the present modelling structure by considering water as a single entity, whether liquid or gas, for the solution of the system of differential equations. However, these changes are only superficial and the numerical resolution techniques remain unchanged. Subsequently, it is also possible to separate water by considering its two phases, knowing the velocity field. Further information and a better understanding of the evolution of the equations in the M^2 model can be found in the study by Wang et al [46].

3.7. Liquid water convective-diffusive flow at the GDL/GC interface: $J_{l,codi}$

As discussed in Section 6.1, if liquid water reaches the GC volume, it is supposed to be in the form of a spray flow, similar to vapour as an ideal gas. $C_{l,gc}$ is the variable used to characterise it. Then, using the convective-diffusive theory discussed in Section ??, it is possible to express the liquid water flow between the GDL/GC interface at the GC side. This flow shown in 33 is considered to be the sorption flow at the GDL/GC interface, as explained in section ??, and is used as a boundary condition at this interface.

$$J_{l,codi} = \begin{cases} h_v \left[C_{l,gc} - C_{l,gc}^{\text{inter}} \right] i, \text{ at the anode} \\ h_v \left[C_{l,gc}^{\text{inter}} - C_{l,gc} \right] i, \text{ at the cathode} \end{cases}$$
(33)

where $J_{l,codi}$ ($mol.m^{-2}.s^{-1}$) is the convective-diffusive flow of liquid water, h_v ($m.s^{-1}$) is the convective-diffusive mass transfer coefficient of vapour, and $C_{l,gc}^{inter}$ ($mol.m^{-3}$) is the liquid water concentration in the GC at its interface with the GDL. The use of h_v is a consequence of the spray hypothesis for liquid water in the GC. Moreover, $J_{l,codi}$ is generally expressed in $mol.m^{-2}.s^{-1}$, contrary to J_{cap} , which is generally expressed as in $kg.m^{-2}.s^{-1}$.

Similar to the discussion in Section ??, it is necessary to have a relationship between $C_{l,gc}^{inter}$ and s_{gdl}^{inter} , which is the liquid water saturation in the GDL at its interface with the GC. However, to the authors' knowledge, this relationship

 $C_{l,gc}^{\rm inter} = f\left(\mathbf{s}_{gdl}^{\rm inter}\right)$ does not exist in the current literature. This is an important research gap and we encourage the community to conduct experiments to determine it. Meanwhile, a major simplification is suggested to perform the calculations. In this study, it is assumed that all the liquid water in the GDL suddenly passes as a spray on contact with the GC boundary, even before crossing it. It is assumed that these droplets are all identical with a spherical volume of radius $r_d = 10^{-4} \, m$ and that their behaviour is similar to that of water vapour studied here. Thus, it is possible to calculate an associated concentration $C_{l,gdl}^{inter}$. Finally, it is assumed that $C_{l,cl}^{inter} = C_{l,gdl}^{inter}$, which leads to the equation (34).

$$J_{l,codi} = \begin{cases} h_{v} \left[C_{l,gc} - \frac{\varepsilon_{gdl}}{N_{a}(\frac{4}{3}\pi r_{d}^{3})} \mathbf{s}_{gdl}^{\text{inter}} \right] \mathbf{i}, \text{ at the anode} \\ h_{v} \left[\frac{\varepsilon_{gdl}}{N_{a}(\frac{4}{3}\pi r_{d}^{3})} \mathbf{s}_{gdl}^{\text{inter}} - C_{l,gc} \right] \mathbf{i}, \text{ at the cathode} \end{cases}$$
(34)

where r_d (m) is the water droplet radius and Na (mol⁻¹) is the Avogadro constant.

3.8. Water phase change rate: S_{vl}

In the stack, it is also important to consider the mole variation of liquid water owing to its evaporation or formation with vapour condensation. From kinetic theory, assuming an ideal gas, by neglecting the interactions between individual molecules, and using constant overall phase change rates [7], the net mass transfer of the evaporation and condensation can be estimated. It is commonly expressed as the following equation 35 [17, 18, 23, 24, 30, 33, 43].

$$S_{vl} = \begin{cases} \gamma_{\text{cond}} \varepsilon \left[1 - \mathbf{s} \right] x_v \left[C_v - C_{v, \text{sat}} \right], & \text{if } C_v > C_{v, \text{sat}} \\ -\gamma_{\text{evap}} \varepsilon \mathbf{s} \frac{\rho_{H_2O}}{M_{H_2O}} RT_{fc} \left[C_{v, \text{sat}} - C_v \right], & \text{if } C_v \le C_{v, \text{sat}} \end{cases}$$
(35)

where S_{vl} ($mol.m^{-3}.s^{-1}$) is the phase transfer rate of condensation and evaporation, that is, the amount of liquid water formed/deformed per unit of volume, γ_{cond} (s^{-1}) is the overall condensation rate constant for water, and γ_{evap} ($Pa^{-1}.s^{-1}$) is the overall evaporation rate constant for water and x_v the mole fraction of vapour.

Both constants γ_{cond} and γ_{evap} should be used carefully as, in the literature, they are given in two different units. A direct comparison of their values is thus impossible. Moreover, several sets of values exist in the literature, as presented in table B.10 in the appendix, and the evaporation rate is usually greater than the condensation rate. The values proposed by Hua Meng: $\gamma_{cond} = 5 \cdot 10^3 \, s^{-1}$ and $\gamma_{evap} = 10^{-4} \, s^{-1} Pa^{-1}$, appear to be the more adapted as the proposed values were well justified by numerical studies conducted in the study [33]. The given values are small owing to the rapid phase transition. This is critical because a modelling algorithm should then have a small time step to track this phenomenon. Thus, it should last longer for computation.

Finally, as the water phase change rates are strongly affected by the local conditions such as mass and heat transfer, the accuracy of this calculation on the macroscopic level remains debatable [7].

3.9. Liquid water saturation dynamic behavior

With all three previous phenomena considered, it is possible to write the dynamic behavior of liquid water as (36a), with its boundary conditions, as (36b).

$$\rho_{H_2O}\varepsilon \frac{\partial \mathbf{s}}{\partial t} = -\nabla \cdot \boldsymbol{J}_{cap} + M_{H_2O}S_{vl}$$
(36a)

$$\begin{cases} \boldsymbol{J}_{l}^{cl,mem} = \boldsymbol{0}, \text{ at the ionomer border} \\ \boldsymbol{J}_{l}^{gdl,gc} = \rho_{H_{2}O} N_{a} \left(\frac{4}{3}\pi r_{d}^{3}\right) \boldsymbol{J}_{l,codi}, \text{ at the GDL/GC border} \end{cases}$$
(36b)

4. Vapor transport in the CL and GDL

4.1. Vapor diffusive flow in the CL and GDL: J_{dif}

Concentration gradients dominate transport in the electrode and convection is thus neglected. Indeed, owing to frictional effects, the velocity of the moving gas stream tends towards zero at the electrode-channel boundary. In

the absence of convective mixing, concentration gradients can form within the stagnant gas of the electrode [8]. To express this flow, a simple Fick equation is used, which is expressed as (??).

$$J_{v,dif} = -D_v^{eff} \nabla C_v \tag{37}$$

where $J_{v,dif}$ is the vapour diffusive flow and D_v^{eff} is the vapour diffusion coefficient.

4.2. Effective diffusion coefficient of two species i and j: $D_{i/i}^{eff}$

The effective diffusivity of two species i/j is a method to consider the real gas diffusion coefficient in the stack regarding the porosity and the tortuosity of the matter plus the space occupied by liquid water. Indeed, the usual binary diffusivity $D_{i/j}$, explained in Section 4.3, is commonly calculated in open space, which is a very different environment. Tortuosity is considered for describing the additional impedance to diffusion caused by a tortuous or convoluted flow path. Notably, the GDL and the CL have different structures and thus matter therefore flows differently in them. Moreover, these structures are anisotropic, which implies that their evolution depends on the spatial direction taken. Thus, it is necessary to consider these differences in the mathematical expressions used to describe the effective diffusivity.

The Bruggeman model is the most commonly used expression [8, 15, 17, 18, 24, 39, 43, 47]. It introduces a coefficient τ which can vary between 1.5–4.0 [8, 48], depending on the pore structure configuration. Highly 'maze-like' or meandering pore structures yield high tortuosity values [8]. However, the Bruggeman model overestimates the effective diffusion coefficient of GDL [49] as it is based on the porosity of packed spherical particles rather than cylindrical fibers that make up the GDL. In contrast, Tomadakis and Sotirchos proposed another model for randomly oriented fibrous porous media to investigate chemical vapour infiltration through fibrous composite matters with the porosity gradients [39]. Based on this, Nam et al. [47] proposed the use of the Bruggeman model for the CL and the Tomadakis and Sotirchos model for the GDL. They also adjusted these models to consider the liquid water saturation. Thus, $D_{i/j}^{eff}$ is expressed as (38).

$$D_{i/j}^{eff} = \begin{cases} \varepsilon^{\tau} [1 - \mathbf{s}]^{\tau} D_{i/j}, & \text{at the CL (Bruggeman model)} \\ \varepsilon \left[\frac{\varepsilon - \varepsilon_{p}}{1 - \varepsilon_{p}} \right]^{\alpha} [1 - \mathbf{s}]^{2} D_{i/j}, & \text{at the GDL (Tomadakis and Sotirchos model)} \end{cases}$$
(38)

where τ is the pore structure coefficient, commonly obtained at $\tau = 1.5$ for PEMFC [39]. Further, $D_{i/j}$ ($m^2.s^{-1}$) is the binary diffusivity of two species in open space, ε_p is the percolation threshold porosity, obtained at 0.11 [24, 39], and α is a fitted value, obtained at 0.521 for in plane direction and at 0.785 for through plan direction [24, 39].

 ε_p is the minimum porosity with an open void space connectivity, which is required for diffusion or permeation through the matter. Tomadakis and Sotirchos found that $\varepsilon_p = 0.11$ was the percolation threshold porosity for a random, two-dimensional (2D) fibrous structure determined by extrapolating the results of their model to the porosity in the absence of mass transport considerations [38, 39].

A different correlation for effective diffusivity also exists; however, is proven to be more accurate only for fuel cells working at high temperature. PEMFC are thus not concerned with this. This correlation is expressed as $D_{i/j}^{eff} = D_{i/j} \frac{\varepsilon_{gdl}}{\tau}$ [8].

Another element that is often neglected in the literature models is the compression of the GDL, described by Bao et al. [40] and discussed in Section 3.4. It is therefore necessary to modify the previously proposed model. It should be noted that this modification concerns only GDL and not CL. The elastic characteristics of GDL results in it deforming to greater degree than CL (or GC), whose deformation can be neglected. Thus, the model of Tomadakis and Sotichos augmented by the work of Bao et al, which can be renamed by the TSB model, yields the following effective diffusion coefficient for the GDL given equation 39.

$$D_{i/j}^{eff} = \begin{cases} \varepsilon^{\tau} [1 - \mathbf{s}]^{\tau} D_{i/j}, & \text{at the CL (Bruggeman model)} \\ \varepsilon \left[\frac{\varepsilon - \varepsilon_p}{1 - \varepsilon_p} \right]^{\alpha} [1 - \mathbf{s}]^2 e^{\beta_2 \varepsilon_c} D_{i/j}, & \text{at the GDL (TSB model)} \end{cases}$$
(39)

where β_2 is a fitted value which varies with the porosity and the diffusion direction of gases according to the following table 3.

eta_2	in-plane	through-plane		
$\varepsilon \approx 0.6$	-2.05	-1.59		
$\varepsilon \approx 0.73$	-1.04	-0.90		

Table 3: Different values of the fitted parameter β_2 according to the porosity and the diffusion direction of gases.

Finally, to present a complete work, it is assumed that the electrolyte has the same tortuosity characteristics as that of the catalyst metal particles.

4.3. Binary diffusion coefficient: $D_{i/j}$

As mentioned before, diffusion coefficient are usually calculated in open space. However, in PEMFC, gas species are not alone during their transport in CLs and GDLs. They are diffused with other species and this coexistence influences their diffusion. For simplicity, only two gases are usually considered at the same time, nitrogen being assumed to not interfere. Consequently, both species in contact share the same diffusion coefficient. This is why we consider binary diffusion coefficients.

For a binary system of two gases i and j, $D_{i/j}$ is a function of temperature, pressure, and the molecular weights of both species [8]. Two close expressions, fitted from experimental data, are available in the literature and expressed as (40) [8] and (41) [18, 24, 39, 43].

$$\begin{cases}
D_{H_2O/H_2} = 1.644 \cdot 10^{-4} \left[\frac{T_{fc}}{333} \right]^{2.334} \left[\frac{101325}{P} \right] \\
D_{H_2O/O_2} = 3.242 \cdot 10^{-5} \left[\frac{T_{fc}}{333} \right]^{2.334} \left[\frac{101325}{P} \right]
\end{cases}$$
(40)

Their background being given, we believe that the expressions (40) which has been emphasised is more adaptable. The expressions (41), mainly used in the literature, originate from a unique source, which do not explain its calculation. Moreover, D_{vc} , which is the vapour diffusion coefficient at the cathode, and D_{O2} , the dioxygen diffusion coefficient, are slightly different in (41) although they are the binary diffusivity of vapour and dioxygen in the GDL and thus should be equal. This may be owing to nitrogen in the fuel cell; however, the explanations were not given in these studies.

$$D_{H_2O/H_2} = 1.005 \cdot 10^{-4} \left[\frac{T_{fc}}{333} \right]^{1.75} \left[\frac{101325}{P} \right]$$
 (41a)

$$\begin{cases}
D_{vc} = 2.982 \cdot 10^{-5} \left[\frac{T_{fc}}{333} \right]^{1.75} \left[\frac{101325}{P} \right] \\
D_{O_2} = 2.652 \cdot 10^{-5} \left[\frac{T_{fc}}{333} \right]^{1.75} \left[\frac{101325}{P} \right]
\end{cases}$$
(41b)

Table 4 presents a comparison of both equations with data obtained from other sources.

	O'Hayre [8]		Yang [18] Hu, Pasaogullari [16, 26]		Nam, Bultel [47, 50]
	(at 353 K and 1.5 atm)	(at 353 K and 1.5 atm)	(at 353 K and 1.5 atm)		
$D_{va}\left(m^2\cdot s^{-1}\right)$	$1.256 \cdot 10^{-4}$	$7.420 \cdot 10^{-5}$	$5.457 \cdot 10^{-5}$	$1 \cdot 10^{-5}$	Ø
$D_{vc}\left(m^2\cdot s^{-1}\right)$	$2.477 \cdot 10^{-5}$	$2.202 \cdot 10^{-5}$	$2.236 \cdot 10^{-5}$	$1 \cdot 10^{-5}$	Ø
$D_{O_2}\left(m^2\cdot s^{-1}\right)$	$2.477 \cdot 10^{-5}$	$1.958 \cdot 10^{-5}$	$1.806 \cdot 10^{-5}$	Ø	$2.9 \cdot 10^{-5}$

Table 4: Comparison between the values given by the mentioned expressions for the binary diffusion coefficients and values found in other works

4.4. Vapor convective-diffusive flow at the GDL/GC interface: $J_{v,codi}$

To obtain a complete model of matter transports in the stack, the sorption flow between the GDL and GC must be considered. This flow, in this work, is approximated by another flow. It is easier to calculate and is named here as vapour convective-diffusive flow at the GDL/GC interface: $J_{v,codi}$. There is a slight difference between these two flows. $J_{v,codi}$ occurs only in the GC and characterises a vapour flow between the GDL/GC interface at the GC side and the core of the GC. Whereas, the desired sorption flow characterises a vapour flow between two layers: the GDL and the GC. However, it is reasonable to conclude that both concentrations at the two interface sides balance instantaneously, considering the tiny volume which characterises the molecules bound at each interface side. Thus, without matter accumulation, the sorption flow at the GDL/GC interface is the same value as that of the convective-diffusive flow $J_{v,codi}$.

In the literature, $J_{v,codi}$ is often referred to as a convective flow [8]. However, the authors believe that this term is confusing and decided to rename it as a convective-diffusive flow. This flow results from the coupling of an external convective mass transfer in the GC flow direction owing to the pressure difference between the inlet and outlet of the GC, and a diffusive mass transfer between the GC interface and its core that transverse to the external convective one. It is expressed as (??), which is based on the diffusive theory, considering the external convective flow characteristics [8, 51]. More information regarding the creation of this equation and the formation of the convective-diffusive mass transfer coefficient h_v are given in Appendix D.2.

$$J_{v,codi} = \begin{cases} h_v \left[C_{v,gc} - C_{v,gc}^{\text{inter}} \right] i, \text{ at the anode} \\ h_v \left[C_{v,gc}^{\text{inter}} - C_{v,gc} \right] i, \text{ at the cathode} \end{cases}$$
 (42)

where h_v ($m.s^{-1}$) is the convective-diffusive mass transfer coefficient of vapour, $C_{v,gc}^{inter}$ ($mol.m^{-3}$) is the vapour concentration in the GC at its interface with the GDL, and ι is a unit vector along the x-axis. Notably, h_v is not an "effective" coefficient because the convective-diffusive flow happens in the GC where vapour moves into an empty space.

To use this equation (??), it is essential to obtain a relationship between $C_{v,gc}^{inter}$ and $C_{v,gdl}^{inter}$, which is the vapour concentration in the GDL at its interface with the GC. Indeed, $C_{v,gc}^{inter}$ is unknown whereas $C_{v,gdl}^{inter}$ is accessible owing to the diffusion theory discussed in ??. This request is similar, although slightly different, to the relationship between λ_{eq} and a_w . Indeed, dissolved water in the membrane is linked with vapour concentration in the triple points region. However, to the best of our knowledge, this relationship $C_{v,gc}^{inter} = f\left(C_{v,gdl}^{inter}\right)$ does not exist in the current literature. This is an important research gap and we encourage the community to conduct experiments to determine it. Meanwhile, the following simplification is suggested: $C_{v,gcl}^{inter} = C_{v,gdl}^{inter}$ which leads to equation (??).

$$J_{\nu,codi} = \begin{cases} h_{\nu} \left[C_{\nu,gc} - C_{\nu,gdl}^{\text{inter}} \right] \mathbf{i}, \text{ at the anode} \\ h_{\nu} \left[C_{\nu,gdl}^{\text{inter}} - C_{\nu,gc} \right] \mathbf{i}, \text{ at the cathode} \end{cases}$$

$$(43)$$

where $C_{v,gdl}^{inter}$ (mol.m⁻³) is the vapor concentration in the GDL at its interface with the GC.

Finally, one implied hypothesis is considered when a convective-diffusive flow is mentioned. The dividing line, or boundary between convective-dominated flow inside the core of the GC and diffusive-dominated flow inside the core of the electrodes must occur at the interface between the GC and the GDL. This is a reasonable assumption for medium current density operation (approximately 1–1.5 $A.cm^{-2}$). However, it can change depending on the flow conditions, flow channel geometry, or electrode structure. For example, at very low gas velocities in the GC, the diffusion layer may stretch out into the middle of the gas channels. In contrast, at extremely high gas velocities, convective mixing may penetrate into the electrode itself, causing the diffusion layer to retreat. However, its exact location is difficult to define and calculating the true diffusion layer thickness in these situations requires sophisticated models [8], such as the one proposed by Kim et al. [37]. They are not considered in this study.

4.5. Water effective convective-diffusive mass transfer coefficient: h_v

For calculating h_v , it is common to use Sherwood number S_h , which links h_v to D_v , as shown in (44) [8]. The Sherwood number is a dimensionless number used in mass-transfer operations to compare convective-diffusion with classical diffusion.

$$h_{\nu} = S_h \frac{D_{\nu}}{H_{\sigma c}} \tag{44}$$

Then, fitting the data given by O'Hayre [8], with a correlation coefficient $R^2 = 0.9869$, the authors obtained the following expression for S_h , which is dependent on channel geometry only. However, equation (45) only applies along with the hypothesis of a uniform density along the gas channel.

$$S_h = 0.9247 \cdot \ln\left(\frac{W_{gc}}{H_{gc}}\right) + 2.3787, \text{ for } \frac{W_{gc}}{H_{gc}} \in [0.2, 10.0]$$
 (45)

where W_{gc} (m) is the width of the gas channel.

4.6. Vapor concentration dynamic behavior in the CL and GDL

Finally, having considered the previous phenomena and knowing that the same phase transfer rate S_{vl} is used to consider condensation and evaporation, the following dynamic behaviour of vapour concentration can be given. (??) corresponds to a molar balance of vapour in the CL or the GDL whereas (??) matches the boundary conditions at the CL/membrane and the GDL/GC interfaces.

$$\varepsilon \frac{\partial}{\partial t} ([1 - \mathbf{s}] C_v) = -\nabla \cdot \mathbf{J}_{v,dif} - S_{sorp} - S_{vl}$$
(46a)

$$\begin{cases} J_{\nu}^{cl,mem} = \mathbf{0}, \text{ at the ionomer border} \\ J_{\nu}^{gdl,gc} = J_{\nu,codi}, \text{ at the GDL/GC border} \end{cases}$$
(46b)

5. Vapor transport in the GC

660

To complete water evolution in the stack, water concentrations in the gas channels must be considered.

5.1. Vapor convective flow in the $GC: J_{v,conv}$

The flow in the gas channels is convection dominated, and the driving force is the pressure at the flow channel inlets [7]. Within the GC, convection ensures that the gas streams are well mixed. This ensures that concentration gradients do not occur [8]. Then, GC being similar to a classical pipe, $J_{v,conv}$ is simply expressed as (??).

$$J_{v,conv} = C_v u_g \tag{47}$$

where u_g ($m.s^{-1}$) is the gas mixture velocity, considering that all gases evolve at the same speed. As gas transports in flow-fields follow classical fluid mechanic equations and are highly dependent on the chosen geometry for the GC, the calculation of the gas mixture velocity u_g is not detailed in this study. Many GC configurations exist and continue to evolve over time. For example, it is possible to consider interdigitated, serpentine, baffle, or porous flow fields. All of them have a major and different impact on the stack performance and each of them require a specific study, which is not the purpose of this study. However, it is important to keep this in mind for in-depth modelling.

5.2. Simplified vapor flows at the inlet and outlet of the GC: $J_{v,in/out}^{gc}$

In real conditions, gas flows at the inlet and outlet of the GC are dependent on the auxiliary system: the nozzles, manifolds, humidifiers, and compressor. Other components can also be added depending on the installation that is simulated. Pukrushpan et al. proposed a very simple model involving these components [9], which has been refined by Xu et al. [52] and Shao and al. [53] while remaining simple. However, this significantly complicates the calculation of the inlet and outlet gas flows. Thus, in practice, during the building of a simulation, it is a good idea to have a simplified model for these flows to first check the accuracy of the matter transport simulation in the stack. The equations mentioned in this study are already numerous, complex, and dependent of one another. Thus, being able to verify the algorithm before using a more complex model is desirable.

Inspired by Pukrushpan's and Clancy's work [9, 54], we propose simplified equations for the inlet and outlet water flows at the GC. Pukrushpan's study is useful in case of the inlet flows whereas Clancy's publication proposes an adapted form of Bernoulli's principle for compressible adiabatic flows of ideal gases, which is useful for the outlet

At the inlets, the goal is to directly link the flows with the current density i_{fc} . Indeed, an increase of i_{fc} means an increase of fuel consumptions and so a need for an increase of fuel inlet flows in order to avoid fuel starvation. Such a link for fuel inlet flows is easy to produce considering that they are injected in the stack proportionally to their consumed flows in the CL. The expressions are given section 7.1. Then, in order to have on an ongoing basis a fix value of the inlet relative humidity, it is necessary to also link water inlet flows with the current density. In practice, these water inlet flows are built based on fuel inlet flows expressions [9] considering that gases are ideals and gas channels have cuboid shape. What makes these equations, given in (48a), simpler is that no auxiliaries are considered and so this amount of matter is directly delivered in the inlet of the GC, whereas in reality it has to pass first through different components which would impact the expressions. A demonstration of these expressions if given Appendix D.3 and Appendix D.4.

At the outlets, the objective is to express the flows as a function of the pressure difference between the GC and the outlet pressures. This expression must be different from the one proposed for the inlet flows because the outlet flows are not controlled by a compressor. They are naturally evacuated owing to pressure differences. Typically, it is assumed that the outlet pressures of the GC directly matches the desired pressures $P_{a,des}$ and $P_{c,des}$, which are fixed by the user. However, the method by which these outlet pressures is achieved is not specified here. With this simplified configuration, it is possible to express the outlet flows, as expressed in equation (??), using Bernoulli's principle for compressible, adiabatic, and steady flows of ideal gases [54]. The assumptions considered here are quite strong, as the flows are not compressible or steady in reality. However, this approach allows for the use of a simple expression that provides initial results while awaiting the implementation of auxiliary systems.

$$\begin{cases} J_{v,\text{in}}^{agc} = \frac{\Phi_{a,\text{in}} P_{\text{sat}}}{P_{a,\text{in}} - \Phi_{a,\text{in}} P_{\text{sat}}} \frac{S_{a}i_{fc}}{2F} \frac{A_{act}}{H_{gc}W_{gc}} \\ J_{v,\text{out}}^{agc} = C_{v} u_{out}^{agc} \\ J_{v,\text{in}}^{cgc} = \frac{\Phi_{c,\text{in}} P_{\text{sat}}}{\Phi_{c,\text{in}} P_{\text{sat}}} \frac{1}{y_{O_{2},ext}} \frac{S_{c}i_{fc}}{4F} \frac{A_{act}}{H_{gc}W_{gc}} \\ J_{v,\text{out}}^{cgc} = C_{v} u_{out}^{cgc} \\ J_{v,\text{out}}^{cgc} = V_{v} u_{out}^{cgc} \end{cases}$$

$$(48a)$$

$$u_{out}^{gc} = \begin{cases} \sqrt{\frac{2}{\rho} \frac{\gamma_{a}}{\gamma_{a-1}} (P_{gc} - P_{des})}, & \text{if } P_{gc} > P_{des} \\ 0, & \text{if } P_{gc} \leqslant P_{des} \end{cases}$$

$$u_{out}^{gc} = \begin{cases} \sqrt{\frac{2}{\rho} \frac{\gamma_a}{\gamma_{a-1}} (P_{gc} - P_{des})}, & \text{if } P_{gc} > P_{des} \\ 0, & \text{if } P_{gc} \le P_{des} \end{cases}$$
(48b)

where A_{act} (m^2) is the active area, u_{out}^{gc} ($m.s^{-1}$) is the outlet velocity of the matter mixture at the GC, P_{des} (Pa) is the desired pressure fixed by the user, and γ_a is the heat capacity ratio of the matter mixture, considered here as the dry air capacity ratio for simplifications, which is $\gamma_a = 1.4$.

5.3. Vapor dynamic behavior in the GC

Finally, assuming that no phase change occurs in the GC, the following dynamic behaviour of vapour concentration can be obtained. (??) corresponds to a molar balance of vapour in the GC and (??) matches the boundary conditions at the GDL/GC interface, inlet, and outlet of the GC.

$$\frac{\partial C_{v}}{\partial t} = -\nabla \cdot \boldsymbol{J}_{v,conv} \tag{49a}$$

$$\begin{cases} J_{\nu}^{gdl,gc} = J_{\nu,codi}, \text{ at the GDL/GC border} \\ J_{\nu}^{in/out,gc} = J_{\nu,in/out}^{gc}, \text{ at the inlet/outlet of the GC} \end{cases}$$
(49b)

6. Liquid water transport in the GC

6.1. Different ways of modeling liquid water in the GC

In the literature there are three major methods for modelling liquid water in the GC. The first, proposed by Pukrushpan et al. [9], is the simplest and involves considering liquid water as a spray flow, as only a small amount of liquid water is supposed to exist there. These liquid droplets are assumed to be finely dispersed (with zero volume) owing to the strong gaseous motion in the GC and to have transport properties identical to those of vapour. Consequently, a new variable is used, that is, the liquid water concentration in the gas channel: $C_{l,gc}$.

Second, several studies have identified similarities between the porous structure of the GDL and the channels of the GC flow-field, although the order of magnitude of the sizes are not the same [18, 55–65]. Thus, they proposed to continue the use of the liquid water saturation variable s and to use Darcy's law, with a porosity equal to 1, for modelling liquid water transport, as dicussed previously in Section 3.3. This attempt further justified by the fact that liquid water can reach up to 10% of the total mass flow rate in the GC [66], which weakens the Pukrushpan hypothesis of a spray flow.

However, as long as 3D complex PEMFC flow-fields are modelled and high current densities are reached ($2 \sim 4$ $A.cm^{-2}$), Darcy's law alone is not sufficient to consider liquid water transport. Thus, Darcy-Forchheimer's law is recommended instead [37]. This is an important consideration because the use of advanced GCs, for example baffles, is becoming the norm in modern fuel cells to achieve much higher power densities. In this scenario, GC geometry often result in gas flow penetrations into the GDL owing to strong convection. Consequently, extensive modelling is required to consider the 3D geometry of the GC and determine the location of the boundary between the convection-dominated flow within the GC core and the diffusion-dominated flow within the GDL core, which is not a flat boundary anymore. This high-level modelling, partially introduced by Kim et al. in 2017 [37], is not that comprehensively discussed in this article.

Pukrushpan's model has been used in this study for modelling liquid water transport in the GC. Darcy-Forchheimer's law requires sophisticated modelling, which is not considered in this study. Moreover, Darcy's law, although compatible in the current stack model, does not fit well into models that consider all the auxiliaries in addition to the stack. To the best of the authors' knowledge, the auxiliaries are generally still modelled using simple equations wherein only gas flows are considered. Therefore, these models require liquid water to be considered as a gas stream and it is more appropriate to consider from the GC.

Finally, as liquid water is modelled as a gas, Section ?? is the referenced Section for transports in the GC. Thus, here equations are presented without deeper explanations.

6.2. Liquid water convective flow in the GC: $J_{l,conv}$

Owing to the GC being similar to a classical pipe, $J_{l,conv}$ is simply expressed as (50).

$$J_{l,conv} = C_{l,gc} u_g \tag{50}$$

where u_g ($m.s^{-1}$) is the gas mixture velocity, considering that liquid water evolves at the same speed as that if the other gases.

6.3. Simplified liquid water flows at the inlet and outlet of the GC: $J_{l,in/out}^{gc}$

To characterise the liquid water outlet flow, a hypothesis is made: liquid droplets are moving at the same speed as that of the gas mixture leaving the GC: u_{out}^{gc} . Consequently, using the definition of a flow, which is the product of the concentration and velocity, it is possible to express a simplified liquid water outflow based on hypothesis made in ??. These flows are expressed as (51).

$$\begin{cases}
J_{l,in}^{agc} = 0 \\
J_{l,out}^{agc} = C_l u_{out}^{agc} \\
J_{l,in}^{cgc} = 0 \\
J_{l,out}^{cgc} = C_l u_{out}^{cgc}
\end{cases}$$
(51)

6.4. Liquid water dynamic behavior in the GC

Finally, assuming that no phase changes occur in the GC, the following dynamic behaviour of liquid water concentration can be obtained. (52a) corresponds to a molar balance of liquid water in the GC and (52b) matches the boundary conditions at the GDL/GC interface and the outlet of the GC.

$$\frac{\partial C_{l,gc}}{\partial t} = -\nabla \cdot \boldsymbol{J}_{l,conv} \tag{52a}$$

$$\begin{cases} J_{l}^{gdl,gc} = J_{l,codi}, \text{ at the GDL/GC border} \\ J_{l}^{in/out,gc} = J_{l,in/out}^{gc}, \text{ at the inlet/outlet of the GC} \end{cases}$$
 (52b)

7. Hydrogen and oxygen transports

The hydrogen and oxygen behaviours are very similar to vapour transport in the stack. Thus, the following governing equations are provided without deeper explanations.

7.1. Hydrogen and oxygen flows: $J_{H_2,dif}$, $J_{H_2,codi}$, $J_{H_2,conv}$, $J_{O_2,dif}$, $J_{O_2,codi}$, $J_{O_2,conv}$

Hydrogen diffusive, convective-diffusive, convective flows, and inlet and outlet flows at the AGC are respectively expressed as (53).

$$\begin{cases}
J_{H_2,dif} = -D_{H_2}^{eff} \nabla C_{H_2} \\
J_{H_2,codi} = h_{H_2} \left[C_{H_2,agc} - C_{H_2,agdl}^{inter} \right] \mathbf{i} \\
J_{H_2,conv} = C_{H_2} \mathbf{u}_g \\
J_{H_2,in} = \frac{S_a i_{fc}}{2F} \frac{A_{act}}{H_g c W_{gc}} \\
J_{H_2,out} = C_{H_2} u_{out}^{agc}
\end{cases} (53)$$

Oxygen diffusive, convective-diffusive, convective flows, and inlet and outlet flows at the CGC are respectively expressed as (54).

$$\begin{cases}
J_{O_2,dif} = -D_{O_2}^{eff} \nabla C_{O_2} \\
J_{O_2,codi} = h_{O_2} \left[C_{H_2,cgdl}^{inter} - C_{O_2,cgc} \right] \mathbf{i} \\
J_{O_2,conv} = C_{O_2} \mathbf{u}_g \\
J_{O_2,in} = \frac{S_c i_{fc}}{4F} \frac{A_{act}}{H_g c W_{gc}} \\
J_{O_2,out} = C_{O_2} u_{out}^{cgc}
\end{cases} (54)$$

7.2. Hydrogen and oxygen consumption at the interface of the triple points: $S_{H_2,cons}$

Hydrogen and oxygen consumption are respectively expressed as (55) and (56).

$$S_{H_2,cons} = \begin{cases} -\frac{i_{fc}}{2FH_{cl}}, & \text{in the ACL} \\ 0, & \text{elsewhere} \end{cases}$$
 (55)

$$S_{H_2,cons} = \begin{cases} -\frac{i_{fc}}{2FH_{cl}}, & \text{in the ACL} \\ 0, & \text{elsewhere} \end{cases}$$

$$S_{O_2,cons} = \begin{cases} -\frac{i_{fc}}{4FH_{cl}}, & \text{in the CCL} \\ 0, & \text{elsewhere} \end{cases}$$
(55)

It is possible to add terms to this hydrogen and oxygen consumption by considering the crossover. Indeed, the membrane is a material chosen to be impermeable to gases so that hydrogen and oxygen do not mix directly, which would prevent any electricity production and would also be dangerous. However, the membrane is not perfectly impermeable to gases and a small amount can pass through it, in both directions. Thus, certain amounts of the hydrogen and oxygen that were supposed to react through the fuel cell mechanism instead pass through the membrane and react via direct contact, producing water. Thus, certain amount of the matter is lost and unused. This phenomenon is referred to as crossover and the equations governing it are described here. The equation describing the production of additional water by crossover is presented in Section 2.9.

The crossover flows are $S_{H_2,co}$ and $S_{O_2,co}$, and are expressed in $mol.m^{-3}.s^{-1}$. It is better to consider them as volume flows because they penetrate the membrane which is dispersed in a volume at the level of the catalytic layer. To calculate them, Fick's law is classically applied between the two interface of the membrane [10, 35, 67–70], represented by a gradient ∇_m , as seen in 57 and 58.

$$S_{H_2,co} = \begin{cases} k_{H_2} \frac{RT_{fc}}{H_{cl}} \nabla_m C_{H_2}, & \text{in the ACL} \\ 0, & \text{elsewhere} \end{cases}$$
 (57)

$$S_{O_2,co} = \begin{cases} k_{O_2} \frac{RT_{fc}}{H_{cl}} \nabla_m C_{O_2}, & \text{in the CCL} \\ 0, & \text{elsewhere} \end{cases}$$
 (58)

where k_i ($mol.m^{-1}.s^{-1}.Pa^{-1}$) is the permeability coefficient of molecule i (hydrogen or oxygen) in the membrane.

An experimental expression for these permeability coefficients was proposed by Weber et al. in 2004 [10, 68, 69] and provides the most accurate prediction to date as this coefficient is a function of both λ and T_{fc} . Another experiment was conducted later by Kocha et al. in 2006 [70], which did not consider the variation of λ in k_i . Gas permeability in PEM fuel cells depends strongly on the conditions of the membrane, such as its hydration level and temperature. Consequently, changes in operational conditions cause fluctuations in k_i [70]. The Weber proposal is expressed as (59) and (60).

$$k_{H_2} = \begin{cases} \left[0.29 + 2.2 f_{\nu}(\lambda) \right] 10^{-14} \exp\left(\frac{E_{act, H_2, \nu}}{R} \left[\frac{1}{T_{ref}} - \frac{1}{T_{fc}} \right] \right) & if \lambda < \lambda_{l, eq} \\ 1.8 \cdot 10^{-14} \exp\left(\frac{E_{act, H_2, l}}{R} \left[\frac{1}{T_{ref}} - \frac{1}{T_{fc}} \right] \right) & if \lambda = \lambda_{l, eq} \end{cases}$$
(59)

$$k_{O_2} = \begin{cases} [0.11 + 1.9f_v(\lambda)] \ 10^{-14} \exp\left(\frac{E_{act,O_2,v}}{R} \left[\frac{1}{T_{ref}} - \frac{1}{T_{fc}}\right]\right) & if \lambda < \lambda_{l,eq} \\ 1.2 \cdot 10^{-14} \exp\left(\frac{E_{act,O_2,l}}{R} \left[\frac{1}{T_{ref}} - \frac{1}{T_{fc}}\right]\right) & if \lambda = \lambda_{l,eq} \end{cases}$$
(60)

where $E_{act,H_2,\nu}=2.1\cdot 10^4 J.mol^{-1}$ and $E_{act,O_2,\nu}=2.2\cdot 10^4 J.mol^{-1}$ are the activation energies of hydrogen and oxygen, respectively, for crossover in the under saturated membrane, $E_{act,H_2,l}=1.8\cdot 10^4 J.mol^{-1}$ and $E_{act,O_2,l}=2.0\cdot 10^4 J.mol^{-1}$ are the activation energies of hydrogen and oxygen, respectively, for crossover in the liquid-equilibrated membrane, $T_{ref}=303.15K$ is the referenced temperature in this study, and f_{ν} the water volume fraction of the membrane described in 2.8.

After the hydrogen and oxygen molecules have passed through the membrane, the consumption of the corresponding complementary molecule, denoted as $S_{i,wasted}$, must be considered. However, the existing equations in the literature oversimplify this process [35]. They assume that the matter passes instantly through the membrane as if it were of zero thickness and that all of the arriving matter reacts immediately with its complementary molecule to form water. Based on this assumption, the equations can be written as (61) and (62).

$$S_{H_2,wasted} = \begin{cases} -2 \cdot S_{O_2,co}, & \text{in the ACL} \\ 0, & \text{elsewhere} \end{cases}$$
 (61)

$$S_{O_2,wasted} = \begin{cases} -0.5 \cdot S_{H_2,co}, & \text{in the CCL} \\ 0, & \text{elsewhere} \end{cases}$$
 (62)

Finally, the corrected expressions of $S_{i,cons}$, considering also the short-circuited current density i_{sc} , is expressed as (63) and (64).

$$S_{H_2,cons} = \begin{cases} -\frac{i_{fc} + i_{sc}}{2FH_{cl}} - \frac{RT_{fc}}{H_{cl}} \left[k_{H_2} \nabla_m C_{H_2} + 2k_{O_2} \nabla_m C_{O_2} \right], & \text{in the ACL} \\ 0, & \text{elsewhere} \end{cases}$$
 (63)

$$S_{O_2,cons} = \begin{cases} -\frac{i_{fc} + i_{sc}}{4FH_{cl}} - \frac{RT_{fc}}{H_{cl}} \left[k_{O_2} \nabla_m C_{O_2} + \frac{k_{H_2}}{2} \nabla_m C_{H_2} \right], & \text{in the CCL} \\ 0, & \text{elsewhere} \end{cases}$$
(64)

7.3. Hydrogen and oxygen concentration dynamic behavior in the CL and GDL

The hydrogen dynamic behaviour is given by the molar balance of H_2 in (65a) and the boundary conditions at the CL/membrane, GDL/GC interfaces, and inlet/outlet of the GC in (65b).

$$\begin{cases} \varepsilon \frac{\partial}{\partial t} \left([1 - \mathbf{s}] C_{H_2} \right) = -\nabla \cdot \boldsymbol{J}_{\boldsymbol{H}_2, dif} + S_{H_2, cons}, & \text{in the anode} \\ \frac{\partial C_{H_2}}{\partial t} = -\nabla \cdot \boldsymbol{J}_{\boldsymbol{H}_2, conv}, & \text{in the AGC} \end{cases}$$
(65a)

$$\begin{cases} \mathcal{E} \frac{\partial}{\partial t} \left([1 - \mathbf{s}] C_{H_2} \right) = -\nabla \cdot J_{H_2,dif} + S_{H_2,cons}, & \text{in the anode} \\ \frac{\partial C_{H_2}}{\partial t} = -\nabla \cdot J_{H_2,conv}, & \text{in the AGC} \end{cases}$$

$$\begin{cases} J_{H_2}^{cl,mem} = \mathbf{0}, & \text{at the CL/membrane border} \\ J_{H_2}^{gdl,gc} = J_{H_2,codi}, & \text{at the GDL/GC border} \\ J_{H_2}^{in/out,gc} = J_{H_2,in/out}, & \text{at the inlet/outlet of the GC} \end{cases}$$

$$(65a)$$

The oxygen dynamic behaviour is given by the molar balance of O_2 in (66a) and the boundary conditions at the CL/membrane, GDL/GC interfaces, and inlet/outlet of the GC in (66b).

$$\begin{cases} \varepsilon \frac{\partial}{\partial t} \left([1 - \mathbf{s}] C_{O_2} \right) = -\nabla \cdot \boldsymbol{J}_{O_2, dif} + S_{O_2, cons}, & \text{in the cathode} \\ \frac{\partial C_{O_2}}{\partial t} = -\nabla \cdot \boldsymbol{J}_{O_2, conv}, & \text{in the CGC} \end{cases}$$
(66a)

$$\begin{cases} J_{O_2}^{cl,mem} = \mathbf{0}, & \text{at the CL/membrane border} \\ J_{O_2}^{gdl,gc} = J_{O_2,codi}, & \text{at the GDL/GC border} \\ J_{O_2}^{in/out,gc} = J_{O_2,in/out}, & \text{at the inlet/outlet of the GC} \end{cases}$$
(66b)

8. Nitrogen transport

800

For nitrogen transport modelling, it is important to assume that N_2 is homogeneous everywhere in the stack (MEA and CGC). This allows us to continue using the binary coefficients for calculating the flow of oxygen and water at the cathode. Thus, in the differential equation shown below as (69), the control volume is the combination of the cathode and CGC volume. The inner flow of nitrogen is not considered. This is a reasonable assumption as no nitrogen is consumed in this process. In this study, the N_2 crossover is not mentioned as it is useful only in very specific modelling tasks. Please refer to [71] for more information.

Thus, nitrogen evolution is fully dependent on the inlet and outlet flows at the CGC. Similar to the vapour situation discussed in Section ??, simplifications of these flows are suggested to obtained preliminary results before the addition of auxiliaries.

8.1. Simplified nitrogen concentration flows at the inlet and outlet of the CGC

The inlet concentration flow of nitrogen in the stack is expressed as (67) and the outlet concentration flow expressed as (68) (the demonstrations are available in the appendix).

$$W_{N_2,\text{in}} = \frac{1 - y_{O_2,in}}{y_{O_2,in}} \frac{S_c i_{fc}}{4F} \frac{A_{act}}{H_{gc} L_{gc} W_{gc}}$$
(67)

$$W_{N_2,\text{out}} = C_{H_2} u_{out}^{agc} \tag{68}$$

Where $\frac{n_{N_2}}{n_{O_2}} = \frac{1 - y_{O_2}}{y_{O_2}}$.

8.2. Nitrogen concentration dynamic behavior in the cathode

The nitrogen dynamic behaviour in the cathode is expressed as (69).

$$\frac{dC_{N_2}}{dt} = W_{N_2, \text{in}} - W_{N_2, \text{out}}$$
 (69)

9. Voltage polarisation

In general, in the literature, the current density i_{fc} is imposed by the operators independent of any other variable, and the resulting voltage is calculated or measured. However, it must be considered that during extreme conditions such as extreme fuel starvation or extreme membrane drying, it is not possible to have an imposed current density. Such a model would lead to false values such as negative voltages. In reality, the stack cannot possibly follow the imposed current density and thus the following equations become false or incomplete. As these extreme situations are not considered here, it is then important to work with acceptable values.

9.1. The apparent voltage: U_{cell}

To calculate the apparent voltage U_{cell} in a fuel cell, many phenomena must be considered. First, the equilibrium voltage U_{eq} yields the maximum amount of energy available in the reaction $H_2(g) + O_2(g) \rightarrow H_2(g)$, using thermodynamics. Consequently, several losses must be considered. To obtain interesting current density values, certain amount of the equilibrium voltage must be sacrificed in driving the chemical reactions on the surface of the electrodes. This voltage loss is referred to as overpotential η . Naturally, a fuel cell provides a very low current density; that is, the cathode exchange current density i_0 . This is because of the kinetics of the reactions at the cathode, which are very slow. However, the electrical load that is imposed is generally much higher. Thus, to keep up with the load, certain amount of the equilibrium voltage is naturally sacrificed to accelerate the rate-limiting step of the reduction reaction. In contrast, at the anode, the overpotential is usually neglected, because the anode kinetics are sufficiently swift.

Then, the concentration losses are indirectly considered in this study as part of the equilibrium voltage's U_{eq} and the overpotential's η expressions. Fuel crossover and internal short circuit current, which also impact U_{cell} , are considered in the expression of the overpotential η . Finally, both proton and electron electrical resistances counterbalance the electrostatic forces at stake and thus reduce the equilibrium voltage.

Based on these assumptions, the following relation (70) is obtained for the cell voltage [5, 7, 8, 15]:

$$U_{cell} = U_{eq} - \eta_c - i_{fc} \left[R_p + R_e \right] \tag{70}$$

where $U_{cell}(V)$ is the cell voltage, $U_{eq}(V)$ is the equilibrium voltage, $\eta_c(V)$ is the cathode overpotential, $R_p(\Omega.m^2)$ is the area specific resistance of the protons, and $R_e(\Omega.m^2)$ is the area specific resistance of the electrons.

9.2. Equilibrium potential at the cathode

In the literature, the anode potential is usually set to zero. Thus, the equilibrium voltage, also referred to as the Nernst equation, is equal to the cathode equilibrium potential and its expression based on thermodynamics is (71) [7–9, 24, 31, 43, 72], where P_{ref} (Pa) is the reference pressure taken at 10^5 Pa.

$$U_{eq} = V_{eq}^{c} = E^{0} - 8.5 \cdot 10^{-4} \left[T_{fc} - 298.15 \right] + \frac{RT_{fc}}{2F} \left[\ln \left(\frac{RT_{fc}C_{H_{2},acl}}{P_{ref}} \right) + \frac{1}{2} \ln \left(\frac{RT_{fc}C_{O_{2},ccl}}{P_{ref}} \right) \right]$$
(71)

where E^0 (V) is the standard-state reversible voltage taken at E^0 = 1.229V, $C_{H_2,acl}$ and $C_{O_2,ccl}$ ($mol.m^{-3}$) are the H_2 concentration at the anode catalyst layer and the O_2 concentration at the cathode catalyst layer, respectively. These concentrations must be considered at the triple point regions as they are the place where the reactions occur and thus the chemical energy is converted here. Choosing the catalyst layer for the fuel concentrations also facilitates the partial incorporation of the concentration loss phenomenon into this expression. This is further discussed in Section 9.5. Thus, the theoretical maximum amount of energy that can be taken from the chemical reactions, that is, the Gibbs free energy, is linked with the fuel concentration in these regions. Then, the Gibbs free energy is transformed to have the expression of a potential, referred to as the equilibrium potential U_{eq} and expressed as 71.

9.3. The overpotential at the cathode η_c

As mentioned before, η_c corresponds to a voltage loss which compensate the energy needed to accelerate the low kinetics reactions that are at stake in the stack. However, the hydrogen oxidation reaction is so fast that the resulting overpotential at the anode is negligible compared to the one at the cathode. So, only the cathode overpotential is considered in this work.

9.3.1. A mistaken trend in the literature

In the literature, many different equations for the cathode overpotential can be found. Each author had their own method for calculating it. Despite their differences, they are similar in their formulation. All are said to be based on the Butler-Volmer equation, which appears in the literature to be a general equation that describes this physical phenomenon, although liberties have been taken in its rewriting. Moreover, certain authors proposed the addition of coefficients to this equation to consider more phenomena, such as drying or flooding of the electrodes. The complex equation (72) that we propose here to illustrate this trend in the literature corresponds to the combination of the expressions proposed by Fan et al. [24], Bao et al. [31], and Dicks [5]. An explanation of the different terms added is presented below.

However, as Dickinson et al. indicated in their article [73], this trend in the literature is not good. The use of the true Butler-Volmer equation has not only been distorted, but also too much is expected from this equation by the authors performing modelling. This criticism is explained in detail later in 9.3.2 and an acceptable, though relatively simple, equation is consequently provided.

$$\begin{cases} i_{fc} + i_n = a_+^{1-2\alpha_c} \left(1 - s_{ccl}\right)^{1.5} i_{0,353}^{ref} \exp\left(\frac{E_{act}}{R} \left[\frac{1}{T_{ref}} - \frac{1}{T_{fc}}\right]\right) \left[\frac{(1 - s_{ccl})\varepsilon_{cl}C_{O_2,ccl}}{C_{O_2}^{ref}}\right]^{\kappa_c} \left[\exp\left(\frac{4F(1 - \alpha_c)}{RT_{fc}}\eta_c\right) - \exp\left(-\frac{4F\alpha_c}{RT_{fc}}\eta_c\right)\right] \\ a_+ = \frac{[\lambda_{ccl} + 1] - \sqrt{[\lambda_{ccl} + 1]^2 - 4\lambda_{ccl}\left[1 - \frac{1}{K_e}\right]}}{2\left[1 - \frac{1}{K_e}\right]} \\ K_e = K_e^0 \exp\left(-\frac{\Delta H^0}{R} \left[\frac{1}{T_{fc}} - \frac{1}{298}\right]\right) \end{cases}$$

$$(72)$$

where a_+ is the activity of solvated protons, i_n $(A.m^{-2})$ is the internal current density, $i_{0,353}^{ref}$ $(A.m^{-2})$ is the referenced exchange current density at the cathode at 353.15K, E_{act} $(J.mol^{-1})$ is the activation energy term, R $(J.mol^{-1}.K^{-1})$ is the universal gas constant, T_{ref} (K) is the referenced temperature taken at 353.15K, C_{02}^{ref} $(mol.m^{-3})$ is the reference concentration of oxygen, κ_c is the overpotential correction exponent, α_c is the charge-transfer coefficient of the cathode, K_e is the acid-base equilibrium constant, K_e^0 is the standard acid-base equilibrium constant, and ΔH^0 $(J.mol^{-1})$ is the standard enthalpy of reaction. In the study by Fan et al., $J_{0,353}^{ref}$ $(A.m^{-3})$ is used and its link with $i_{0,353}^{ref}$ $(A.m^{-2})$ is: $i_{0,353}^{ref} = J_{0,353}^{ref} H_{cl}$.

Next, certain explanations are provided to globally understand each of these terms, although as discussed later, the use of a few of them is discouraged or should be modified.

First, the internal current density i_n is used here to consider the fuel crossover in the membrane [5], as explained in Section 9.1.

Then, the activity of solvated protons a_+ , is used here to consider the influence of a significantly dry membrane on the exchange current density. It is done for analysing start operation and current ignition [31]. Moreover, as shown in Figure 8, at T = 353K and $\lambda > 1$, $a_+ \approx 1$. Thus, it does not impact the equation for a hydrated membrane.

The purpose of $(1 - s_{ccl})^{1.5}$ is to consider the impact of the flooding on the stack voltage by examining the covering effect of liquid water on the active area of the catalyst. If the liquid saturation at the CCL increases, the active area of the catalyst becomes covered by liquid water and the cell voltage drops. Moreover, Xu et al. proposed to replace this term with: $\frac{s_{lim}-s_{ccl}}{s_{lim}}$. The idea is similar although reaching a certain value strictly between 0 and 1 (referred to as s_{lim} here) is sufficient to make the cell voltage drop to zero. Indeed, the surface of the active area, where the reactions occur, could be completely filled with water before its volume is covered. However, the value of s_{lim} was not given by the author and thus it would add another undetermined parameter in the model, which must be numerically estimated. One method to determine an analytical expression for s_{lim} is suggested in Section 2.7. However, these terms are a very simple method to consider the cathode flooding impact on the voltage as the relations are linear.

In this equation, the referenced exchange current density at the cathode $i_{0,353}^{ref}$ is a referenced constant obtained at a given O_2 concentration and at 353K. Thus, to obtain the working value of the exchange current density $i_{0,c}$, it is necessary to convert $i_{0,353}^{ref}$ by adding other terms. First, the expression $\exp\left(\frac{E_{act}}{R}\left[\frac{1}{T_{ref}}-\frac{1}{T_{fc}}\right]\right)$ is a way to convert $i_{0,353}^{ref}$

necessary to convert $i_{0,353}^{ref}$ by adding other terms. First, the expression $\exp\left(\frac{E_{act}}{T_{ref}} - \frac{1}{T_{fc}}\right)$ is a way to convert $i_{0,353}^{ref}$ from its referenced temperature to the working one. Subsequently, $\left[\frac{(1-s_{cct})\varepsilon_{ct}C_{O_2,cct}}{C_{O_2}^{ref}}\right]^{\kappa}$ converts $i_{0,353}^{ref}$ from its referenced

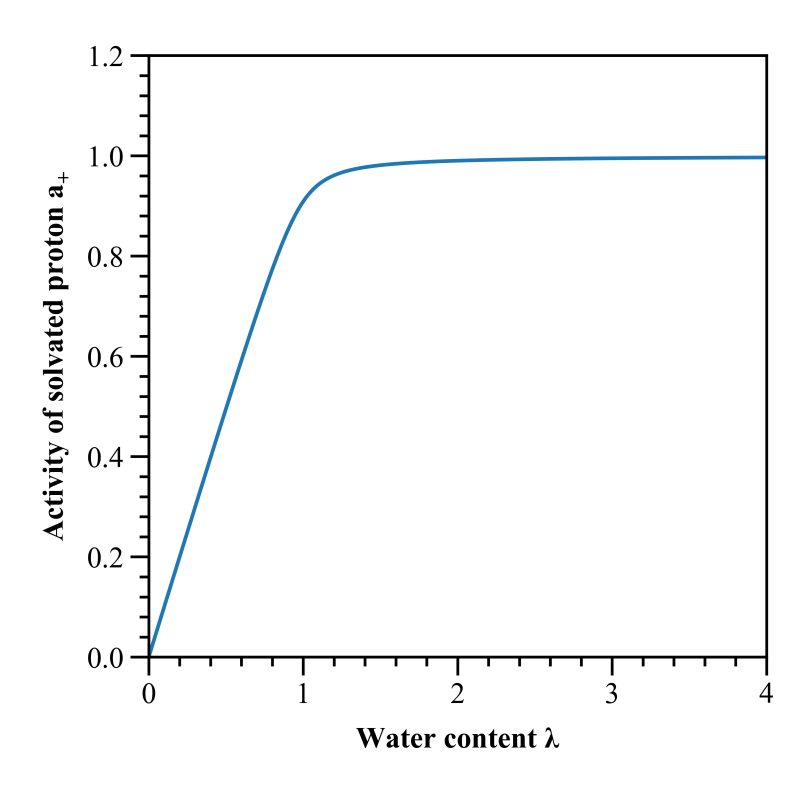


Figure 8: Plot of the activity of the solvated protons function of the water content

values of C_{O_2} to the working ones. The overpotential correction exponent κ_c is introduced in this study and is an undefined positive number usually between [0.25, 4.0], although it is possible to exceed this interval. It should be estimated for each specific stack [15, 24, 31, 48, 72, 73].

The term $\exp\left(\frac{4F(1-\alpha_c)}{RT_{fc}}\eta_c\right) - \exp\left(-\frac{4F\alpha_c}{RT_{fc}}\eta_c\right)$ is the last piece to link the current density i_{fc} to the overpotential η_c . The parameter α_c is referred to as the 'charge-transfer coefficient' and is the proportion of the electrical energy applied that is harnessed in changing the rate of an electrochemical reaction by changing the size of the activation barrier. Its value depends on the reaction involved and the material used for the electrode; however, it must be in the range 0–1.0. For most electrochemical reactions, α_c ranges within approximately 0.2–0.5 . At the oxygen electrode, the charge-transfer coefficient exhibits greater variation; however, it is still between approximately 0.1–0.5 in most circumstances. For 'symmetric' reactions, α_c is generally taken as 0.5 [5, 8].

Furthermore, it is important to use $C_{O_2,ccl}$ in the calculation of η_c , because the overpotential occurs at the triple point region. This indirectly contributes to the modelling of the concentration losses, as discussed in 9.5.

Finally, to obtain an explicit expression of the η_c function of i_{fc} , simplifications are made. The first solution involves simplifying one of the two exponentials in (72), that is, the negative one. $\exp\left(-\frac{4F\alpha_c}{RT_{fc}}\eta_c\right)$ is negligible at every working condition. However, this simplification yields false results for very low current densities, and the breaking value of i_{fc} for which it is not usable is dependent on the constant value chosen for the expression of η_c . Thus, it is difficult to obtain a reliable threshold. However, according to our results, this simplification should be sufficient for current densities greater than 0.01 $A.cm^{-2}$. The expression built and expressed as (73) is a Tafel form as it refers to the early work of the Swiss chemist Julius Tafel who determined this equation based on experimental data.

$$\begin{cases} \eta_{c} = \frac{RT_{fc}}{4F(1-\alpha_{c})} ln \left(\frac{1}{a_{+}} \frac{1}{(1-s_{ccl})^{1.5}} \frac{i_{fc} + i_{n}}{i_{0.353}^{ref}} \frac{1}{\exp\left(\frac{E_{act}}{R} \left[\frac{1}{T_{ref}} - \frac{1}{T_{fc}} \right]\right)} \left[\frac{C_{O2}^{ref}}{(1-s_{ccl})E_{cl}C_{O_{2}.ccl}} \right]^{\kappa_{c}} \right) \\ a_{+} = \frac{[\lambda_{ccl} + 1] - \sqrt{|\lambda_{ccl} + 1|^{2} - 4\lambda_{ccl} \left[1 - \frac{1}{K_{e}} \right]}}{2\left[1 - \frac{1}{K_{c}} \right]} \\ K_{e} = K_{e}^{0} \exp\left(-\frac{\Delta H^{0}}{R} \left[\frac{1}{T_{fc}} - \frac{1}{298} \right] \right) \end{cases}$$

$$(73)$$

Another method to obtain an explicit expression of η_c function of i_{fc} is to impose the value of α_c to 0.5. This way, the two exponentials are symmetrical and the mathematical function *sinh* appears, which can be easily reversed. This equation, expressed as (74), offers the advantage of being usable for all current densities.

$$\begin{cases}
\eta_{c} = \frac{RT_{fc}}{4F(1-\alpha_{c})} \operatorname{arsinh} \left(\frac{1}{2a_{+}} \frac{1}{(1-s_{ccl})^{1.5}} \frac{i_{fc} + i_{n}}{i_{0.353}^{ref}} \frac{1}{\exp\left(\frac{E_{act}}{R} \left[\frac{1}{T_{ref}} - \frac{1}{T_{fc}}\right]\right)} \left[\frac{C_{O_{2}}^{ref}}{(1-s_{ccl})\varepsilon_{cl}C_{O_{2},ccl}} \right]^{\kappa_{c}} \right) \\
a_{+} = \frac{[\lambda_{ccl} + 1] - \sqrt{[\lambda_{ccl} + 1]^{2} - 4\lambda_{ccl} \left[1 - \frac{1}{K_{e}}\right]}}{2\left[1 - \frac{1}{K_{e}}\right]} \\
K_{e} = K_{e}^{0} \exp\left(-\frac{\Delta H^{0}}{R} \left[\frac{1}{T_{fc}} - \frac{1}{298}\right]\right)
\end{cases} (74)$$

One important point in the expressions of η_c in the literature is that it is linked with many undetermined parameters: α_c , $i_{0.353}^{ref}$ and κ_c . The modelers must adjust them using experimental data for each fuel stack studied. It is not possible to use predefined values for these parameters because the Butler-Volmer equation is in essence an empirical treatment that does not mechanically model electrochemical processes [8, 73]. This parameter estimation should be performed only once per stack studied. Any changes in operating conditions following this adjustment should always lead to consistent results when a good model has been established. Moreover, adjustments to these parameters must be made within given ranges that make physical sense. It is generally legitimate to restrict their minimum and maximum values with physical considerations. These notions will be addressed in a future study.

9.3.2. A fair use of the Butler-Volmer equation

Dickinson et al. [73] highlighted two important features of the overpotential equation. First, the general form proposed in (72) originates from a misreading of the Butler-Volmer equation, although it has been copied many times and is now the most popular version of that equation. This is because this equation contains a single dependence on oxygen concentration and this applies equally between the two processes of oxidation and reduction (each modelled by an exponential), which is contrary to the essence of the Butler-Volmer equation. It is true that this error disappears in practice when the simplifying assumptions appear, giving rise to the (73) and (74) equations; however, but it is important to not create a model on the wrong basis.

Second, the Butler-Volmer equation is not derived from a theory that correctly describes the processes involved in the overpotential for a fuel cell. It is derived from a theory that describes much simpler processes, and its use for stacks is in fact a major simplification. It is therefore illusory to add terms to it in the hope of improving its predictions. Dickinson recommends using only the Nernst equation to model the hydrogen oxidation reaction (or even using a linearised Butler-Volmer equation, but this is not covered here as it is negligible under most operating conditions) and the Tafel equation to model the oxygen reduction reaction. This reduces the overall complexity of the models, makes them clearer to the community because the number of variants is reduced, reduces the number of undetermined parameters involved, which will have to be estimated experimentally when the model is put into practice on a real stack, and reduces the numerical instability of the models under abnormal operating conditions.

This simple Tafel equation, which is recommended for use, is expressed as (75).

$$i_{fc} + i_n = i_{0,c}^{ref} \left[\frac{C_{O_2,ccl}}{C_{O_2}^{ref}} \right]^{\kappa_c} \exp\left(\frac{F\alpha_c}{RT_{fc}} \eta_c \right)$$
(75)

where $i_{0,c}^{ref}$ is the referenced exchange current density at the cathode. To improve precision in the calculation of the model voltage, or to consider certain defects such as electrode flooding, the Butler-Volmer equation must be abandoned and a rigorous multi-step mechanism-based model must be implemented. This type of model still needs considerable research before it can be used [73].

9.4. Internal current density: crossover and short circuit

In the fuel cell, there is a slight amount of matter that naturally crosses the membrane, although it is supposed to be impermeable to it. This causes a voltage drop. This can be oxygen or hydrogen and is referred to as a crossover, or in case of electrons it is referred to as an electronic short circuit. These two phenomena together correspond to the internal current density, as expressed by 76.

$$i_n = i_{co,H_2} + i_{co,O_2} + i_{sc} (76)$$

where $i_{co.i}$ (A.m⁻²) is the internal crossover current density of the molecule i (hydrogen or oxygen) and i_{sc} (A.m⁻²) is the internal short circuit current density.

During a crossover, the matter that was supposed to react according to the fuel cell mechanism instead passes through the membrane and reacts with its complementary molecule by direct contact. Thus, matter is lost and unused, as are the electrons it carries. This crossover volume flow of matter through the membrane, $S_{i,co}$, discussed in Section 7.2, can be linked to a flow of lost electrons for calculating i_{co} , knowing the number of electrons that every molecule carries. This is expressed as 77.

$$\begin{cases} i_{co,H_2} = 2FH_{cl}S_{H_2,co} = 2Fk_{H_2}RT_{fc}\nabla_mC_{H_2} \\ i_{co,O_2} = 4FH_{cl}S_{O_2,co} = 4Fk_{O_2}RT_{fc}\nabla_mC_{O_2} \end{cases}$$
(77)

During an electronic short circuit through the membrane, the reaction between oxygen and hydrogen occurs normally on either side of the membrane, except that the electrons released by the hydrogen do not pass through the external circuit. Consequently, they do not contribute to i_{fc} and manage to pass through the membrane as well, although it is designed to resist them. There are few articles on this subject. The equation presented here, which has been standardised since the work of Giner-Sanz et al. [67] for more general use and expressed as (78), contains several assumptions that severely restrict its use. This is an experimental work, performed on a single commercial Nafion®117 membrane, which used linear voltammetry. The measurements were performed under constant temperature and relative humidity of the incoming gases, with only the pressures being varied independently at the anode and cathode without the need for them to be equal. It was therefore considered that the pressure is the determining variable for calculating i_{sc} , although in reality at least the temperature is a dependent variable as well. Moreover, the pressure variations are relatively small: between 1.12-1.45 bar at the cathode and only between 1.01-1.06 bar at the anode. Considering these strong limitations, further and larger experimental tests are required to refine these results [67].

$$\begin{cases} i_{sc} = \frac{U_{cell}}{r_{sc}} \\ r_{sc} = 1.79 \cdot 10^{-2} \left[\frac{P_{agc}}{101325} \right]^{-9.63} \left[\frac{P_{cgc}}{101325} \right]^{0.38} \end{cases}$$
 (78)

where r_{sc} ($\Omega .m^2$) is the area specific short circuit resistance.

Giner-Sanz et al. proposed a physical explanation for the link between the inlet pressures of the stack and the internal electronic short circuit. Increasing the gas pressure in a PEMFC can result in two opposing effects on the shortcircuit resistance. It can increase the effective interfacial contact area between layers, thereby decreasing resistance. However, it can cause porosity and morphological changes, which may increase or decrease resistance depending on the specific characteristics of the PEMFC. Whether an increase in pressure will result in increased or decreased resistance depends on the relative importance of these two effects. However, further research is needed to confirm this hypothesis [67].

Next, on a more general level, it is interesting to understand how this internal current density affects the voltage of the stack. To the authors' knowledge, there is no clear information on this in the literature. Here we present a possible physical explanation that would aid in understanding this link. The crossed hydrogen and oxygen molecules do not all react directly with their complementary molecule, although they are located in the same layer of matter. The distance and the presence of other molecules prevent easy contact between them and thus a high number of reactions per second. However, they are drawn to the catalytic sites because of the attraction generated by the overpotential of the stack, which enhances their reaction kinetics. By participating in this attraction, they is an additional weight to the overpotential, which must be higher to produce the same current through the stack. Similarly, the internal short circuit current density is an additional weight to the overpotential as certain electrons that need to be supplied to the external circuit are kept inside the stack by passing directly through the membrane. Thus, certain amount of the attraction produced by the overpotential has been wasted.

Mathematically, this impact translates into the addition of i_n to i_{fc} as expressed in 75. However, as mentioned by O'Hayre et al. [8] and contrary to that proposed by Dicks et al. [5], the addition of i_n to i_{fc} only concerns the overpotential and not the electronic and proton resistances. Indeed, these resistances are only concerned with the external current density and not its internal losses.

Finally, it is important to know that the internal current density is weak, approximately 0.01– $0.05 \ A.cm^{-2}$. At normal working conditions it is highly negligible. However, at low current density, it has a major impact. It is responsible for the open circuit voltage of fuel cells being approximately $0.95 \ V$, which is far lower than the Nernst potential of approximately $1.2 \ V$. Thus, accurate modelling of these losses is essential to develop PEMFC models that accurately replicate the experimental behaviour of PEMFCs operating at low current densities.

9.5. Concentration losses

1010

Under bad operating conditions, O_2 and H_2 concentrations can dramatically drop leading to a major voltage loss. This happens because U_{cell} is directly linked with fuel concentrations, as discussed previously. Several causes could lead to this phenomenon, referred to as concentration loss.

Diffusion between the GC and the CL could lead to two different concentration losses. First, even if a good control on the auxiliary system stabilises the fuel concentrations in the GC (which is generally the case), a rise in fuel consumption at the CL, which is inherent to the increase in current density, reduces the fuel concentration at the CL to increase the fuel diffusion from the GC to CL and reach equilibrium. This is an inevitable concentration loss (at constant pressure in the GC) and is dependent on the diffusion characteristics of the stack, load, and fuel concentrations in the GC (and so the operating conditions) [8]. Second, diffusion flow in GDL has physical limits that cannot be overcome. Thus, near these limits, diffusion could be sufficient to fill the first active sites near the inlets of the GC, but insufficient for satisfying those close to the outlets. In these last regions, fuel concentrations could quickly reach zero, which would dramatically reduce the voltage (and cause important degradations to the cells) [8].

Moreover, without a good drainage system, liquid water can build up and reduce the flow of oxygen to the catalyst sites. This reduction can quickly saturate the ability to recharge the catalytic layer with oxygen, resulting in a concentration loss.

In addition, N_2 crossover through the membrane could also lead to H_2 concentration loss as its accumulation leads to a reduction in the H_2 partial pressure at a fixed total pressure. However, this can be overcome by wisely using an ejector at the anode outlet, which ejects the gases in the AGC when N_2 is very important. This situation is comparable with saturated vapour and liquid water accumulation in the anode.

Finally, one method of avoiding concentration losses is to have high stoichiometries, for example greater than 1.5. It automatically leads to higher fuel concentrations in the stack and thus delays concentration losses. Moreover, the minor and temporary concentration losses during the transitory state are more likely to have very low impacts on the voltage as, being ruled by logarithm laws, voltage losses only occur at low fuel concentrations. In addition, having high concentrations at the inlet of the GC helps to avoid concentration losses at the outlet. It works as a safety margin.

To consider all these phenomena, the following expression (79) [8] is mainly used in the literature.

$$\Delta V_{conc} = \frac{RT}{4F} \left(1 + \frac{1}{\alpha_c} \right) ln \left(\frac{j_L}{j_L - j} \right)$$
 (79)

where j_L ($A.m^{-2}$) is the limiting current density. The value of j_L is approachable and discussed in [8]. However, this relation is a simplified approach of the concentration loss. It is only useful for black box and equivalent electrical models for which the concentrations at the triple point zone are not accessible. Moreover, it has a big disadvantage of

being dependant on experiments. The value of j_l changes with the stack technology and with the operating conditions. However, for all relations present in the literature, j_l is presented as a parameter and no expressions are given. Thus, it cannot accurately predict the concentration losses when the operating conditions change and is therefore limited.

Nevertheless, when the inside of PEMFC is modelled as in this study, the information regarding the concentration losses are already there. Indeed, the concentrations at the CL are followed. So, concentration losses are already considered in both equilibrium potential U_{eq} , as in 9.2, and overpotential η_c , as in 9.3 [8]. Any other voltage drop should be added in this case.

9.6. Proton conductive resistance

9.6.1. Proton conductivity of the membrane: σ_m

The proton conductivity σ is generally defined as (80).

$$\frac{1}{R_p} \stackrel{\triangle}{=} \sigma \frac{dS}{dx} \tag{80}$$

A confusing habit is present in the literature. The resistance R_p commonly refers to the area specific resistance r_p , in $\Omega.m^2$. In theory, we have $r_p = R_p dS$. However, in practice, the resistance is the area specific resistance, and the symbol R_p is still used: " $r_p = R_p$ ". Thus, with this confusing convention, we have the following definition for the proton conductivity (equation (81)).

$$\frac{1}{R_p} = \frac{\sigma}{dx} \tag{81}$$

Then, to calculate the resistance R_p , an expression of the proton conductivity in the membrane σ_m was obtained experimentally by Springer et al in 1991 [13] and is widely used in the literature [7, 15, 17, 18, 24, 26, 30, 31, 43]. It is expressed as (82).

$$\sigma_m = \begin{cases} [0.5139\lambda - 0.326] \exp\left(1268 \left[\frac{1}{303.15} - \frac{1}{T_{fc}}\right]\right), & \text{for } \lambda \ge 1\\ 0.1879 \exp\left(1268 \left[\frac{1}{303.15} - \frac{1}{T_{fc}}\right]\right), & \text{for } \lambda < 1 \end{cases}$$
(82)

The linear part $0.5139\lambda - 0.326$ is obtained from measurement at 30°C and the exponential part allows the consideration of other temperature ranges. An activation energy $E_{act} = 10542 \ J.mol^{-1}$ was measured and considered independent of λ . Then, the coefficient 1268 was calculated using $1268 = \frac{E_{act}}{R} = \frac{10542}{8.314}$. Moreover, below one water molecule per charge site (λ < 1), the conductivity is assumed to be constant. The shape of this function is showed figure 9.

In certain papers, this expression was inadvertently revised when $\lambda < 1$, using a linear decreasing with λ , as in (83) [30]. The goal was to "avoid negative conductivity".

$$\sigma_m = 0.1879\lambda \exp\left(1268 \left[\frac{1}{303.15} - \frac{1}{T_{fc}}\right]\right), \text{ for } \lambda < 1$$
 (83)

We discourage its use, although it intends to fix the σ_m expression, which reaches negative values if its expression for $\lambda \ge 1$ is used for $\lambda < 1$. However, the constant part in (82) is mentioned in Springer's original work [13], although only in the text and not in equation, which may be the source of the confusion. Moreover, although it is right to have a conductivity that decreases with λ for a 117 Nafion®membrane, it is exaggerated to yield $\sigma_m = 0$ $\Omega^{-1}.m^{-1}$ when $\lambda = 0$ and thus to obtain a perfect insulator with achievable conditions.

However, this expression (82) has limits for modern models as it was evaluated using outdated membranes [19]. Recent models exist [20], however none of them became widespread in the literature as they suffer from negative aspects. Either they are based from outdated data, the data used are not accessible, or the use of the equation is limited to one-phase consideration only, without liquid water. Thus, a strong study well documented with few limitations over a large brand of membranes is highly expected from the community.

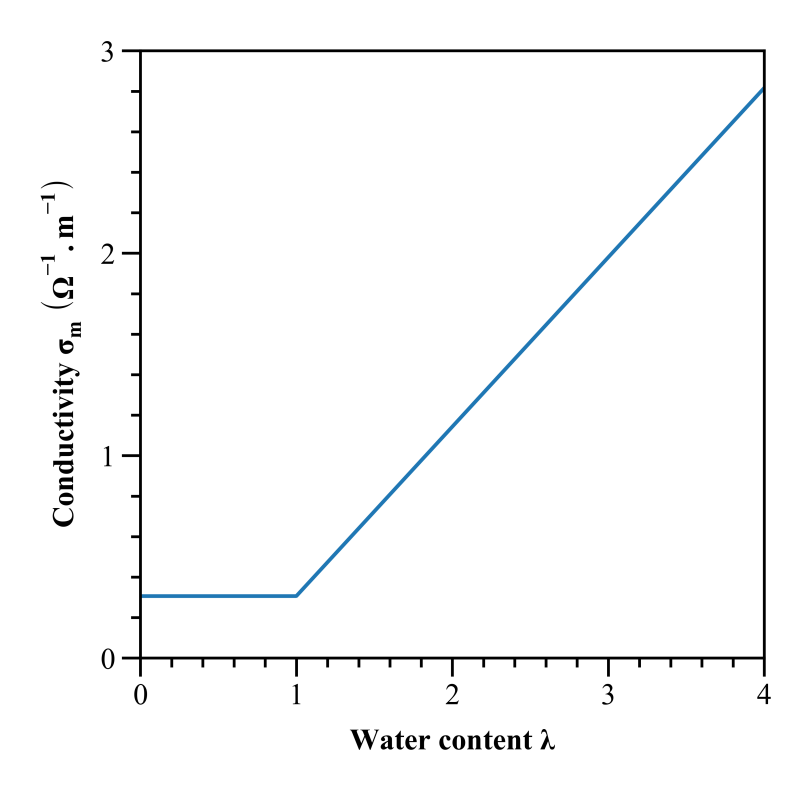


Figure 9: Shape of the conductivity σ_m function of the water content λ at $T_{fc} = 343.15K$

Moreover, (82) has the disadvantage of being built in two parts (and thus has a discontinuous derivative), which could introduce parasitic oscillations in the models when the discontinuous point is reached at $\lambda \approx 1$. To avoid this, the expression by Ramousse et al. can be used [74], which is expressed as (84). However, it is based on outdated and hardly accessible data and it yields $\sigma_m = 0$ $\Omega^{-1}.m^{-1}$ when $\lambda = 0$. A comparison between Springer and Ramousse expressions is presented in Figure 10.

$$\begin{cases}
\sigma_m = \left[0.0013\lambda^3 + 0.0298\lambda^2 + 0.2658\lambda \right] \exp\left(E_A \left[\frac{1}{353} - \frac{1}{T_{fc}} \right] \right) \\
E_A = 2640 \exp\left(-0.6\lambda \right) + 1183
\end{cases}$$
(84)

9.6.2. Proton conductivity resistance: R_p

The proton conductivity resistance R_p accounts for both the proton resistance in the membrane and the proton resistance in the catalyst layer at the triple point, considering the path between the membrane and the reaction sites. However, Springer's relationship yields the conductivity in the membrane but not in the catalyst layer. Thus, other studies have linked the catalyst resistance to the conductivity in the membrane. According to the transmission line model [15, 75, 76], the CCL resistance is equal to one-third of a membrane resistance of the shape of the CCL (H_{cl} , ε_{mc} and the tortuosity τ considered). The ACL resistance is also neglected. This second simplification is made because the hydrogen oxidation reaction is kinetically facile and gas-diffusion resistances for pure H2 are negligible. Thus, its reaction occurs in close proximity to the membrane, rendering a short path for proton transport and thus resulting in minimal voltage loss in anode [15, 75, 76]. Finally, the following equation (85) must be used [15, 26, 43, 75, 76].

$$R_p = R_{mem} + \frac{1}{3}R_{ccl} = \int_{mem} \frac{dx}{\sigma_m} + \frac{1}{3}\int_{ccl} \frac{dx}{\varepsilon_{mc}^{\tau}\sigma_m}$$
(85)

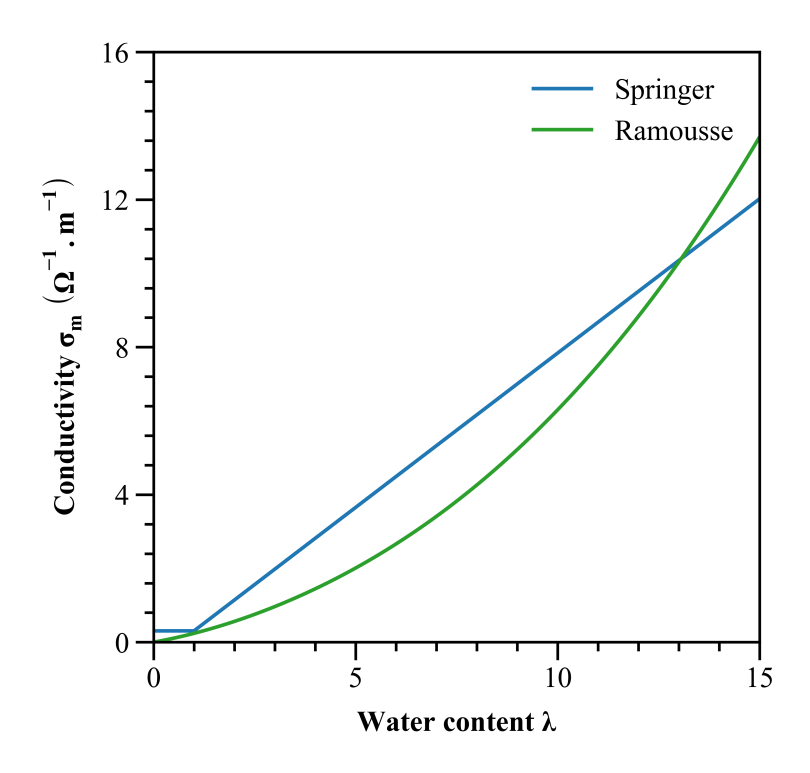


Figure 10: Comparison between Springer and Ramousse expressions for the conductivity at $T_{fc} = 343.15K$

10. Summary and outlook

This study attempted to synthesise and document the matter transport and voltage polarisation governing laws proposed in the literature. New laws, being the combination of several ideas presented in the literature, have also been presented. Certain expressions were discussed in detail, as they were more representative of the physics phenomena at stake. A synthesis is presented in tables 5,6, 7, and 8.

Finally, certain perspectives are discussed in this last section.

10.1. Model development

From this review, it is noted that more investigations are needed to model more clearly and precisely the processes at stake. In particular, explorations should be undertaken to improve the water sorption at the triple points in a biphasic state, the matter sorption at the GDL/GC interface, and the flooding impact on the voltage. Better modelling of these processes requires more targeted experimental investigation at both the material and cell levels.

10.2. Model parameter identification

The values of involved parameters are determinative for model performance. As shown in Tables B.10 and B.11, different parameters are selected and used in both mater transport and voltage polarisation models. The unclarified selection and use conditions of these parameters could lead to poor model performance, and even model invalidity. In addition, most of the available experimental data dedicated to model identification in the literature are outdated. The data were mainly extracted from experiments at the beginning of the 1990s. When more recent expressions are given, they are often based on outdated experimental or hardly accessible data, or usable only with strong limitations. Thus, a strong well documented study with few limitations over a large brand of fuel cells must be conducted to update the electro-osmotic drag, equilibrium water content, capillary pressure, and protonic conductivity expressions. The components have evolved during the last years and the modern measurement protocols have become more precise [19]. It is therefore highly necessary to update the database dedicated to model parameter identification. Overall, the limitations of the identified model parameters should be well noted in the model development and use stages.

However, the authors recognise that doing these precise experimentations is very challenging. This explains why the equations in the literature are not unified, as they were done by different teams on different stacks and under different conditions. It is therefore difficult to separate equations that model the same physical phenomenon but are different. It also remains to be demonstrated that these equations from different operating conditions remain valid in combination in a global model.

10.3. Targeted multiscale experiments

The development of both the matter and voltage polarisation models involves multiscale physicochemical phenomena. The global operating conditions can only be controlled and assigned at the macroscopic level. However, the matter transport and electrochemical processes are concerned at microscale to mesoscale. Most existing models were developed without considering the link between the different scales. For instance, processes at the microscale to mesoscale are often concerned with modelling the mass transport along the MEA and GDL. The corresponding models were thus often built using the data from ex-situ characterisations without considering the impacts of dynamic macroscopic operating parameters. It is questionable that the developed model can still conserve the performance when the multiscale interactions must be considered, which is the condition in practice. Thus, to achieve more reliable models, experiments and model development must be undertaken with multiscale characterisations and analysis. In these experiments, it is often necessary to combine macroscopic in-situ characterisations at the stack/system level and ex-situ microscopic characterisations at the component/cell level. Moreover, the in-situ and operando characterisation techniques are promising tools to gather the relevant microscopic data during operation [77].

10.4. Model resolution

As discussed in this review, the matter transport models, developed based on different theories, are governed by partial differential equations (PDEs) based on the Navier-Stokes equations. It is mainly the conservation equations which were used, as most flows are Fick-like ones [78]. However, for more complex models that consider multidimensional space (from 2D to 3D) or that consider convective flows within the GDL and CL, it is necessary to add the Navier-Stokes momentum balance equations to obtain a solvable model. These PDEs, in most cases, can be solved only by numerical simulations [79]. The high computation complexity renders it difficult to upscale the developed models in terms of space and time. In addition, the PDEs governed models are naturally not able to satisfy the requirements of certain model applications. For instance, inferring material properties must solve inverse problems, that is, calculating model parameters from online measured data. The inverse problems of PDEs and molecular simulations are prohibitively expensive and require complex formulations, and new algorithms [80]. Moreover, the models represented by PDEs cannot handle the noisy boundary data [81]. This results in the development of reduced-order modeling (ROM) that seeks to build low-dimensional models for efficient solutions with noisy boundary data [82]. Particularly, recent studies have shown that machine learning can be adopted as an efficient ROM tool and provide robust and efficient model resolutions [83].

10.5. Model use

The reviewed matter transport and voltage polarisation models are essential for optimisation of cell design, materials preparation, and operating conditions. It should be noted that different uses of the models recall different requirements for model order reduction, simplification, and formulation [84]. Nowadays, the analysis and optimisation of high-power fuel cell stacks/systems and the prediction of performance degradation has become increasingly important for fuel cell large deployment. In these large spatial-tempo scale applications, how to maintain the high-fidelity model performance without losing the model efficiency remains a challenging issue [85].

To proceed further, the authors have also built a one-dimensional two-phases model in a complementary work and the numerical results are discussed there. It is an interesting application to observe the deeper simplifications that were made to adapt the following equations for a control-command use. In addition, a review of the preponderant degradation phenomena is scheduled. In combination with these reviews and the one-dimensional two-phases model, these works are expected to allow a more accurate control on running devices, such as buses, to extend their lifetime and help to reach the European goal of 25,000 operating hours by 2023 [86].

11. Acknowledgments

This work has been supported by French National Research Agency via project DEAL (Grant no. ANR-20-CE05-0016-01), the Region Provence-Alpes-Côte d'Azur, the EIPHI Graduate School (contract ANR-17-EURE-0002) and the Region Bourgogne Franche-Comté.

Differential equations and boundary conditions	Matter flow expressions								
Dissolved water									
$\begin{cases} \frac{\rho_{\text{mem}}}{M_{\text{eq}}} \frac{\partial \lambda_{\text{mem}}}{\partial t} = -\nabla \cdot \boldsymbol{J}_{mem}, \text{ in the bulk membrane} \\ \frac{\rho_{mem} \varepsilon_{mc}}{M_{eq}} \frac{\partial \lambda_{cl}}{\partial t} = -\nabla \cdot \boldsymbol{J}_{mem} + S_{sorp} + S_{prod}, \text{ in the CL} \end{cases} $ (25a)	$S_{\text{prod}} = \begin{cases} 2k_{O_2} \frac{RT_{fc}}{H_{cl}} \nabla_m C_{O_2}, & \text{in the ACL} \\ \frac{i_{fc} + i_{sc}}{2FH_{cl}} + k_{H_2} \frac{RT_{fc}}{H_{cl}} \nabla_m C_{H_2}, & \text{in the CCL (24)} \\ 0, & \text{elsewhere} \end{cases}$								
$J_{mem}^{cl,mem} = 0$, at the ionomer border (25b)	$S_{sorp} = \gamma_{sorp} \frac{\rho_{mem}}{M_{eq}} \left[\lambda_{eq} - \lambda \right] (20)$ $J_{mem} = \frac{2.5}{22} \frac{i_{fc}}{F} \lambda \iota - \frac{\rho_{mem}}{M_{eq}} D(\lambda) \nabla \lambda (3)$								
Liquid water in th	e GDL and the CL								
$\rho_{H_2O}\varepsilon_{\frac{\partial s}{\partial t}} = -\nabla \cdot \boldsymbol{J}_{l,cap} + M_{H_2O}S_{vl} $ (36a)	$S_{vl} = \begin{cases} \gamma_{\text{cond}} \varepsilon \left[1 - \mathbf{s} \right] x_v \left[C_v - C_{\text{v,sat}} \right], & \text{if } C_v > C_{\text{v,sat}} \\ -\gamma_{\text{evap}} \varepsilon \mathbf{s} \frac{\rho_{H_2O}}{M_{H_2O}} RT_{fc} \left[C_{\text{v,sat}} - C_v \right], & \text{if } C_v \le C_{\text{v,sat}} \end{cases} $ (35)								
$ \begin{cases} J_{l}^{cl,mem} = 0, \text{ at the ionomer border} \\ J_{l}^{gdl,gc} = \rho_{H_{2}O} N_{a} \left(\frac{4}{3}\pi r_{d}^{3}\right) \mathbf{J}_{l,codi}, \text{ at the GDL/GC border} \end{cases} (36) $	$J_{l,cap} = -\sigma \frac{K_0}{v_l} \cos(\theta_c) \sqrt{\frac{\varepsilon}{K_0}} \mathbf{s}^{\mathbf{e}} \left[1.417 - 4.24\mathbf{s} + 3.789\mathbf{s}^2 \right] \nabla \mathbf{s} $ (27) $J_{l,codi} = \pm h_v \left[C_{l,gc} - \frac{\varepsilon_{gdl}}{N_a \left(\frac{4}{3} \pi r_d^3 \right)} \mathbf{s}_{gdl}^{\text{inter}} \right] \boldsymbol{\iota} $ (34)								
Vapor in the G	DL and the CL								
$\varepsilon \frac{\partial}{\partial t} \left([1 - \mathbf{s}] C_{\nu} \right) = -\nabla \cdot \boldsymbol{J}_{\nu, dif} - S_{sorp} - S_{\nu l} (46a)$	$\boldsymbol{J}_{\boldsymbol{v},dif} = -D_{\boldsymbol{v}}^{eff} \boldsymbol{\nabla} C_{\boldsymbol{v}} (37)$								
$\begin{cases} J_{v}^{cl,mem} = 0, & \text{at the ionomer border} \\ J_{v}^{gdl,gc} = J_{v,codi}, & \text{at the GDL/GC border} \end{cases} $ (46b)	$\boldsymbol{J_{v,codi}} = \pm h_v \left[C_{v,gc} - C_{v,gdl}^{\text{inter}} \right] \boldsymbol{\iota} (43)$								
Vapor in	n the GC								
$\frac{\partial C_{v}}{\partial t} = -\nabla \cdot \boldsymbol{J}_{v,conv} $ (49a)	$J_{v,conv} = C_v u_g (47)$ $J_{v,in}^{agc} = \frac{\Phi_{a,in} P_{sat}}{P_{a,in} - \Phi_{a,in} P_{sat}} \frac{S_a i_{fc}}{2F} \frac{A_{act}}{H_{gc} W_{gc}} (48a)$								
$\begin{cases} J_{\nu}^{gdl,gc} = J_{\nu,codi}, \text{ at the GDL/GC border} \\ J_{\nu}^{in/out,gc} = J_{\nu,\text{in/out}}^{gc}, \text{ at the inlet/outlet of the GC} \end{cases} $ (49b)	$J_{v,\text{in}}^{cgc} = \frac{\Phi_{c,\text{in}} P_{\text{sat}}}{P_{c,\text{in}} - \Phi_{c,\text{in}} P_{\text{sat}}} \frac{1}{y_{O_2,\text{in}}} \frac{S_c i_{fc}}{4F} \frac{A_{act}}{H_{gc} W_{gc}} $ (48a) $J_{v,\text{out}}^{gc} = C_v u_{out}^{gc} $ (48a)								
Liquid water	er in the GC								
$\frac{\partial C_{l,gc}}{\partial t} = -\nabla \cdot \boldsymbol{J}_{l,conv} $ (52a)	$\boldsymbol{J}_{l,conv} = C_{l,gc} \boldsymbol{u}_{g} \ (50)$								
$ \begin{cases} J_l^{gdl,gc} = J_{l,codi}, \text{ at the GDL/GC border} \\ J_l^{in/out,gc} = J_{l,in/out}^{gc}, \text{ at the inlet/outlet of the GC} \end{cases} (52b) $	$J_{l,in}^{gc} = 0 (51)$ $J_{l,out}^{gc} = C_l u_{out}^{gc} (51)$								

 $Table \ 5: \ Synthesis \ of \ the \ partial \ differential \ equations \ and \ the \ spotlighted \ matter \ transport \ expressions \ (1/2)$

Differential equations and boundary conditions	Matter flow expressions						
Hydrogen in the	GDL and the CL						
$\varepsilon_{\frac{\partial}{\partial t}}([1-s]C_{H_2}) = -\nabla \cdot \boldsymbol{J}_{H_2,dif} + S_{H_2,cons} (65a)$	$S_{H_2,cons} = \begin{cases} -\frac{i_f c^{+} i_{sc}}{2FH_{cl}} - \frac{RT_{fc}}{H_{cl}} \left[k_{H_2} \nabla_m C_{H_2} + 2k_{O_2} \nabla_m C_{O_2} \right], \text{ACL} \\ 0, \text{ elsewhere} \end{cases}$ (63)						
$ \begin{cases} J_{H_2}^{cl,mem} = 0, & \text{at the CL/membrane border} \\ J_{H_2}^{gdl,gc} = J_{H_2,codi}, & \text{at the GDL/GC border} \end{cases} (65b) $	$\boldsymbol{J}_{H_2,dif} = -D_{H_2}^{eff} \nabla C_{H_2} $ (53)						
, -	$J_{H_2,codi} = h_{H_2} \left[C_{H_2,agc} - C_{H_2,cgdl}^{inter} \right] \iota (53)$						
Hydrogen	in the GC						
$\frac{\partial C_{H_2}}{\partial t} = -\nabla \cdot \boldsymbol{J}_{H_2,conv} $ (65a)	$J_{H_2,conv} = C_{H_2} u_g (53)$						
$\begin{cases} J_{H_2}^{gdl,gc} = J_{H_2,codi}, \text{ at the GDL/GC border} \\ J_{H_2}^{in/out,gc} = J_{H_2,in/out}, \text{ at the inlet/outlet of the GC} \end{cases} $ (65b)	$J_{H_2, \text{in}} = \frac{S_{a}i_{fc}}{2F} \frac{A_{act}}{H_{gc}W_{gc}} $ (53)						
	$J_{H_2,\text{out}} = C_{H_2} u_{out}^{agc} (53)$						
Oxygen in the C	GDL and the CL						
$\varepsilon_{\partial t}^{\underline{\partial}} ([1-s] C_{O_2}) = -\nabla \cdot \boldsymbol{J}_{O_2, dif} + S_{O_2, cons} (66a)$	$S_{O_2,cons} = \begin{cases} -\frac{i_{fc} + i_{sc}}{4FH_{cl}} - \frac{RT_{fc}}{H_{cl}} \left[k_{O_2} \nabla_m C_{O_2} + \frac{k_{H_2}}{2} \nabla_m C_{H_2} \right], \text{CCL} \\ 0, \text{elsewhere} \end{cases} $ (64)						
$\begin{cases} J_{O_2}^{cl,mem} = 0, \text{ at the CL/membrane border} \\ J_{O_2}^{gdl,gc} = J_{O_2,codi}, \text{ at the GDL/GC border} \end{cases} $ (66b)	$\boldsymbol{Jo_{2,dif}} = -D_{O_2}^{eff} \boldsymbol{\nabla} C_{O_2} (54)$						
	$J_{O_2,codi} = h_{O_2} \left[C_{O_2,cgdl}^{inter} - C_{O_2,cgc} \right] \iota (54)$						
Oxygen i	n the GC						
$\frac{\partial C_{O_2}}{\partial t} = -\nabla \cdot \boldsymbol{J}_{O_2,conv} $ (66a)	$J_{O_2,conv} = C_{O_2} u_g $ (54)						
$ \begin{cases} J_{O_2}^{gdl,gc} = J_{O_2,codi}, \text{ at the GDL/GC border} \\ J_{O_2}^{in/out,gc} = J_{O_2,in/out}, \text{ at the inlet/outlet of the GC} \end{cases} (66b) $	$J_{O_2,\text{in}} = \frac{S_c i_{fc}}{4F} \frac{A_{act}}{H_{gc} W_{gc}} $ (54)						
` -	$J_{O_2,\text{out}} = C_{O_2} u_{out}^{cgc} $ (54)						
Nitr	ogen						
$\frac{dC_{N_2}}{dt} = W_{N_2, \text{in}} - W_{N_2, \text{out}} $ (69)	$W_{N_2,\text{in}} = \frac{1 - y_{O_2,in}}{y_{O_2,in}} \frac{S_c i_{fc}}{4F} \frac{A_{act}}{H_{gc} L_{gc} W_{gc}} $ (67)						
	$W_{N_2,\text{out}} = C_{N_2} u_{out}^{cgc} (68)$						

 $Table \ 6: \ Synthesis \ of \ the \ partial \ differential \ equations \ and \ the \ spotlighted \ matter \ transport \ expressions \ (2/2)$

Coefficients associated to the dissolved water in the membrane $D(\lambda) = 4.1 \times 10^{-10} \left[\frac{\lambda}{25.0} \right]^{0.15} \left[1.0 + \tanh\left(\frac{\lambda - 2.5}{1.4}\right) \right] (7)$ $a_w(C, s) = \frac{C}{C_{sat}} + 2s (15)$ $\lambda_{eq} = \frac{1}{2} \left[0.300 + 10.8a_w - 16.0a_w^2 + 14.1a_w^3 \right] \cdot \left[1 - \tanh\left(100 \left[a_w - 1 \right] \right) \right]$ $+\frac{1}{2}\left[9.2+8.6\left[1-\exp\left(-K_{\text{shape}}\left[a_{w}-1\right]\right)\right]\right]\cdot\left[1+\tanh\left(100\left[a_{w}-1\right]\right)\right]$ $\gamma_{sorp}(\lambda, T) = \begin{cases} \frac{1.14 \cdot 10^{-5} f_{v}(\lambda)}{H_{cl}} e^{2416 \left[\frac{1}{303} - \frac{1}{T_{fc}}\right]}, & \text{absorption flow} \\ \frac{4.59 \cdot 10^{-5} f_{v}(\lambda)}{H_{cl}} e^{2416 \left[\frac{1}{303} - \frac{1}{T_{fc}}\right]}, & \text{desorption flow} \end{cases}$ Coefficients associated to liquid water in the GDL and the CL $f_{\nu}(\lambda) = \frac{\lambda V_{w}}{V_{\text{mem}} + \lambda V_{w}}$ (20) $\begin{cases} e = 3, & \text{if } \varepsilon \in [0.1, 0.4] \\ e \in [4, 5], & \text{if } \varepsilon \in [0.6, 0.8] \end{cases}$ $K_0(\varepsilon) = \frac{\varepsilon}{8\ln(\varepsilon)^2} \frac{\left[\varepsilon - \varepsilon_p\right]^{\alpha + 2} r_f^2}{\left[1 - \varepsilon_p\right]^{\alpha} \left[\left[\alpha + 1\right]\varepsilon - \varepsilon_p\right]^2} e^{\beta_1 \varepsilon_c} \tag{30}$ $\sigma(T) = 235.8 \times 10^{-3} \left[\frac{647.15 - T_{fc}}{647.15} \right]^{1.256} \left[1 - 0.625 \frac{647.15 - T_{fc}}{647.15} \right] (31)$ $C_{l,gc}^{\text{inter}} = \frac{\sigma[\cos(\theta_c)]}{RT_{fc}} \sqrt{\frac{\varepsilon}{K_0}} \left[1.417 \mathbf{s}_{gdl}^{\text{inter}} - 2.12 \left(\mathbf{s}_{gdl}^{\text{inter}} \right)^2 + 1.263 \left(\mathbf{s}_{gdl}^{\text{inter}} \right)^3 \right] (34)$ $\mathbf{Coefficients \ associated \ to \ vapor \ in \ the \ GDL \ and \ the \ CL}$ $D_{i/j}^{eff} = \begin{cases} \varepsilon^{\tau} \left[1 - \mathbf{s} \right]^{\tau} D_{i/j}, & \text{at the CL} \\ \varepsilon \left[\frac{\varepsilon - \varepsilon_p}{1 - \varepsilon_p} \right]^{\alpha} \left[1 - \mathbf{s} \right]^2 e^{\beta_2 \varepsilon_c} D_{i/j}, & \text{at the GDL} \end{cases} (39)$ $h_v = S_h \frac{D_v}{H_{gc}} (44)$ $S_h = 0.9247 \cdot \ln\left(\frac{W_{gc}}{H_{gc}}\right) + 2.3787 (45)$

Table 7: Synthesis of the spotlight flow coefficients

	Spotlighted voltage polarization expressions											
The apparent voltage $U_{cell} = U_{eq} - \eta_c - i_{fc} \left[R_p + R_e \right]$ (70)												
The equilibrium potential	$U_{eq} = E^{0} - 8.5 \cdot 10^{-4} \left[T_{fc} - 298.15 \right] + \frac{RT_{fc}}{2F} \left[\ln \left(\frac{RT_{fc}C_{H_{2,acl}}}{P_{ref}} \right) + \frac{1}{2} \ln \left(\frac{RT_{fc}C_{O_{2,ccl}}}{P_{ref}} \right) \right] (71)$											
The overpotential	$\eta_c = \frac{RT_{fc}}{\alpha_c F} ln \left(\frac{i_{fc} + i_n}{i_{0,c}^{ref}} \left[\frac{C_{O_2}^{ref}}{C_{O_2,ccl}} \right]^{k_c} \right) (75) \qquad i_n = i_{co,H_2} + i_{co,O_2} + i_{sc} (76)$											
	$\begin{cases} i_{sc} = \frac{U_{cell}}{r_{sc}} \\ r_{sc} = 1.79 \cdot 10^{-2} \left[\frac{P_{agc}}{101325} \right]^{-9.63} \left[\frac{P_{cgc}}{101325} \right]^{0.38} \end{cases} (78) $ $\begin{cases} i_{co,H_2} = 2Fk_{H_2} \nabla_m P_{H_2} \\ i_{co,O_2} = 4Fk_{O_2} \nabla_m P_{O_2} \end{cases} (77)$											
The proton resistance	$\begin{cases} i_{sc} = \frac{U_{cell}}{r_{sc}} \\ r_{sc} = 1.79 \cdot 10^{-2} \left[\frac{P_{agc}}{101325} \right]^{-9.63} \left[\frac{P_{cgc}}{101325} \right]^{0.38} \end{cases} (78) \qquad \begin{cases} i_{co,H_2} = 2Fk_{H_2} \nabla_m P_{H_2} \\ i_{co,O_2} = 4Fk_{O_2} \nabla_m P_{O_2} \end{cases} (77) \\ \sigma_m = \begin{cases} [0.5139\lambda - 0.326] \exp\left(1268 \left[\frac{1}{303.15} - \frac{1}{T_{fc}} \right] \right), & \text{for } \lambda \ge 1 \\ 0.1879 \exp\left(1268 \left[\frac{1}{303.15} - \frac{1}{T_{fc}} \right] \right), & \text{for } \lambda < 1 \end{cases} (82)$											

Table 8: Synthesis of the spotlighted voltage polarization expressions

12. ORCID

1160

Raphaël Gass https://orcid.org/0000-0002-9586-0884 Zhongliang Li https://orcid.org/0000-0001-7021-2103 Rachid Outbib https://orcid.org/0000-0002-9157-5269 Daniel Hissel https://orcid.org/0000-0003-0657-3320 Samir Jemei https://orcid.org/0000-0003-0195-903X

Nomenclature

	Physica	al quantities	J	molar transfer flow $(mol.m^{-2}.s^{-1})$						
	A_{act}	active area (m^2)	J(s)	Leverett function						
	a_w	water activity in the pores of the CL	K	permeability (m^2)						
	C	molar concentration $(mol.m^{-3})$	k	permeability coefficient in the membrane						
	D	diffusion coefficient of water in the membrane		$(mol.m^{-1}.s^{-1}.Pa^{-1})$						
		$(m^2.s^{-1})$	K_e	acid-base equilibrium constant						
1170	D_c	capillary diffusion coefficient $(kg.m^{-1}.s^{-1})$	L_{gc}	length of the gas channel (<i>m</i>)						
	$D_{i/j}$	binary diffusivity of two species i and j in open	M	molecular weight $(kg.mol^{-1})$						
•,,,	space $(m^2.s^{-1})$	n	number of moles (mol)							
	E^0	standard-state reversible voltage (V)	Na	Avogadro constant (mol^{-1})						
	E_{act}	activation energy $(J.mol^{-1})$	P	pressure (Pa)						
	F	Faraday constant $(C.mol^{-1})$	R	universal gas constant $(J.mol^{-1}.K^{-1})$						
	f_{v}	water volume fraction of the membrane	r_d	water droplet radius (m)						
	H	thickness (m)	R_e/R_p	electron/proton conduction resistance $(\Omega.m^2)$						
	h	convective-conductive mass transfer coefficient	r_f	carbon fiber radius (m)						
		$(m.s^{-1})$	S	matter conversion at the interface of the triple						
1180	i	current density per unit of cell active area		points $(mol.m^{-3}.s^{-1})$						
		$(A.m^{-2})$	S_a/S_c	stoichiometric ratio at the anode/cathode						

1200	S_h	Sherwood number		φ_{sp}	Surface proportion function			
	S_{vl}	phase transfer rate of condensation and evapo-		α, β_1, β_2	2 fitted values			
		ration $(mol.m^{-3}.s^{-1})$	$\stackrel{\triangle}{=}$	equality by definition				
	T_{fc}	fuel cell temperature (K)		∇	gradient notation			
	U	voltage (V)	Subsc	cripts and superscripts				
	и	velocity $(m.s^{-1})$	a	anode				
	V	molar volume $(m^3.mol^{-1})$		c	cathode			
	W_{gc}	width of the gas channel (m)		cap	capillarity			
	X	space variable (<i>m</i>)		conv	convective			
	$\mathcal{X}_{\mathcal{V}}$	mole fraction of vapor		dif	diffusion			
1210	y_{O_2}	molar fraction of O_2 in dry air		eff	effective			
	е	capillary exponent		eq	equilibrium			
	S	liquid water saturation		fc	fuel cell			
	α_c	charge-transfer coefficient of the cathode		H_2	dihydrogen			
	ΔH^0	standard enthalpy of reaction $(J.mol^{-1})$		in	inlet			
	η	overpotential (V)	1250	liquid	liquid			
	γ	rate constant (s^{-1})		mem	membrane			
	γ_a	heat capacity ratio of dry air		N_2	dinitrogen			
γ _{sor} κ	γ_{sorp}	sorption rate (s^{-1})		O_2	dioxygen			
	К	overpotential correction exponent		out	outlet			
1220	λ	water content		prod	production			
	μ	dynamic viscosity (Pa.s)		sat	saturated			
	v_l	liquid water kinematic viscosity $(m^2.s^{-1})$		sorp	sorption			
	Φ	relative humidity		v	vapor			
	ho	density $(kg.m^{-3})$		Abbr	eviation			
	σ	surface tension of liquid water $(N.m^{-1})$	1260	ACL	anode catalyst layer			
	σ_m	conductivity of the membrane $(\Omega^{-1}.m^{-1})$		AGC	anode gas channel			
	au	pore structure coefficient		AGDL	anode gas diffusion layer			
	θ_c	contact angle of GDL for liquid water (°)		CCL	cathode catalyst layer			
	ε	porosity		CGC	cathode gas channel			
1230	$\boldsymbol{arepsilon}_{c}$	compression ratio	CGDL	cathode gas diffusion layer				
	Mathe	ematical symbols	CL	catalyst layer				
	ı	unit vector along the x-axis		EOD	electro-osmotic drag			
	K_{shape}	shape mathematical factor		GC	gas channel			
	'n	temporal derivative of $n \ (mol.s^{-1})$		GDL	gas diffusion layer			

70 Appendix A. Other useful equations

In this part, useful equations are given to link certain basic physical quantities with the temperature.

Appendix A.1. Vapor saturated pressure: $P_{v,sat}$

The vapour saturated pressure is expressed as (??). This is a correlation that provides acceptable agreement with the experimental data in the temperature range from -50 to 100 °C [7, 18, 23, 24, 27, 43].

$$P_{\text{v sat}} = 101325 \cdot 10^{-2.1794 + 0.02953} [T_{fc} - 273.15] - 9.1837 \cdot 10^{-5} [T_{fc} - 273.15]^2 + 1.4454 \cdot 10^{-7} [T_{fc} - 273.15]^3$$
(A.1)

Appendix A.2. Liquid water density: ρ_{H_2O}

Liquid water density expression is expressed as (A.2) [87]. At 70°C, this expression yields $\rho_{H_2O} = 977.77 \text{ kg.m}^{-3}$.

$$\rho_{H_2O} = \frac{999.83952 + 16.945176 \left[T_{fc} - 273.15 \right] - 7.9870401 \cdot 10^{-3} \left[T_{fc} - 273.15 \right]^2 - 46.170461 \cdot 10^{-6} \left[T_{fc} - 273.15 \right]^3}{1 + 16.879850 \cdot 10^{-3} \left[T_{fc} - 273.15 \right]} + \frac{105.56302 \cdot 10^{-9} \left[T_{fc} - 273.15 \right]^4 - 280.54253 \cdot 10^{-12} \left[T_{fc} - 273.15 \right]^5}{1 + 16.879850 \cdot 10^{-3} \left[T_{fc} - 273.15 \right]}$$
(A.2)

Appendix A.3. Liquid water dynamic viscosity: μ_l

Liquid water dynamic viscosity is expressed as (A.3) [24].

$$\mu_l = 2.414 \cdot 10^{-5 + \frac{247.8}{T_{fc} - 140.0}} \tag{A.3}$$

The following table A.9 compares this equation with data from other sources. Equation (A.3) is evaluated there at 70° C.

		Fan [24]	Hu [16]	Yang [18]	Bao [31]
Ì	$\mu_l (10^{-4} \text{ Pa.s})$	4.01	3.56	3.517	3.508

Table A.9: Comparison between the values given by the mentioned expression for the liquid water dynamic viscosity and values found in other works

Appendix A.4. Liquid water kinematic viscosity: v_1

Liquid water kinematic viscosity is expressed as (A.4). At 70°C, this expression yields $v_l = 4.10 \cdot 10^{-7} m^2 . s^{-1}$, which is a close to $v_l = 3.7 \cdot 10^{-7} m^2 . s^{-1}$ obtained from [16].

$$\nu_l \triangleq \frac{\mu_l}{\rho_{H_2O}} \tag{A.4}$$

Appendix B. Synthesis of the constant values founded in the literature

The goal of this appendix is to provide a large range of constants used by the precedent researchers. They are presented in tables B.10 and B.11.

References	[15]	[43]	[24]	[16]	[31]	[7]	[18]	[47]	[23]	[30]	[33]	[26]	[14]
Year	2021	2020	2017	2016	2015	2011	2011	2009	2008	2007	2007	2005	2003
	'				Operati	ng inpu	its						
$T_{fc}(K)$	343	353	353		353		343	343					353
P _{in} (Pa)	[1.3 – 1.5]-		101325		202650			101325			202650		303975
	105												
S_a	1.4	2.0	2.0							6 a			1.5
S_c	1.8	3.0	1.5						3	3 a			1.5
$\Phi_{a,in}$									1	1			
$\Phi_{c,in}$		0.6							1	1			
				I	Physical	consta	nts						
$F(C.mol^{-1})$							96485						
$R(J.mol^{-1}.K^{-1})$							8.314						
M_{H2O} $(kg.mol^{-1})$							0.018						
$\gamma_{O_2,in} (C.mol^{-1})$ K_e^0							0.2095						
K_e^0					6.2								
$\Delta H^0 (J.mol^{-1})$					5.23 ·								
					10^{4}								
μ_{cg} (Pa.s)				1.881		2.075						1.881	
				10^{-5}		10^{-5}						10^{-5}	

 $[^]a$ at 1 $A.cm^{-2}$

Table B.10: Comparison of constant values from different sources (1/2)

Appendix C. Synthesis of the hypothesis made in this work

The goal of the appendix is to sum up and classify all the hypothesis that have been made in this study.

Appendix C.1. Globally

- The stack described in these equations is composed of 1 cell.
- The stack temperature is considered constant and uniform (the cooling system is not represented).
- All the gas species behave ideally [15].
- The effect of gravity is ignored.
- The cell is operated with pure hydrogen, thus no contamination effects are considered.
- Nitrogen is supposed to be homogenous in all the cathode and the CGC.

Appendix C.2. In the membrane

- The experimental equations were generally measured on Nafion®-117 membrane [13, 27, 31].
- Certain experiments were conducted at a fixed temperature of 30°C or 80°C. It is assumed that these data can be used at any working PEMFC temperature [13, 27, 31].
- Schroeder's paradox is considered for describing the equilibrium water content of the membrane [15].
- The thickness of the membrane at different water contents is assumed to be identical. The membrane expansion is ignored [28].
- Water generated at the triple points is produced in dissolved form in the membrane [7].
- Water that crosses the membrane to the CL is in vapour form [28].
- N_2 crossover is neglected. Please refer to [71] for more information.

References	[15]	[43]	[5]	[24]	[16]	[31]	[17]	[7]	[18]	[47]	[23]	[30]	[33]	[26]	[50]	[75]	[14]	[22]
Year	2021	2020	2018	2017	2016				2011	2009	2008	2007	2007	2005	2005	2005	2003	2000
								sical p										
$L_{gc}(m)$	12	0.1		0.1	1.298	0.9282			0.2			0.2						1.36
$H_{gc}(m)$	5 ·	10^{-3}		10-3	10^{-3}	10^{-3}	5 .		5 .	10^{-3}		5 .	10^{-3}	10^{-3}			2 ·	7.6.
	10^{-4}						10^{-4}		10^{-4}			10^{-4}					10^{-3}	10^{-4}
$W_{gc}(m)$	8 ·	10^{-3}		8 .			7.5.		10^{-3}			10^{-3}					10^{-3}	1.59-
	10^{-4}			10-4			10-4											10^{-3}
$H_{gdl}(m)$	2.3.	3 ·		4.2.	2.1.	3 ·	3.8⋅	2 ·	2 ·	2.5.	2.5.	1.8-	3 ·	3 ·				
	10^{-4}	10^{-4}		10^{-4}	10^{-4}	10^{-4}	10^{-4}	10^{-4}	10^{-4}	10^{-4}	10^{-4}	10^{-4}	10^{-4}	10^{-5}				
$oldsymbol{arepsilon}_{gdl}$		0.7		0.6	0.6	0.4	0.4		0.7		0.5	0.7	0.6	0.5				
$H_{cl}(m)$	10^{-5}	10^{-5}		10^{-5}	10^{-5}			10^{-5}	10^{-5}	10^{-5}	1.6⋅	1.5.	10^{-5}	10^{-5}			5 ·	
											10^{-5}	10^{-5}					10^{-5}	
$arepsilon_{cl}$	0.2	0.3		0.3	0.6				0.2	0.2-	0.12	0.2	0.12					
										0.3								
$oldsymbol{arepsilon}_{mc}$	0.2	0.25^{a}		0.22/0.2	27						0.393		0.4	0.2		0.15		
S_{lim}	0.2735b	b																
$H_{mem}(m)$	2.5.	2.5.		5 ·	2.5.	5 ·		5 ·	2.5.		5 ·	5 ·	2.5.	5 ·			2 ·	1.5-
	10^{-5}	10^{-5}		10^{-5}	10^{-5}	10^{-5}		10^{-5}	10^{-5}		10^{-5}	10^{-5}	10^{-5}	10^{-5}			10^{-4}	10^{-4}
$\rho_{mem} (kg.m^{-3})$		1980		1980	1980	2000	2000	1980	1980				1980	1980		2000		2000
$\rho_{mem} (kg.m^{-3})$ $M_{eq} (kg.mol^{-1})$		1.1		1.1	1.1	1.1	1.1	1.1	1.1				1.1	1.1				1.1
A_{act} (m^2)	2.91.																	5 ·
	10^{-2}																	10^{-3}
		Cons	tants	based	on th	ne inte	eractio	on bet	ween	wate	r and	the st	ructu	re				
$\frac{\gamma_v(s^{-1})}{\gamma_{cond}(s^{-1})}$	1.3			1.3				1.3										
$\gamma_{cond} (s^{-1})$		5 ·		5 ·	10 ⁴		10 ²	[1, 10 ⁴]	10 ²		10 ²	1.0	5 ·					
		10^{3}		10^{3}									10^{3} c					
$\gamma_{evap} (Pa^{-1}.s^{-1})$		10^{-4}		10^{-4}			10^{-3}		10^{-3}		10^{-3}	5 ·	10^{-4c}					
												10^{-5}						
$\frac{\theta_c^{cl}\left(\right)}{\theta_c^{gdl}\left(\right)}$	120	95		95	110		120		95				95	110				
θ_c^{gdl} ()	120	110		120	110		120		110				110	110				
						Re	feren	ced v	alues			'					'	
$i_n (A.m^{-2})$			20															
$i_{0,c} (A.m^{-2})$			0.67			150^{d}				0.1	0.01				0.42			
$i_{0,c} (A.m^{-3})$		120^{d}		120^{d}								10 ⁴ e		120				
$i_{0,a} (A.m^{-3})$				10 ⁸ d									10 ⁹		10 ⁸			
α_c		0.5	0.5	0.5		0.18				1	1	1	1	1			1	
$E_{act} (J.mol^{-1})$		6.568-		6.568-		7.32-												
		104		104		104												
$C_{O_2}^{ref} (mol.m^{-3})$		3.39		3.39		40.89	3.39			40.89	5.55	5.24 ^e	40					
$C_{O_2}^{ref} (mol.m^{-3})$ $C_{H_2}^{ref} (mol.m^{-3})$		56.4		56.4		40.89	56.4						40					
$P_{ref}(Pa)$		23.1		10 ⁵		105	23.1	10 ⁵										
1 rej (1 u)				10			hema	tical f	actor	s l								
K _{shape}	5					2		.icai i	1									
snape	٥					-												

Table B.11: Comparison of constant values from different sources (2/2)

^aoptimal value according to [43] ^bvalue obtained with experimental fits from [15] ^coptimal value according to [33] ^dat 353.15 K ^eat 343 K

Appendix C.3. In the CLs

- The gas flow in the CL is laminar flow.
- The electrolyte in the CL is assumed to have the same tortuosity characteristics as that if the catalyst metal particles.
- The CLs are modelled as an agglomerate of packed spherical particles.

Appendix C.4. In the GDLs

- The GDLs are modelled as a fibrous porous media composed of randomly oriented cylindrical fibers.
- To characterise the water transport in GDLs, the Leverett function is used. It is based on experimental data of structures that are different from the one in PEMFC. However, it is still widely used [7].
- The gas flow in the GDL is laminar flow.
- The deformation of the porous environment is considered negligeable and water flow must be sufficiently slow to have small Reynold's number under stationary conditions [36].
- Gases motions haul liquid water, which generate a convective flow $J_{l,conv}$. However, being minor compared to the capillary flow $J_{l,cap}$, this flow is neglected.

Appendix C.5. In the GCs

1330

- The gas flow in the channel is predominantly convective.
- A small amount of liquid water is permitted to move out of the CGC as a spray flow. Liquid droplets are finely dispersed (with zero volume) in the two-phase flow and have transport properties identical to those of vapor [13, 15].
- Liquid droplets are moving at the same velocity as that of the gas mixture.
- All gases have the same velocity in the gas mixture.
- Water phase change is ignored in the GC.
- The 'dividing line,' or boundary between convective-dominated flow inside the core of the GC and diffusive-dominated flow inside the core of the electrodes, is assumed to occur at the interface between the GC and the GDL.
- Without better knowledge, it is considered that both concentrations at the two side of the GDL/GC interface are instantaneously equal. This is available for all gases : $C_{gc}^{inter} = C_{gdl}^{inter}$.

Appendix C.6. For the voltage

- It is assumed that the stack can follow the imposed current density.
- Anode overpotential is neglected.
- Anode potential is set to zero.
- Among the four elementary steps of the oxidation reduction reaction on the $Pt_{(111)}$ surface, OH formation reaction is the rate-limiting step [31].

Appendix D. Demonstrations

Appendix D.1. Additional information concerning the capillary flow $J_{l,cap}$ and the convective flow $J_{l,conv}$

To give a better comprehension of $J_{l,cap}$ and $J_{l,conv}$, certain additional information are presented here. First, an adaptation of Darcy's law with the variables of this study is expressed as D.1 [88]:

$$\boldsymbol{J}_{l} = -\frac{K_{l}}{v_{l}} \boldsymbol{\nabla} \boldsymbol{P}_{l} \tag{D.1}$$

where J_l is the liquid water flow, K_l (m^2) is the liquid phase permeability, and P_l (Pa) is the liquid-phase pressure.

Then, the common method to calculate P_l is to consider the capillary pressure P_c using its definition expressed as (D.2). Indeed P_c depends only on the pore geometry, fluid physical properties, and phase saturation. It is therefore a measurable quantity.

$$P_c \stackrel{\triangle}{=} P_g - P_l \tag{D.2}$$

where P_g (Pa) is the gas-phase pressure. For information, within a liquid, the intermolecular cohesive forces (e.g., hydrogen bonding for water) compensate each other. Each molecule generates interaction forces in all directions in a isotropic manner with neighbouring molecules, the resultant of these forces is therefore zero. However, at the surface, this is not the case (interactions with gas molecules are negligible) and the resultant of the forces for the molecules at the surface is directed towards the interior of the liquid. Therefore, there is an additional force, which counterbalances the pressure of the liquid at its surface; this is the capillary pressure Pc. In fact, wherever we are in the liquid, the pressure is globally the same (if we set aside gravity) and is mainly owing to the concentration of the species and their temperature. However, the surface molecules are slowed down, which reduces the pressure at the surface. As this surface pressure is at equilibrium equal to the gas pressure, it follows that liquid water is at a higher pressure, which is logical as it is a much more condensed phase (and at the same temperature at equilibrium).

Subsequently, using again Darcy's law to link the gas phase pressure P_g to its velocity u_g , (D.3) is obtained. Consequently, it is possible to identify two different flows: the capillary flow discussed in 3.3 and the convective flow discussed in 3.6.

$$\boldsymbol{J}_{l} = \frac{K_{l}}{v_{l}} \nabla \boldsymbol{P}_{c} + \frac{\mu_{g}}{v_{l}} \frac{K_{l}}{K_{g}} \boldsymbol{u}_{g} = \boldsymbol{J}_{l,conv}$$
 (D.3)

where μ_g (Pa.s) is the gas mixture dynamic viscosity, $K_l = K_0 s^e$ (m^2) is the liquid water phase permeability, $K_g = K_0 (1 - s)^e$ (m^2) is the gas mixture phase permeability, and u_g ($m.s^{-1}$) is the gas mixture velocity.

The capillary flow still needs more development to be usable. Thus, now we have (D.4).

$$J_{l,cap} = \frac{K_l}{\gamma_l} \nabla P_c \tag{D.4}$$

The next step is to highlight s, the liquid water saturation, one mainly used variable in this work. For this, the gradient ∇ is moved from P_c to s and (D.4) is seen as a Fick-like equation in (D.5), with D_{cap} ($kg.m^{-1}.s^{-1}$) its capillary diffusion coefficient.

$$\begin{cases} J_{l,cap} = -D_{cap} \nabla \mathbf{s} \\ D_{cap} = -\frac{K_{l}}{v_{l}} \frac{\partial P_{c}}{\partial \mathbf{s}} \end{cases}$$
(D.5)

Next, the liquid phase permeability can be calculated using D.6 and the capillary pressure P_c correlates to the properties of porous materials as follows in D.7 [7, 17, 23, 26, 30].

$$K_l = K_0 s^e \tag{D.6}$$

$$P_c = -\sigma \left| \cos \left(\theta_c \right) \right| \sqrt{\frac{\varepsilon}{K_0}} J(\mathbf{s}) \tag{D.7}$$

where K_0 (m^2) is the intrinsic permeability and J(s) is the Leverett function.

For information, it is also possible to find k_{rl} in the literature, which is the relative permeability of liquid phase and is a function of phase saturation alone, expressed as D.8.

$$k_{rl} = \frac{K_l}{K_0} = s^{e} \tag{D.8}$$

Then, it is the Leverett function J which brings the experimental part. This function showed in D.9 is based on experimental data of homogeneous soil or a sand bend with uniform wettability, which are different from the GDL and CL structures in PEMFC. Other experimental measurements have been conducted in an attempt to assess the real

situation in PEMFC. However, the results do not agree with each other very well. Therefore, this equation is still widely used for PEMFC studies [7].

$$J(s) = 1.417s - 2.12s^{2} + 1.263s^{3}$$
(D.9)

Finally, all of this considered, it is possible to derive the mainly used expression of J_{Lcap} showed in 27.

Appendix D.2. Additional information concerning the convective-diffusive flow at the GDL/GC interface J_{v,codi}

The expression of $J_{v,codi}$ in (??) needs further explanations. This flow is primary based on the diffusive theory, which rules that a diffusive flow is proportional to the gradient of its characteristic variable, which is the vapour concentration, as shown in (D.10).

$$J_{v,dif} = D_v \nabla \mathbf{C} \tag{D.10}$$

However, this theory is applicable only in case of a very thin volume at the GDL/GC interface at the GC side, where diffusion is the dominant flow. The thickness of this thin volume is demoted as ε_{gc} . Elsewhere in the GC, convection is dominant and leads reasonably, for simple modelling, to an homogeneous value of the concentration in the x direction (see figure 1). This homogeneity is only valid along the thickness. Thus, in the GC outside the mentioned thin volume, $C_{v,gc}$ is not function of x anymore. Then, considering that ε_{gc} is very small, the diffusive flow can be rewritten as in (D.11).

$$J_{v,dif} = \pm D_v \frac{C_{v,gc} - C_{v,gc}^{\text{inter}}}{\varepsilon_{gc}} \iota$$
 (D.11)

 ε_{gc} is a variable that depends not only on the GC geometry but also on the flows characteristics. This difficulty in measuring ε_{gc} is classically and artificially passed to an adimensional number, the Sherwood number S_h , as it is more convenient and generalisable to discuss about the values of an adimensional number. It is defined as follow:

$$S_h = \frac{H_{gc}}{\varepsilon_{gc}} \tag{D.12}$$

with H_{gc} the characteristic thickness of the GC. Then, the equation naturally becomes (D.13).

$$J_{v,dif} = \pm S_h \frac{D_v}{H_{gc}} \left[C_{v,gc} - C_{v,gc}^{\text{inter}} \right] \iota$$
 (D.13)

As $C_{v,gc}$ is free of the x direction owing to convection, it is easy to obtain its value. Finally, all of these coefficients are embedded in h_v , as discussed in 4.5, leading to (??).

Appendix D.3. Simplified flows at the inlet and outlet of the AGC

The consumed molar rate of hydrogen is given by the following equation. It is important to extract the active area from the fuel flow as MEA and GC have different flow areas.

$$\dot{n}_{H_2,\text{cons}} = J_{H_2,c} A_{\text{act}} = \frac{i_{fc}}{2F} A_{\text{act}}$$
 (D.14)

where \dot{n} ($mol.s^{-1}$) is the temporal derivative of the number of moles n.

1400

In the simplified model, the inlet flow of hydrogen at the anode is selected to be a certain amount of time $\dot{n}_{H_2, \mathrm{cons}}$. This coefficient is the anode stoichiometric ratio of hydrogen : S_a .

$$\dot{n}_{H_2,\text{in}} = \frac{S_a i_{fc}}{2F} A_{\text{act}} \tag{D.15}$$

Using the ideal gas law and the definition of the relative humidity, a link between n_{H_2} and n_{H_2O} is obtained as:

$$\frac{n_{H_2O}}{n_{H_2}} = \frac{P_{H_2O}}{P_{H_2}} = \frac{\Phi_a P_{sat}}{P - \Phi_a P_{sat}}$$
(D.16)

Thus:

$$\dot{n}_{H_2O,in} = \frac{\Phi_{a,in} P_{sat}}{P_{a,in} - \Phi_{a,in} P_{sat}} \frac{S_a i_{fc}}{2F} A_{act}$$
 (D.17)

Finally, the simplified flow of water at the inlet of the AGC is

$$J_{v,in}^{agc} = \frac{\dot{n}_{H_20,in}}{H_{gc}W_{gc}}$$

$$= \frac{\Phi_{a,in}P_{sat}}{P_{a,in} - \Phi_{a,in}P_{sat}} \frac{S_a i_{fc}}{2F} \frac{A_{act}}{H_{gc}W_{gc}}$$
(D.18)

Appendix D.4. Simplified flows at the inlet and outlet of the CGC

The consumed molar rate of oxygen is given by the following equation:

$$\dot{n}_{O_2,\text{cons}} = \frac{i_{fc}}{4F} A_{\text{act}} \tag{D.19}$$

In this model, the inlet flow of oxygen at the cathode is selected to be a certain amount of time $\dot{n}_{0_2,\text{cons}}$. This coefficient is the cathode stoichiometric ratio of oxygen: S_c .

$$\dot{n}_{O_2,\text{in}} = \frac{S_c i_{fc}}{4F} A_{\text{act}} \tag{D.20}$$

Using the ideal gas law and the definition of the relative humidity, a link between the dry air n_a , composed of $y_{O_2,in} = 20.95\%$ of O_2 and $O_2,in = 20.95\%$ of O_2 and O_2

$$\frac{n_{H_2O}}{n_a} = \frac{P_{H_2O}}{P_a} = \frac{\Phi_c P_{sat}}{P - \Phi_c P_{sat}}$$
 (D.21)

Moreover, by definition:

$$y_{O_2} = \frac{n_{O_2}}{n_a} \tag{D.22}$$

1410 Thus:

$$\dot{n}_{H_2O,in} = \frac{\Phi_{c,in} P_{sat}}{P_{c,in} - \Phi_{c,in} P_{sat}} \frac{1}{y_{O_2,in}} \frac{S_c i_{fc}}{4F} A_{act}$$
 (D.23)

Finally, the simplified flow of water at the inlet of the CGC is

$$J_{v,in}^{cgc} = \frac{\dot{n}_{H_20,in}}{H_{gc}W_{gc}}$$

$$= \frac{\Phi_{c,in}P_{sat}}{P_{c,in} - \Phi_{c,in}P_{sat}} \frac{1}{y_{O_2,in}} \frac{S_c i_{fc}}{4F} \frac{A_{act}}{H_{gc}W_{gc}}$$
(D.24)

References

- [1] The Future of Hydrogen. Seizing today's opportunities, https://www.iea.org/reports/the-future-of-hydrogen (Jun. 2019).
- [2] Y. Wang, K. S. Chen, J. Mishler, S. C. Cho, X. C. Adroher, A review of polymer electrolyte membrane fuel cells: Technology, applications, and needs on fundamental research, Applied Energy 88 (4) (2011) 981–1007. doi:10.1016/j.apenergy.2010.09.030.
- [3] The Paris Agreement. United Nations., https://www.un.org/en/climatechange/paris-agreement.
- [4] Stratégie nationale pour le développement de l'hydrogène décarboné en France. Dossier de presse. (Sep. 2020).
- [5] A. Dicks, D. A. J. Rand, Fuel Cell Systems Explained, third edition Edition, Wiley, Hoboken, NJ, 2018.
- [6] K. Jiao, J. Xuan, Q. Du, Z. Bao, B. Xie, B. Wang, Y. Zhao, L. Fan, H. Wang, Z. Hou, S. Huo, N. P. Brandon, Y. Yin, M. D. Guiver, Designing the next generation of proton-exchange membrane fuel cells, Nature 595 (7867) (2021) 361–369. doi:10.1038/s41586-021-03482-7.

- [7] K. Jiao, X. Li, Water transport in polymer electrolyte membrane fuel cells, Progress in Energy and Combustion Science 37 (3) (2011) 221-291. doi:10.1016/j.pecs.2010.06.002.
- [8] R. P. O'Hayre, S.-W. Cha, W. G. Colella, F. B. Prinz, Fuel Cell Fundamentals, third edition Edition, Wiley, Hoboken, New Jersey, 2016.
- [9] J. T. Pukrushpan, H. Peng, A. G. Stefanopoulou, Control-Oriented Modeling and Analysis for Automotive Fuel Cell Systems, Journal of Dynamic Systems, Measurement, and Control 126 (1) (2004) 14–25. doi:10.1115/1.1648308.
- [10] A. Z. Weber, J. Newman, Transport in Polymer-Electrolyte Membranes, Journal of The Electrochemical Society 15.
- [11] G. A. Futter, P. Gazdzicki, K. A. Friedrich, A. Latz, T. Jahnke, Physical modeling of polymer-electrolyte membrane fuel cells: Understanding water management and impedance spectra, Journal of Power Sources 391 (2018) 148–161. doi:10.1016/j.jpowsour.2018.04.070.
- [12] J. Newman, K. E. Thomas-Alyea, Electrochemical Systems, 3rd Edition, John Wiley & Sons, 2004.

1440

1450

- [13] T. E. Springer, T. A. Zawodzinski, S. Gottesfeld, Polymer Electrolyte Fuel Cell Model, Journal of The Electrochemical Society 138 (8) (1991) 2334–2342. doi:10.1149/1.2085971.
 - [14] A. A. Kulikovsky, Quasi-3D Modeling of Water Transport in Polymer Electrolyte Fuel Cells, Journal of The Electrochemical Society 150 (11) (2003) A1432. doi:10.1149/1.1611489.
 - [15] L. Xu, Z. Hu, C. Fang, L. Xu, J. Li, M. Ouyang, A reduced-dimension dynamic model of a proton-exchange membrane fuel cell, International Journal of Energy Research 45 (12) (2021) 18002–18017. doi:10.1002/er.6945.
 - [16] J. Hu, J. Li, L. Xu, F. Huang, M. Ouyang, Analytical calculation and evaluation of water transport through a proton exchange membrane fuel cell based on a one-dimensional model, Energy 111 (2016) 869–883. doi:10.1016/j.energy.2016.06.020.
 - [17] L. Xing, P. K. Das, X. Song, M. Mamlouk, K. Scott, Numerical analysis of the optimum Membrane/Ionomer water content of PEMFCs: The interaction of Nafion® ionomer content and cathode relative humidity, Applied Energy 138 (2015) 242–257. doi:10.1016/j.apenergy. 2014.10.011.
 - [18] X.-G. Yang, Q. Ye, P. Cheng, Matching of water and temperature fields in proton exchange membrane fuel cells with non-uniform distributions, International Journal of Hydrogen Energy 36 (19) (2011) 12524–12537. doi:10.1016/j.ijhydene.2011.07.014.
 - [19] M. B. Karimi, F. Mohammadi, K. Hooshyari, Recent approaches to improve Nafion performance for fuel cell applications: A review, International Journal of Hydrogen Energy 44 (54) (2019) 28919–28938. doi:10.1016/j.ijhydene.2019.09.096.
 - [20] E. J. F. Dickinson, G. Smith, Modelling the Proton-Conductive Membrane in Practical Polymer Electrolyte Membrane Fuel Cell (PEMFC) Simulation: A Review, Membranes 10 (11) (2020) 310. doi:10.3390/membranes10110310.
 - [21] T. A. Zawodzinski, M. Neeman, L. O. Sillerud, S. Gottesfeld, Determination of water diffusion coefficients in perfluorosulfonate ionomeric membranes, The Journal of Physical Chemistry 95 (15) (1991) 6040–6044. doi:10.1021/j100168a060.
 - [22] S. Motupally, A. J. Becker, J. W. Weidner, Diffusion of Water in Nafion 115 Membranes, Journal of The Electrochemical Society 147 (9) (2000) 3171. doi:10.1149/1.1393879.
 - [23] X. Wang, T. V. Nguyen, Modeling the Effects of Capillary Property of Porous Media on the Performance of the Cathode of a PEMFC, Journal of The Electrochemical Society 155 (11) (2008) B1085. doi:10.1149/1.2965512.
 - [24] L. Fan, G. Zhang, K. Jiao, Characteristics of PEMFC operating at high current density with low external humidification, Energy Conversion and Management 150 (2017) 763-774. doi:10.1016/j.enconman.2017.08.034.
 - [25] H. P. L. H. van Bussel, F. G. H. Koene, R. K. A. M. Mallant, Dynamic model of solid polymer fuel cell water management, Journal of Power Sources 71 (1) (1998) 218–222. doi:10.1016/S0378-7753(97)02744-4.
 - [26] U. Pasaogullari, C.-Y. Wang, Two-Phase Modeling and Flooding Prediction of Polymer Electrolyte Fuel Cells, Journal of The Electrochemical Society 152 (2) (2005) A380. doi:10.1149/1.1850339.
 - [27] J. T. Hinatsu, M. Mizuhata, H. Takenaka, Water Uptake of Perfluorosulfonic Acid Membranes from Liquid Water and Water Vapor, Journal of The Electrochemical Society 141 (6) (1994) 1493–1498. doi:10.1149/1.2054951.
 - [28] S. Ge, X. Li, B. Yi, I.-M. Hsing, Absorption, Desorption, and Transport of Water in Polymer Electrolyte Membranes for Fuel Cells, Journal of The Electrochemical Society 152 (6) (2005) A1149. doi:10.1149/1.1899263.
 - [29] T. Zawodzinskijr, T. Springer, F. Uribe, S. Gottesfeld, Characterization of polymer electrolytes for fuel cell applications, Solid State Ionics 60 (1-3) (1993) 199–211. doi:10.1016/0167-2738(93)90295-E.
 - [30] Q. Ye, T. V. Nguyen, Three-Dimensional Simulation of Liquid Water Distribution in a PEMFC with Experimentally Measured Capillary Functions, Journal of The Electrochemical Society 154 (12) (2007) B1242. doi:10.1149/1.2783775.
 - [31] C. Bao, W. G. Bessler, Two-dimensional modeling of a polymer electrolyte membrane fuel cell with long flow channel. Part I. Model development, Journal of Power Sources 275 (2015) 922–934. doi:10.1016/j.jpowsour.2014.11.058.
- [32] H. Wu, P. Berg, X. Li, Modeling of PEMFC Transients with Finite-Rate Phase-Transfer Processes, Journal of The Electrochemical Society 157 (1) (2010) B1. doi:10.1149/1.3248005.
 - [33] H. Meng, A two-phase non-isothermal mixed-domain PEM fuel cell model and its application to two-dimensional simulations, Journal of Power Sources 168 (1) (2007) 218–228. doi:10.1016/j.jpowsour.2007.03.012.
 - [34] H. Wu, Mathematical Modeling of Transient Transport Phenomena in PEM Fuel Cells, Ph.D. thesis, University of Waterloo, Waterloo, Ontario, Canada (2009).
 - [35] J. Nam, P. Chippar, W. Kim, H. Ju, Numerical analysis of gas crossover effects in polymer electrolyte fuel cells (PEFCs), Applied Energy 87 (12) (2010) 3699-3709. doi:10.1016/j.apenergy.2010.05.023.
 - [36] S. Whitaker, The Method of Volume Averaging, Vol. 13 of Theory and Applications of Transport in Porous Media, Springer Netherlands, Dordrecht, 1999. doi:10.1007/978-94-017-3389-2.
 - [37] J. Kim, G. Luo, C.-Y. Wang, Modeling two-phase flow in three-dimensional complex flow-fields of proton exchange membrane fuel cells, Journal of Power Sources 365 (2017) 419–429. doi:10.1016/j.jpowsour.2017.09.003.
 - [38] M. M. Tomadakis, T. J. Robertson, Viscous Permeability of Random Fiber Structures: Comparison of Electrical and Diffusional Estimates with Experimental and Analytical Results, Journal of Composite Materials 39 (2) (2005) 163–188. doi:10.1177/0021998305046438.
 - [39] Z. Fishman, A. Bazylak, Heterogeneous Through-Plane Distributions of Tortuosity, Effective Diffusivity, and Permeability for PEMFC GDLs, Journal of The Electrochemical Society 158 (2) (2011) B247. doi:10.1149/1.3524284.
 - [40] Z. Bao, Y. Li, X. Zhou, F. Gao, Q. Du, K. Jiao, Transport properties of gas diffusion layer of proton exchange membrane fuel cells: Effects of

- compression, International Journal of Heat and Mass Transfer 178 (2021) 121608. doi:10.1016/j.ijheatmasstransfer.2021.121608.
- [41] N. Zamel, X. Li, Effective transport properties for polymer electrolyte membrane fuel cells With a focus on the gas diffusion layer, Progress in Energy and Combustion Science 39 (1) (2013) 111–146. doi:10.1016/j.pecs.2012.07.002.
- [42] S.-D. Yim, B.-J. Kim, Y.-J. Sohn, Y.-G. Yoon, G.-G. Park, W.-Y. Lee, C.-S. Kim, Y. C. Kim, The influence of stack clamping pressure on the performance of PEM fuel cell stack, Current Applied Physics 10 (2) (2010) S59–S61. doi:10.1016/j.cap.2009.11.042.
- [43] Y. Wang, T. Liu, H. Sun, W. He, Y. Fan, S. Wang, Investigation of dry ionomer volume fraction in cathode catalyst layer under different relative humilities and nonuniform ionomer-gradient distributions for PEM fuel cells, Electrochimica Acta 353 (2020) 136491. doi:10.1016/j.electacta.2020.136491.
- [44] N. B. Vargaftik, B. N. Volkov, L. D. Voljak, International Tables of the Surface Tension of Water, Journal of Physical and Chemical Reference Data 12 (3) (1983) 817–820. doi:10.1063/1.555688.
- [45] U. Pasaogullari, C.-Y. Wang, Two-phase transport and the role of micro-porous layer in polymer electrolyte fuel cells, Electrochimica Acta (2004).
- [46] C. Y. Wang, P. Cheng, A multiphase mixture model for multiphase, multicomponent transport in capillary porous media I. Model development.
- [47] J. H. Nam, K.-J. Lee, G.-S. Hwang, C.-J. Kim, M. Kaviany, Microporous layer for water morphology control in PEMFC, International Journal of Heat and Mass Transfer 52 (11-12) (2009) 2779–2791. doi:10.1016/j.ijheatmasstransfer.2009.01.002.
- [48] B. Xie, M. Ni, G. Zhang, X. Sheng, H. Tang, Y. Xu, G. Zhai, K. Jiao, Validation methodology for PEM fuel cell three-dimensional simulation, International Journal of Heat and Mass Transfer 189 (2022) 122705. doi:10.1016/j.ijheatmasstransfer.2022.122705.
- [49] N. Zamel, X. Li, J. Shen, Correlation for the Effective Gas Diffusion Coefficient in Carbon Paper Diffusion Media, Energy & Fuels 23 (12) (2009) 6070–6078. doi:10.1021/ef900653x.
- [50] Y. Bultel, K. Wiezell, F. Jaouen, P. Ozil, G. Lindbergh, Investigation of mass transport in gas diffusion layer at the air cathode of a PEMFC, Electrochimica Acta 51 (3) (2005) 474–488. doi:10.1016/j.electacta.2005.05.007.
- [51] J. Taine, TAINE+ENGUEHARD+PETI, Transferts thermiques introduction aux transferts d'énergie: cours et exercices d'application, DUNOD., 2014.
- [52] L. Xu, J. Hu, S. Cheng, C. Fang, J. Li, M. Ouyang, W. Lehnert, Robust control of internal states in a polymer electrolyte membrane fuel cell air-feed system by considering actuator properties, International Journal of Hydrogen Energy 42 (18) (2017) 13171-13191. doi: 10.1016/j.ijhydene.2017.03.191.
 - [53] Y. Shao, L. Xu, X. Zhao, J. Li, Z. Hu, C. Fang, J. Hu, D. Guo, M. Ouyang, Comparison of self-humidification effect on polymer electrolyte membrane fuel cell with anodic and cathodic exhaust gas recirculation, International Journal of Hydrogen Energy 45 (4) (2020) 3108–3122. doi:10.1016/j.ijhydene.2019.11.150.
 - [54] L. Clancy, Isentropic flow, in: Aerodynamics, pitman publishing Edition, London, 1975, Ch. 3.11, p. 28.

- [55] T. Kotaka, Y. Tabuchi, U. Pasaogullari, C.-Y. Wang, Impact of Interfacial Water Transport in PEMFCs on Cell Performance, Electrochimica Acta 146 (2014) 618–629. doi:10.1016/j.electacta.2014.08.148.
- [56] L. Hao, K. Moriyama, W. Gu, C.-Y. Wang, Modeling and Experimental Validation of Pt Loading and Electrode Composition Effects in PEM Fuel Cells, Journal of The Electrochemical Society 162 (8) (2015) F854–F867. doi:10.1149/2.0221508jes.
- [57] Y. Wang, S. Basu, C.-Y. Wang, Modeling two-phase flow in PEM fuel cell channels, Journal of Power Sources 179 (2) (2008) 603-617. doi:10.1016/j.jpowsour.2008.01.047.
 - [58] F. Jiang, C.-Y. Wang, Numerical modeling of liquid water motion in a polymer electrolyte fuel cell, International Journal of Hydrogen Energy 39 (2) (2014) 942–950. doi:10.1016/j.ijhydene.2013.10.113.
 - [59] Y. Li, S.-C. Yao, Porous Media Modeling of Microchannel Cooled Electronic Chips with Nonuniform Heating, Journal of Thermophysics and Heat Transfer 29 (4) (2015) 695–704. doi:10.2514/1.T4509.
 - [60] J. Jie Liu, H. Zhang, S. C. Yao, Y. Li, Porous Media Modeling of Two-Phase Microchannel Cooling of Electronic Chips With Nonuniform Power Distribution, Journal of Electronic Packaging 136 (2) (2014) 021008. doi:10.1115/1.4027420.
 - [61] U. Imke, Porous media simplified simulation of single- and two-phase flow heat transfer in micro-channel heat exchangers, Chemical Engineering Journal 101 (1-3) (2004) 295–302. doi:10.1016/j.cej.2003.10.012.
 - [62] C.-Y. Wang, M. Groll, S. Rösler, C.-J. Tu, Porous medium model for two-phase flow in mini channels with applications to micro heat pipes, Heat Recovery Systems and CHP 14 (4) (1994) 377–389. doi:10.1016/0890-4332(94)90041-8.
 - [63] D. Sugumar, K.-K. Tio, Thermal Analysis of Inclined Micro Heat Pipes, Journal of Heat Transfer 128 (2) (2006) 198–202. doi:10.1115/1.2137763.
 - [64] K.-K. Tio, C. Y. Liu, K. C. Toh, Thermal analysis of micro heat pipes using a porous-medium model, Heat and Mass Transfer 36 (1) (2000) 21–28. doi:10.1007/s002310050359.
 - [65] S. Basu, J. Li, C.-Y. Wang, Two-phase flow and maldistribution in gas channels of a polymer electrolyte fuel cell, Journal of Power Sources 187 (2) (2009) 431–443. doi:10.1016/j.jpowsour.2008.11.039.
 - [66] Y. Wang, C.-Y. Wang, Modeling Polymer Electrolyte Fuel Cells with Large Density and Velocity Changes, Journal of The Electrochemical Society 152 (2) (2005) A445. doi:10.1149/1.1851059.
- [67] J. Giner-Sanz, E. Ortega, V. Pérez-Herranz, Hydrogen crossover and internal short-circuit currents experimental characterization and modelling in a proton exchange membrane fuel cell, International Journal of Hydrogen Energy 39 (25) (2014) 13206–13216. doi: 10.1016/j.ijhydene.2014.06.157.
 - [68] N. T. Truc, S. Ito, K. Fushinobu, Numerical and experimental investigation on the reactant gas crossover in a PEM fuel cell, International Journal of Heat and Mass Transfer 127 (2018) 447–456. doi:10.1016/j.ijheatmasstransfer.2018.07.092.
 - [69] R. Ahluwalia, X. Wang, Buildup of nitrogen in direct hydrogen polymer-electrolyte fuel cell stacks, Journal of Power Sources 171 (1) (2007) 63–71. doi:10.1016/j.jpowsour.2007.01.032.
 - [70] S. S. Kocha, J. Deliang Yang, J. S. Yi, Characterization of gas crossover and its implications in PEM fuel cells, AIChE Journal 52 (5) (2006) 1916–1925. doi:10.1002/aic.10780.
- [71] K. D. Baik, M. S. Kim, Characterization of nitrogen gas crossover through the membrane in proton-exchange membrane fuel cells, International Journal of Hydrogen Energy 36 (1) (2011) 732–739. doi:10.1016/j.ijhydene.2010.09.046.

- [72] Z. Yang, Q. Du, Z. Jia, C. Yang, K. Jiao, Effects of operating conditions on water and heat management by a transient multi-dimensional PEMFC system model, Energy 183 (2019) 462–476. doi:10.1016/j.energy.2019.06.148.
- [73] E. J. F. Dickinson, G. Hinds, The Butler-Volmer Equation for Polymer Electrolyte Membrane Fuel Cell (PEMFC) Electrode Kinetics: A Critical Discussion, Journal of The Electrochemical Society 166 (4) (2019) F221-F231. doi:10.1149/2.0361904jes.
- [74] J. Ramousse, J. Deseure, O. Lottin, S. Didierjean, D. Maillet, Modelling of heat, mass and charge transfer in a PEMFC single cell, Journal of Power Sources 145 (2) (2005) 416–427. doi:10.1016/j.jpowsour.2005.01.067.
- [75] R. Makharia, M. F. Mathias, D. R. Baker, Measurement of Catalyst Layer Electrolyte Resistance in PEFCs Using Electrochemical Impedance Spectroscopy, Journal of The Electrochemical Society 152 (5) (2005) A970. doi:10.1149/1.1888367.
- [76] K. C. Neyerlin, W. Gu, J. Jorne, A. Clark, H. A. Gasteiger, Cathode Catalyst Utilization for the ORR in a PEMFC, Journal of The Electrochemical Society 154 (2) (2007) B279. doi:10.1149/1.2400626.
- [77] Q. Meyer, Y. Zeng, C. Zhao, In Situ and Operando Characterization of Proton Exchange Membrane Fuel Cells, Adv. Mater. (2019).
- [78] A. Z. Weber, R. L. Borup, R. M. Darling, P. K. Das, T. J. Dursch, W. Gu, D. Harvey, A. Kusoglu, S. Litster, M. M. Mench, R. Mukundan, J. P. Owejan, J. G. Pharoah, M. Secanell, I. V. Zenyuk, A Critical Review of Modeling Transport Phenomena in Polymer-Electrolyte Fuel Cells, Journal of The Electrochemical Society (2014).
- [79] G. Zhang, Multi-phase models for water and thermal management of proton exchange membrane fuel cell_ A review, Journal of Power Sources (2018).
- [80] G. Karniadakis, I. Kevrekidis, L. Lu, et al., Physics-informed machine learning, Nat Rev Phys 3 (2021) 422–440doi:10.1038/ s42254-021-00314-5.
- [81] K. Shukla, P. C. Di Leoni, J. Blackshire, D. Sparkman, G. E. Karniadakis, Physics-informed neural network for ultrasound nondestructive quantification of surface breaking cracks (May 2020). arXiv: 2005.03596.
- [82] W. Chen, Q. Wang, J. S. Hesthaver, C. Zhang, Physics-informed machine learning for reduced-order modeling of nonlinear problems, Journal
- of Computational Physics 446 (2021) 110666. doi:10.1016/j.jcp.2021.110666.
 [83] R. Ding, S. Zhang, Y. Chen, Z. Rui, K. Hua, Y. Wu, X. Li, X. Duan, X. Wang, J. Li, J. Liu, Application of Machine Learning in Optimizing Proton Exchange Membrane Fuel Cells: A Review, Energy and AI 9 (2022) 100170. doi:10.1016/j.egyai.2022.100170.
- [84] M. Mayur, M. Gerard, P. Schott, W. G. Bessler, Lifetime Prediction of a Polymer Electrolyte Membrane Fuel Cell under Automotive Load Cycling Using a Physically-Based Catalyst Degradation Model (2018).
- [85] T. Jahnke, Performance and degradation of Proton Exchange Membrane Fuel Cells: State of the art in modeling from atomistic to system scale. Journal of Power Sources (2016).
- [86] Fuel Cells and Hydrogen 2 Joint Undertaking (FCH 2 JU). Addendum to the Multi Annual Work Plan 2014 2020 (FCH 2 JU, 2018) (2018).
- [87] G. S. Kell, Density, thermal expansivity, and compressibility of liquid water from 0.Deg. to 150.Deg.. Correlations and tables for atmospheric pressure and saturation reviewed and expressed on 1968 temperature scale, Journal of Chemical & Engineering Data 20 (1) (1975) 97–105. doi:10.1021/je60064a005.
- [88] S. P. Neuman, Theoretical derivation of Darcy's law, Acta Mechanica 25 (3-4) (1977) 153-170. doi:10.1007/BF01376989.